Perturbation theory and molecular simulation of nonprimitive model electrolyte solutions

Von der Fakultät Energie-, Verfahrens- und Biotechnik der Universität Stuttgart zur Erlangung der Würde eines Doktors der Ingenieurwissenschaft (Dr.-Ing.) genehmigte Abhandlung

Vorgelegt von
Florian Drunsel
aus Lörrach

Hauptberichter: Prof. Dr.-Ing. Joachim Groß
Mitberichter: Prof. Dr.-Ing. habil. Jadran Vrabec

Tag der mündlichen Prüfung: 22.07.2021

Institut für Technische Thermodynamik und Thermische Verfahrenstechnik der Universität Stuttgart

2021

Eidesstattliche Erklärung zu meiner Dissertation mit dem Titel:

Perturbation theory and molecular simulation of nonprimitive model electrolyte solutions

Hiermit erkläre ich, dass ich die beigefügte Dissertation selbstständig verfasst und keine anderen als die angegebenen Hilfsmittel genutzt habe. Alle wörtlich oder inhaltlich übernommenen Stellen habe ich als solche gekennzeichnet.

Ich versichere außerdem, dass ich die beigefügte Dissertation nur in diesem und keinem anderen Promotionsverfahren eingereicht habe und dass diesem Promotionsverfahren keine endgültig gescheiterten Promotionsverfahren vorausgegangen sind.

Ort, Datum	Unterschrift

Contents

Kurzzusammenfassung

In der vorliegenden Arbeit wird ein neuer Störungsansatz für Elektrolytlösungen entwickelt. Bei der Anwendung von Störungstheorien auf Elektrolytlösungen, die mit Hilfe des nichtprimitiven Modells modelliert werden, ergibt sich aufgrund der Langreichweitigkeit der elektrostatischen Wechselwirkungen das Problem von divergierenden Korrelationsintegralen. Um dieses Problem zu umgehen werden hier die elektrostatischen Wechselwirkungspotentiale in kurzreichweitige und langreichweitige Anteile aufgetrennt. Die kurzreichweitigen Anteile werden zur Formulierung einer Störungstheorie dritter Ordnung verwendet. Die zu den langreichweitigen Potentialanteilen gehörende Helmholtzenergie wird durch einen analytischen Korrekturterm, der aus der 'local molecular field' (LMF) Theorie resultiert, berücksichtigt. Mit Hilfe von Daten aus Molekularsimulationen wird der grundlegende Ansatz, eine Störungstheorie für kurzreichweitige Paarpotentiale und einen analytischen Korrekturterm zu verwenden, validiert. Die selben Daten werden verwendet, um die Störungstheorie dritter Ordnung zu bewerten und systematisch Möglichkeiten zu deren weiterer Verbesserung zu identifizieren.
Um das nichtprimitive Modellfluid von harten dipolaren und ionisch geladenen Kugeln umfänglicher zu beleuchten, werden zusätzlich Simulationsdaten für das chemische Potential dieser Modellelektrolytlösung erzeugt. Diese Daten können zur Bewertung von physikalisch basierten Zustandsgleichungen sowie zur Anpassung solcher Gleichungen an die Simulationsdaten verwendet werden.

Summary

In this work, a new perturbation approach for electrolyte solutions is developed. When applying perturbation theory to electrolyte solutions described with the nonprimitive model, the problem of diverging correlation integrals occurs due to the long-ranged behavior of the electrostatic interactions. To overcome this problem, the electrostatic pair potentials are here divided into a short- and a long-ranged part. For the short-ranged part a third order perturbation expansion is developed. The Helmholtz energy contribution arising from the long-ranged part is accounted for by an analytical term resulting from 'local molecular field' (LMF) theory. Using molecular simulation data, the basic approach of using short-ranged pair potentials and and the analytical correction is validated. The same simulation data is employed for assessing third order perturbation expansion itself and to systematically identify possibilities for further improvements of the theory.

In order to further analyze the nonprimitive model fluid consisting of dipolar and charged hard spheres, molecular simulation data for mean ionic chemical potentials of such model electrolyte solutions are produced. This data can be used for assessing physically-based equations of state and to adjust such equations of state to the simulation data.

Journal publications

This thesis led to the following publications:

- First publication, Ref. 1:
  F. Drunsel, W. Zmpitas, J. Gross, A new perturbation theory for electrolyte solutions, The Journal of Chemical Physics 141 (5) (2014) 054103

  W. Zmpitas was a discussion partner for various aspects during deriving the new perturbation expansion. He also cross-checked the expressions of the orientational averaged short ranged potentials. J. Gross had the role of a daily supervisor and was involved in editing the manuscript.

- Second publication, Ref. 2:
  F. Drunsel, J. Gross, Theory of model electrolyte solutions: Assessing the short- and longranged contributions by molecular simulations, Fluid Phase Equilibria 430 (2016) 195

  J. Gross had the role of a daily supervisor and was involved in editing the manuscript.

- Third publication, Ref. 3:
  F. Drunsel, J. Gross, Chemical potential of model electrolyte solutions consisting of hard sphere ions and hard dipoles from molecular simulations, Fluid Phase Equilibria 429 (2016) 205

  J. Gross had the role of a daily supervisor and was involved in editing the manuscript.

Major parts of chapters 2, 3 and 4 are literal quotes taken from those publications. At the beginning of each chapter, it is clarified which section of the chapter is taken from which publication. Whenever parts of the original publication are omitted, this is marked with '[...]'. For obtaining a well readable document, some passages were added to the originally published text. Whenever this is done, the text that was added is written within curly brackets ('{text that was added}').
Furthermore, for obtaining a consistent document, cross references of sections and equations have been changed compared to the originally published text passages.

1 Introduction

1.1 Basics of thermodynamic perturbation theory

Statistical Thermodynamics provides the link between molecular interactions and macroscopic properties of pure substances and mixtures. This link is given by partition functions that connect thermodynamic potentials with the energy resulting from molecular interactions. In this work, the key quantity is Helmholtz energy A, given as (see, e.g. Refs. 4 and 5)

$$A = -\frac{1}{\beta} \ln \left[\frac{1}{N!\ \Lambda^{3N}} \int \exp\left(-\beta U(\widetilde{\mathbf{r}}^N)\right) \mathrm{d}\widetilde{\mathbf{r}}^N \right] \tag{1.1}$$

where the corresponding partition function is contained in the brackets, as the argument of the logarithm[4,5]. Further, $\beta = 1/kT$ with k being the Boltzmann constant and T as temperature, N is the particle number, Λ the de Broglie wavelength and $U(\widetilde{\mathbf{r}})$ the total energy arising from the molecular interactions. The short notation $\widetilde{\mathbf{r}}$ comprises the positions of the molecules as well as their orientation, and $\int ... \mathrm{d}\widetilde{\mathbf{r}}^N$ is a shorthand notation for the N-dimensional integral over all possible molecular positions and orientations.

For determining the energy $U(\widetilde{\mathbf{r}}^N)$ of a microstate it is in many cases sufficient to only consider pair interactions between the particles, i.e. to neglect multi body interactions[5]. Specifically, the energy $U(\widetilde{\mathbf{r}}^N)$ of a system of fixed (partial) charges can exactly be expressed as the sum of pairwise interactions. Similarly, a system of hard particles is exactly described through only pairwise interactions. Then, the total energy is given by

$$U(\widetilde{\mathbf{r}}^N) = \sum_{i=1}^{N} \sum_{j>i}^{N} u_{ij}(ij) \tag{1.2}$$

where $u_{ij}(ij)$ is a shorthand notation for $u_{ij}(\widetilde{\mathbf{r}}_i, \widetilde{\mathbf{r}}_j)$ and represents the pair potential between two particles i and j.

When formulating a perturbation expansion according to Zwanzig[6], the intermolecular pair potential is divided into a reference part $u_{ij}^{\mathrm{ref}}(ij)$ and a perturbation part $w_{ij}(ij)$. Both parts need to be additive, thus the sum of reference and perturbation part recovers $u_{ij}(ij)$, representing the pair potential of interest. In addition, a coupling parameter λ that ranges between 0 and 1 is introduced according to

$$u_{\lambda,ij}(ij) = u_{ij}^{\mathrm{ref}}(ij) + \lambda \cdot w_{ij}(ij). \tag{1.3}$$

For $\lambda = 0$ the intermolecular pair potential is solely the reference potential, whilst for $\lambda = 1$ the pair potential of interest is approached. With this definition, the total energy

U, and consequently also Helmholtz energy A is a function of λ. Thus, the Helmholtz energy of the system of interest, $A(\lambda = 1)$, can be described by a Taylor expansion in terms of λ as

$$A(\lambda = 1) = \sum_{n=0}^{\infty} \frac{1}{n!} \left(\frac{\partial^n A}{\partial \lambda^n} \right)_{\lambda=0} \tag{1.4}$$

In practice, of course, such an expansion can only be formed to a limited order of n, and thus the expansion can in practice not be exact. The required order of the expansion for sufficiently converged results depends on the system of interest and on the reference potential that is employed[4]. For example, for describing simple soft core potentials such as Lennard-Jones-Potential, two prominent perturbation approaches that use different reference potentials (and, accordingly, different perturbation potentials) exist. For describing the Lennard-Jones-Fluid, the theory of Barker and Henderson[7,8] requires a second order expansion to reach acceptable accuracy, whilst for the theory of Weeks, Chandler and Anderson[9–11] a first order expansion is sufficient. A systematic analysis of both expansions to higher order was recently given by van Westen and Gross[12]. Another requirement for the Taylor expansion is a differentiable function, which limits the expansion to conditions, where the reference fluid does not undergo a phase transition (for example to a solid phase).

From the above equations, the perturbation term of first order can for a homogeneous system be derived as (for details, see Appendix B or Refs. 4 and 5)

$$A = A(\lambda = 0) + \left(\frac{\partial A}{\partial \lambda} \right)_{\lambda=0} = A^{\mathrm{ref}} + \frac{\rho^2}{2} \int w_{12}(12)\; g^{\mathrm{ref}}(12) \mathrm{d}\tilde{\mathbf{r}}_1 \mathrm{d}\tilde{\mathbf{r}}_2 \tag{1.5}$$

with $\rho = {}^{N}/_{V}$ as particle density and $g^{\mathrm{ref}}(12)$ as two-particle correlation function of the reference system. The integral in Eq. (1.5), and accordingly similar integrals occurring in the higher order terms, are referred to as correlation integrals. Often, for engineering models, analytic expressions (ansatz functions) are parametrized for such correlation integrals, and thus Helmholtz energy is given as explicit function of Temperature T, Volume V and particle number N.

As can be seen from Eq. (1.5), precise knowledge of the reference system is required for obtaining a viable theory: $A^{\mathrm{ref}}(T, \rho)$ needs to be described, the two-particle correlation function $g^{\mathrm{ref}}(12)$ is required, and for the higher order terms also higher correlation functions need to be known with sufficient accuracy.

Hard sphere (HS) model is one of the most widely used models to describe the behavior of fluids and also one of most studied ones[13]. It is also a common choice for the reference system. The advantage of this reference fluid is its simplicity. The only molecular interaction that is considered is infinite repulsion, leading to a trivial tem-

perature dependence. The dimensionless Helmholtz energy $\beta A/N$ is independent of temperature. Many equations of state exist for HS fluids, the most prominent one being the equation of Carnahan and Starling[14]. An extensive overview of over 80 equations of state for the hard sphere fluid is given in Ref. 15, and a comprehensive discussion of the thermodynamic properties and the multi-particle correlation functions has been published in Ref. 13. Besides being a well studied system, HS system yields the major advantage that the two-particle correlation function $g^{\mathrm{hs}}(12)$ as well as the multi-particle correlation functions only depend on density and are independent of temperature. Thus, the correlation integrals are also a function of density only (given of course that $w_{12}(12)$ is also independent from temperature), so that analytic expressions (ansatz functions) of those integrals can be parametrized as simple functions of density.

1.2 Statistical thermodynamic approaches for electrolyte solutions

Some reviews on equations of state for electrolyte solutions that include equations based on statistical thermodynamics have appeared[16–18]. Here, the most important approaches and the available molecular models are discussed.

In statistical thermodynamic approaches, there are two different classes of models that have been employed for modeling electrolyte solutions. In the first one, referred to as 'primitive model', the multipolar solvent is modeled as continuum and is characterized by its static dielectric constant ε. Only the ions are modeled explicitly as point charges, either with or without a repulsive core. Thus, only the interactions between the ions have to be considered explicitly, resulting in only three types of interactions that occur in that model (cation-cation, anion-anion, cation-anion). According to Coulomb's law, the intermolecular potential of the point charges scales linearly with ε^{-1}. The static dielectric constant needs to be known quite precisely for obtaining accurate results from primitive model approaches[19–24]. The main advantage of this model is its simplicity. The disadvantage is in the requirement for providing the dielectric constant, which itself is a state function dependent on temperature, pressure and composition.

The second molecular model employed for electrolyte solutions is called 'nonprimitive model'. Nonprimitive model electrolyte solutions consist of explicitly modeled ions surrounded by an also explicitly modeled solvent of multipolar (in many cases dipolar) solvent species. For that model, all electrostatic interaction sites are superimposed with a repulsive core. Since all intermolecular interactions are considered explicitly, at

least five types of interactions occur (cation-cation, anion-anion, cation-anion, cation-multipole, anion-multipole, multipole-multipole). That leads to a higher complexity, but also to a more physically based model compared to primitive model. Because the solvent is modeled explicitly, nonprimitive models have the advantage that there is no need to have precise knowledge of ε.

Besides distinguishing different molecular models for electrolyte solutions, one can also distinguish two different statistical mechanical approaches that can be employed for describing the thermophysical properties of those models. In addition to perturbation theory (PT) as introduced in section 1.1, integral equation theories can be employed. Those theories are based on the Ornstein-Zernike equation[4,25]

$$h(r_{12}) = c(r_{12}) + \rho \int c(r_{13})h(r_{23})\mathrm{d}\mathbf{r}_3 \tag{1.6}$$

with which the pair correlation function $g(r_{12})$ is determined. Once $g(r_{12})$ is known, other thermodynamic quantities can be derived. In Eq. (1.6), $h(r_{12})$ is defined as $g(r_{12}) - 1$, further $c(r_{ij})$ is the direct correlation function of particles i and j and r_{ij} is the distance between them. For fluids with orientation-dependent interactions, the generalized coordinates $\widetilde{\mathbf{r}}_i$ and $\widetilde{\mathbf{r}}_{ij}$ can be introduced in Eq. (1.6) including the orientational coordinates, and for mixtures, a sum over all types of species for particle 3 is introduced[5]. Integral equations require a ‚closure', which is an ansatz function for the short-ranged direct correlation function $c(r_{ij})$. The difficulty of integral equations is that suitable closures of a fluid are a priori not known and defining them requires a good deal of empirical knowledge and serendipity.
For electrolyte solutions, the probably most prominent closure relation for solving the Ornstein-Zernike equation are hypernetted chain (HNC) and mean spherical approximation (MSA). HNC is known to be accurate[26], but its main disadvantage is that it requires solving a set of highly nonlinear equations which makes it computationally demanding[4]. Further it is known to show non-physical behavior for low densities, as analyzed by Høye et al.[27]. MSA is less accurate, but it allows deriving equations that are explicit in terms of thermodynamic quantities[4,28,29]. Thus, MSA is much more commonly used than HNC.

Primitive model theories

The most prominent approach employing the primitive molecular model is Debye-Hückel[30] (DH) theory. In DH theory, the ionic charges are not superimposed by a repulsive core, and thus it is quite imprecise at high ion concentrations. Nonetheless,

the original equation as well as extended versions are still in use today. The theory is especially valuable for describing the behavior of electrolyte solutions at infinite dilution. In that limit, DH theory is exact. In fact, the behavior of the mean ionic activity $\gamma_{\pm}$ at infinite dilution is only possible to explain due to DH theory[18].

For primitive model electrolyte solutions, an MSA approximation was given by Waisman and Lebowitz[31,32] for equal size ions and by Blum and Høye[28,29] for ions with arbitrary diameters. Comparison of MSA with DH theory showed that the results of both approaches are basically of equivalent quality and that the results are dominated by the dielectric constant ε[24,33]. Comparison of primitive model MSA with data from Monte Carlo (MC) simulations reveal that the internal energy is not estimated satisfyingly by the theory[34–36].

In several studies, primitive model MSA has been applied to real electrolyte solutions[37–40]. In those studies, the ion diameter was treated as parameter that was adjusted to experimental data. It was shown that the approach then matches experimental osmotic and activity coefficients astonishingly well.

Perturbation theories have also been applied to the primitive molecular model of electrolyte solutions. A perturbation approach was presented by Stell and Lebowitz[41]. In the work of Larsen et al.[42], MSA and the theory of Stell and Lebowitz were compared to data obtained from MC simulations for 1:1 and 2:2 electrolyte solutions. For that comparison, model electrolyte solutions with well defined dielectric constants and equal hard sphere diameters of cations and anions were used. It was shown that both approaches give nearly identical results for both, 1:1 and 2:2 electrolyte solutions and that those results are in good agreement with the MC data for the 1:1 electrolyte solution. In a later work, Chan[43] applied the theory of Stell and Lebowitz to real electrolyte systems. In that work, the ion diameters were adjusted to experimental data of activity coefficients. Although the experimental data could be reproduced rather accurately, ion diameters that differ significantly from Pauling diameters had to be used.

Nonprimitive model theories

A nonprimitive MSA approach was derived by Blum[44] and Adelman and Deutch[45] for equal size particles and by Wei and Blum[46,47] for particles with arbitrary size. Nonprimitive MSA was compared to MC simulation data in several works[34–36,48]. The studies reveal that internal energy as well Helmholtz energy predicted by nonprimitive MSA are only in moderate agreement to the simulation data. One reason for that is that the ion-dipole contribution to internal energy estimated by MSA is of poor accuracy since the orientation of the dipolar solvent around the ions is not captured by the

theory[34].

Nonprimitive MSA has been applied to real electrolyte solutions by Li et al.[34], Seyfkar et al.[49] and Herzog et al.[50]. In those studies, the ion diameters have been treated as parameters that were adjusted to experimental data. The mean ionic activity coefficients as well as the osmotic coefficients of real electrolyte systems could be described as a function of ion concentration for a variety of electrolyte solutions with fair accuracy.

The main challenge with a perturbation approach for nonprimitive model electrolyte solutions is that some of the correlation integrals of the theory diverge due to the long-range nature of the ionic interactions. The first perturbation approach for nonprimitive model electrolyte solutions has been presented by Henderson, Blum and Tani[51] (HBT theory). They overcame the problem of diverging terms by approximating a finite value for the sum of terms of third order theory that contain diverging correlation integrals. As result, they obtained an explicit expression for Helmholtz energy as a power series in terms of $\beta^{1/2}$.

Subsequent studies, however, showed that their theory does not give satisfactory results. The most obvious deficiency is that the Padé approximation suggested by Henderson et al. has singularities for some ion concentrations[1,52].

Wu et al.[53] and Liu et al.[35,36] compared the results of HBT theory to data for internal energy obtained from MC simulations. The predictions of the theory show mayor deviations from the simulation results. Furthermore, it is shown that primitive as well as nonprimitive model MSA is more accurate than the HBT approach[35,36]. Chan[54] employed HBT theory for calculating activity coefficients of real electrolyte solutions. The author concludes that the theory does not satisfactorily predict the experimental data.

All of the above mentioned studies conclude that HBT theory suffers from significant inaccuracies. Therefore, a detailed analysis of that theory has been carried out as part of this work. Besides some minor errors that are easy to correct, an inaccurate approximation that is crucial for resummation of the diverging integrals has been found. A detailed discussion of our analysis is given in Appendix A.

Besides HBT theory, some other perturbation approaches for nonprimitive model electrolytes have been proposed. As one part of an extensive study of the charged and dipolar hard sphere mixture[55–58], Eggebrecht and Ozler developed a perturbation theory[58] that is very similar to the one of Henderson et al. They employed MC simulation data for evaluating prefactors of some of the terms of their theory, i.e. they changed the factors by adjusting them to MC simulation results. Furthermore, they employed an expression for static dielectric constant depending on the dipolar strength and used

a Padé approximation different from the one suggested by Henderson et al. As part of their study, they compared the results of their modified HBT theory to MC data of internal energy, Helmholtz energy and compressibility and showed that their theory is quite accurate[58].

An entirely different approach for overcoming the problem of diverging correlation integrals was presented by Wu et al.[53]. Instead of using the resummation technique as suggested by Henderson et al. and Eggebrecht and Ozler, they considered a mixture of charged and neutral hard spheres as reference system. This way, no diverging terms occur since the long-ranged ionic interactions are captured in the reference part. For describing the reference system, they employed the MSA approach of Blum and Høye. By comparison with MC simulation data of internal energy, they showed that their theory is much more accurate than HBT theory.

Quite similar hybrid theories consisting of MSA and a perturbation expansion have been proposed by Cong et al.[59] and Liu et al.[35,36]. In their theories, they replaced the ion-ion-interaction term of HBT theory with a term obtained from the primitive model MSA approach of Blum and Høye. However, Liu et al. showed that this kind of theory gives less accurate results than nonprimitive model MSA[35,36].

As part of their study, Liu et al.[35,36] conducted a comparison of MSA and perturbation approaches for polar fluids and ion-dipole mixtures. The results show that perturbation theories are more accurate than MSA for polar systems. The only system of their study for which perturbation theory gave less accurate results than MSA is the mixture of charged and dipolar hard spheres for which they employed HBT theory. Because some errors have been made when deriving HBT theory, the work of Liu et al. gives rise to the hope that a properly formulated perturbation expansion for electrolyte solutions can outperform integral equation theories, such as MSA.

1.3 Chemical potential of electrolyte solutions from molecular simulations

Two different pathways for determining macroscopic properties from intermolecular pair potentials exist: (i) fluid theories, i.e. integral theories or perturbation theories as discussed in Sec. 1.1 and 1.2 and (ii) molecular simulations.

In general, molecular simulations yield the advantage of giving exact results within their statistical uncertainty. On the other hand side, they are computationally demanding and therefore time-consuming. Thus, molecular simulation is not a suitable tool for practical engineering applications, such as process simulation and optimization.

Fluid theories, in contrast, can be cast into a set of algebraic equations that can be solved quickly and with low computational cost. To reach that goal, simplifications and approximations need to be applied. Thus, fluid theories can only provide approximate descriptions of a chosen molecular model.

It is obvious that molecular simulation provides a powerful tool for developing, assessing and refining fluid theories. Simulations yield one decisive advantage over data of real systems: they provide exact data of the chosen molecular model. Thus, the accuracy of the fluid theory can be judged entirely independent from the quality of the molecular model itself.

For the model electrolyte solution used in this work, i.e. the ion-dipole HS mixture as described in Sec. 2.1, existing studies that compare theories with MC data are limited to internal energy, Helmholtz energy and compressibility. The reason is that only this simulation data is available in literature. Chemical potential data has not been reported yet, although this data is particularly important, being the key quantity for phase equilibrium calculation. Therefore, mean ionic chemical potential data for the ion-dipole HS mixture has been determined in MC simulations as part of this work.

For primitive model electrolytes, plenty of simulation studies have been published so far[26,60–74]. For this model, standard Widom test particle method[75] can be used for determining the chemical potential of the ions, noting only that ion pairs have to be sampled simultaneously. This simple and efficient method fails for electrolytes for which the the solvent is modeled explicitly. For nonprimitive models, special sampling techniques are required, and only few studies on chemical potentials exist. In the following, an overview of the different techniques employed in those studies is given. A similar overview has been presented by Nezbeda et al.[76] and also in our third publication, Ref. 3.

Chemical potential calculations using thermodynamic integration have been carried out by Ferrario et al.[77], Sanz and Vega[78], Aragones et al.[79] as well as Benavides et al.[80]. All those authors employ Kirkwood thermodynamic integration schemes[81], i.e. methods similar to what is referred to as 'λ-integration method' in Sec. 3.2 of this work for determining chemical potentials of real electrolyte solutions. The advantage of such methods is that they are easy to implement and they are well established techniques. The main disadvantage is that a number of independent simulations are required for obtaining one data point. Thus, they are demanding with respect to computation time. More efficient methods with which chemical potential can be computed in one single simulation have been used by Lísal et al.[82], Moučka, Smith and coworkers[83–88], Panagiotopoulos and coworkers[89–91] and Paluch et al.[92,93].

In the works of Lísal et al. and Moučka, Smith and coworkers, chemical potential has

been determined by Osmotic Ensemble simulations[82,83]. In this ensemble, chemical potential of the ions is in fact determined indirectly since it is an input to the simulation. During the simulations, the particle number of the solvent is kept constant, whilst the number of ions fluctuates. Thus, the composition of liquid is determined for a given chemical potential of the ions. Whilst Lísal et al. employed a molecular dynamics algorithm, Moučka, Smith and coworkers used MC simulations.
Panagiotopoulos and coworkers determined the chemical potential of the ions via Bennett Acceptance Ratio Method[94] in molecular dynamics simulations.
The method that has been employed by Paluch et al. and also in this work is expanded ensemble transition matrix method[95,96] with a biasing function determined by Wang-Landau method[97].
It is worth mentioning that all of the above studies used soft core potentials and molecular force fields that aim for representing real electrolyte solutions. Thus, for this work, their results play a subordinate role.

2 New perturbation theory for non-primitive model electrolyte solutions

Parts of this chapter are literal quotes from the first two publications, Ref. 1 and Ref. 2. In both of those works, the newly developed perturbation theory is described. To obtain a well readable document, parts from both publications are quoted to this chapter.
The origin of the sections is as follows:

- *Section 2.1 has not been published previously.*
- *Major parts of section 2.2 are a literal quote from the first publication, Ref. 1, where the section was published as 'II. Thermodynamic perturbation theory of nonprimitive model electrolyte solutions'.*
- *Section 2.3 is a literal quote from the second publication, Ref. 2, where the section was published as '2. Short- and long–ranged electrostatic interactions from LMF theory'.*
- *Major parts of section 2.4 are a literal quote from the second publication, Ref. 2, where the section was published as '3.1. Third order perturbation theory' and '3.2 Further development of the theory'.*
- *Major parts of section 2.5 are a literal quote from the first publication, Ref. 1, where the section was published as 'C. Application of 3rd order perturbation theory to the decomposed potential'.*
- *Section 2.6 has not been published previously. A graphical representation of the data of the static dielectric constant ε from molecular simulations given in this section, however, has been published in the first publication, Ref. 1.*
- *Sections 2.7.1 and 2.7.2 are literal quotes from the second publication, Ref. 2. Section 2.7.1 was published in Ref. 2 as 'Appendix A. Correlation integrals from*

molecular simulations', subsection 2.7.2 as '3.3. Assessing Kirkwood superposition approximation'.

2.1 Molecular model

In this entire work, electrolyte solutions are modeled as a mixture of charged and dipolar hard spheres.

The basic intermolecular pair potentials that occur in our model mixture can be described as a superposition of the hard sphere potential $u^{\mathrm{hs}}(12)$ and an electrostatic potential $u^{\mathrm{es}}(12)$, i.e. $u(12) = u^{\mathrm{hs}}(12) + u^{\mathrm{es}}(12)$. Here, the short notation '(12)' comprises the intermolecular distance $\mathbf{r}_{12}$ as well as the orientation $\boldsymbol{\omega}_1$ and $\boldsymbol{\omega}_2$ of the particles.

The hard sphere contribution to the potential is defined as

$$u^{\mathrm{hs}}(12) = \begin{cases} \infty, & \text{for } r_{12} \leq \frac{1}{2}(\sigma_1 + \sigma_2) \\ 0, & \text{for } r_{12} > \frac{1}{2}(\sigma_1 + \sigma_2) \end{cases} \tag{2.1}$$

where σ_i denotes the hard sphere diameter of a particle and r_{12} is the scalar distance between the particles, $r_{12} = |\mathbf{r}_{12}|$.

The electrostatic pair potentials that are relevant for a mixture containing point charges (index 'c') and point dipoles (index 'd') are the charge-charge-potential $u_{cc}(12)$, the charge-dipole-potential $u_{cd}(12)$ and the dipole-dipole-potential $u_{dd}(12)$. Those are

$$u_{cc}(12) = \frac{q_1 q_2}{r_{12}} \tag{2.2}$$

$$u_{cd}(12) = \frac{q_1 \mu_2}{r_{12}^2} \left(\hat{\boldsymbol{\mu}}_2 \cdot \hat{\mathbf{r}}_{12}\right) \tag{2.3}$$

$$u_{dd}(12) = -\frac{\mu_1 \mu_2}{r_{12}^3} \left[3 \left(\hat{\boldsymbol{\mu}}_1 \cdot \hat{\mathbf{r}}_{12}\right) \left(\hat{\boldsymbol{\mu}}_2 \cdot \hat{\mathbf{r}}_{12}\right) - \left(\hat{\boldsymbol{\mu}}_1 \cdot \hat{\boldsymbol{\mu}}_2\right)\right] \tag{2.4}$$

where q_i is the charge of the ions, μ_i is the dipole moment of the solvent (both in CGS units), $\hat{\boldsymbol{\mu}}_i$ is the unit direction vector of a dipole and $\hat{\mathbf{r}}_{ij}$ is the unit direction vector between the particles.

For obtaining a compact theory, some simplifying definitions are made. The first one is that all components, cations, anions and the dipolar component have identical hard sphere diameters σ. The second one is that only monovalent ions are regarded, and $q = q_+ = -q_-$ where the indice '+' and '−' denote cations and anions, respectively. This leads to the simplification that the ionic species can be comprised as charged species without further distinguishing between cations and anions. Due to electroneutrality, the mole fraction of cations, x_+, and the mole fraction of anions, x_-, are the same. Thus, the composition of the mixture can be described by one ion mole fraction $x = x_+ + x_-$. The mole fraction of the solvent is then $(1 - x)$.

With the above simplifications, the complexity of the perturbation theory presented in the upcoming sections reduces significantly because these definitions allow regarding the model solution as a quasi–binary mixture of hard sphere ions and dipoles.
In addition to the simplifications discussed above, it is useful to regard the model parameters as dimensionless quantities. The dimensionless squared charge of an ion is defined as

$$q^{*\,2} = \frac{\beta q^2}{\sigma}, \tag{2.5}$$

the dimensionless squared dipole moment is

$$\mu^{*\,2} = \frac{\beta \mu^2}{\sigma^3} \tag{2.6}$$

and the dimensionless intermolecular distance is defined as

$$r_{12}^* = r_{12}/\sigma. \tag{2.7}$$

With those definitions, the pair potentials can be rewritten in terms of dimensionless quantities as

$$\beta u^{\mathrm{hs}}(12) = \begin{cases} \infty, & \text{for } r_{12}^* \leq 1 \\ 0, & \text{for } r_{12}^* > 1 \end{cases} \tag{2.8}$$

and

$$\beta u_{cc}(12) = \frac{q_1^* q_2^*}{r_{12}^*} \tag{2.9}$$

$$\beta u_{cd}(12) = \frac{q_1^* \mu_2^*}{r_{12}^{*\,2}} \left(\hat{\boldsymbol{\mu}}_2 \cdot \hat{\mathbf{r}}_{12}\right) \tag{2.10}$$

$$\beta u_{dd}(12) = -\frac{\mu_1^* \mu_2^*}{r_{12}^{*\,3}} \left[3 \left(\hat{\boldsymbol{\mu}}_1 \cdot \hat{\mathbf{r}}_{12}\right) \left(\hat{\boldsymbol{\mu}}_2 \cdot \hat{\mathbf{r}}_{12}\right) - \left(\hat{\boldsymbol{\mu}}_1 \cdot \hat{\boldsymbol{\mu}}_2\right)\right]. \tag{2.11}$$

Introducing dimensionless quantities yields not only the advantage of a more compact notation. By using q^* and μ^*, the dependance on temperature is comprised in those quantities. When additionally introducing the dimensionless particle number density

$$\rho^* = \rho \sigma^3 \tag{2.12}$$

where $\rho = N/V$ with N as number of particles and V as system volume, a thermodynamic equilibrium state is fully defined by q^*, μ^*, ρ^* and x.

2.2 General perturbation approach for the charged and dipolar hard sphere mixture

According to perturbation theory, as introduced by Zwanzig[6], the intermolecular pair potential $u(12)$ is divided into a reference part $u^{\mathrm{ref}}(12)$ and a perturbation part $w(12)$ according to

$$u_\lambda(12) = u^{\mathrm{ref}}(12) + \lambda \cdot w(12) \tag{2.13}$$

where the coupling parameter λ ranges from 0 to 1. [...] The full Hamiltonian is obtained from Eq. (2.13) for $u_{\lambda=1}(12)$, i.e., for the coupling parameter $\lambda = 1$. The reference system can, for example, be a Lennard-Jones fluid or a hard sphere fluid. For the remainder of this study we consider the hard-sphere fluid (index 'hs') as the reference. The perturbation part represents in our case the electrostatic potential [...]. With the definition of $u_\lambda(12)$, the Helmholtz energy is given by

$$A_\lambda = -\frac{1}{\beta} \ln Q_\lambda \tag{2.14}$$

with the partition function

$$Q_\lambda = \frac{1}{N!\,\Lambda^{3N}} \int \exp\left(-\beta U(\widetilde{\mathbf{r}}^N, \lambda)\right) \mathrm{d}\widetilde{\mathbf{r}}^N \tag{2.15}$$

where for brevity we use $\widetilde{\mathbf{r}}$ for the space coordinate $\mathbf{r}$ as well as the orientational vector $\boldsymbol{\omega}$. The configurational energy of the system is $U(\widetilde{\mathbf{r}}^N, \lambda) = \sum_i^N \sum_{j>i}^N u_{\lambda,ij}(ij)$. The total Helmholtz energy of the system can then be written as a Taylor expansion around $\lambda = 0$, as

$$\begin{aligned} A =& A^{\mathrm{ref}} + \left(\frac{\partial A}{\partial \lambda}\right)_{\lambda=0} \lambda + \frac{1}{2}\left(\frac{\partial^2 A}{\partial \lambda^2}\right)_{\lambda=0} \lambda^2 \\ &+ \frac{1}{6}\left(\frac{\partial^3 A}{\partial \lambda^3}\right)_{\lambda=0} \lambda^3 + \mathcal{O}(\lambda^4) \end{aligned} \tag{2.16}$$

evaluated at $\lambda = 1$.

The partial derivatives in Eq. (2.16) are obtained using Eq. (2.14) and (2.15). The derivation of the theory up to 3rd order is lengthy and is provided [...] {in appendix B}. Here we only state the final result for a nonprimitive model electrolyte solution as a ternary mixture of cations, anions and dipolar solvent. The dimensionless residual

Helmholtz energy $a^{\mathrm{res}} = \beta(A - A^{\mathrm{hs}})/N$ is approximately (to third order), given as

$$\begin{aligned} a^{\mathrm{res}} = &- \frac{1}{4}\rho\beta^2 \sum_{\alpha=1}^{3}\sum_{\gamma=1}^{3} x_\alpha x_\gamma \int g^{\mathrm{hs}}_{\alpha\gamma}(12) \left\langle w^2_{\alpha\gamma}(12)\right\rangle \mathrm{d}\mathbf{r}_{12} \\ &+ \frac{1}{6}\rho^2\beta^3 \sum_{\alpha=1}^{3}\sum_{\gamma=1}^{3}\sum_{\tau=1}^{3} x_\alpha x_\gamma x_\tau \\ &\times \int g^{\mathrm{hs}}_{\alpha\gamma\tau}(123) \left\langle w_{\alpha\gamma}(12) w_{\alpha\tau}(13) w_{\gamma\tau}(23)\right\rangle \mathrm{d}\mathbf{r}_{12}\mathrm{d}\mathbf{r}_{13} \end{aligned} \tag{2.17}$$

with ρ as the number density, x_α denotes the molar fraction of component α and $g^{\mathrm{hs}}_{\alpha\gamma}(12)$ and $g^{\mathrm{hs}}_{\alpha\gamma\tau}(123)$ are the pair- and the three-particle correlation functions of the hard sphere fluid, respectively. The angular brackets indicate that the squared pair and the three-particle potentials are averaged over the orientations of the dipolar solvent. Other terms that would appear are zero for the model we use due to electroneutrality and the fact that the orientational averaged dipole-dipole-potential is zero.

When applying the coulomb $1/r_{12}$ and the dipolar $1/r^3_{12}$ potential to Eq. (2.17), the correlation integrals containing two or more ionic particles in both, 2nd and 3rd order term, diverge. The rest of the terms converge and could be directly solved. The main challenge when developing a PT for electrolyte solutions is to deal with the diverging integrals.

{For obtaining converging correlation integrals the electrostatic potentials are decomposed into a short-ranged pair potential and a long-ranged part. The division is similar to what is known as the Ewald summation in molecular simulations. For the short-ranged part of the electrostatic interactions we propose a perturbation theory. That is possible, because for a short-ranged potential the perturbation theory does not suffer from diverging correlation integrals. The Helmholtz energy due to the long-ranged part of the potential is described through the local molecular field (LMF) theory[98], which for electrostatic interactions delivers an appropriate analytic expression. In the next section, the key features of LMF theory are presented. Additionally, it is made clear why this approach is particularly suitable for applying it together with a perturbation theory of the charged and dipolar hard sphere mixture.}

2.3 Short- and long-ranged electrostatic interactions from LMF theory

LMF theory provides a general framework for capturing long-ranged parts of intermolecular pair potentials in a mean field manner. When applying LMF theory to any

molecular system (homogeneous as well as inhomogeneous systems), the intermolecular pair potential u_{ij} is split into a short-ranged part u_{ij}^{sr} and a long-ranged part u_{ij}^{lr},

$$u_{ij} = u_{ij}^{\mathrm{sr}} + u_{ij}^{\mathrm{lr}}. \tag{2.18}$$

Both parts, u_{ij}^{sr} as well as u_{ij}^{lr} have to fulfill well defined prerequisites. Those are

$$F_{ij}^{\mathrm{sr}} = -\frac{\partial u_{ij}^{\mathrm{sr}}}{\partial r_{ij}} \approx 0 \quad \text{for large } r_{ij} \tag{2.19}$$

$$F_{ij}^{\mathrm{lr}} = -\frac{\partial u_{ij}^{\mathrm{lr}}}{\partial r_{ij}} \approx 0 \quad \text{for small } r_{ij} \tag{2.20}$$

and thus, that the force F_{ij}^{sr} arising from the short-ranged potential determines the (short-ranged) fluid structure without any impact of the long-ranged force F_{ij}^{lr}. When applying LMF theory to electrostatic systems, the split of the charge-charge pair potential $u_{cc,ij}$ according to

$$\beta u_{cc,ij} = \frac{q_i^* q_j^*}{r_{ij}^*} = \beta u_{cc,ij}^{\mathrm{sr}} + \beta u_{cc,ij}^{\mathrm{lr}} \tag{2.21}$$

with

$$\beta u_{cc,ij}^{\mathrm{sr}} = \frac{q_i^* q_j^*}{r_{ij}^*} \cdot \operatorname{erfc}\left(\frac{r_{ij}^*}{\alpha^*}\right) \tag{2.22}$$

$$\beta u_{cc,ij}^{\mathrm{lr}} = \frac{q_i^* q_j^*}{r_{ij}^*} \cdot \operatorname{erf}\left(\frac{r_{ij}^*}{\alpha^*}\right) \tag{2.23}$$

fulfills the above conditions, given that the damping parameter α^* is within a carefully chosen range. [...] In the limit of $\alpha^* \to 0$, the complementary error function $\operatorname{erfc}\left(r_{ij}^*/\alpha^*\right)$ is zero, and $\beta u_{cc,ij} = \beta u_{cc,ij}^{\mathrm{lr}}$. For $\alpha^* \to \infty$, $\operatorname{erfc}\left(r_{ij}^*/\alpha^*\right)$ is one, and $\beta u_{cc,ij} = \beta u_{cc,ij}^{\mathrm{sr}}$. For any α^* between those limits, the short- and the long-ranged part of the potential contribute to the total pair potential, and the short-ranged contribution increases with increasing α^*. When also charge-dipole and dipole-dipole interactions are taken into account, as is the case in the perturbation theory presented in Sec. 2.2, the short-ranged charge-dipole and dipole-dipole interactions, $u_{cd,ij}^{\mathrm{sr}}$ and $u_{dd,ij}^{\mathrm{sr}}$, can be obtained from Eq. (2.22). Those are (see also Ref. 1)

$$\beta u_{cd,ij}^{\mathrm{sr}} = \frac{q_i^* \mu_j^*}{r_{ij}^{*\,2}} K_{ij}\left(\hat{\boldsymbol{\mu}}_j \cdot \hat{\mathbf{r}}_{ij}\right) \tag{2.24}$$

$$\beta u_{dd,ij}^{\mathrm{sr}} = -\frac{\mu_i^* \mu_j^*}{r_{ij}^{*\,3}}\left[M_{ij}\left(\hat{\boldsymbol{\mu}}_i \cdot \hat{\mathbf{r}}_{ij}\right)\left(\hat{\boldsymbol{\mu}}_j \cdot \hat{\mathbf{r}}_{ij}\right) - K_{ij}\left(\hat{\boldsymbol{\mu}}_i \cdot \hat{\boldsymbol{\mu}}_j\right)\right] \tag{2.25}$$

with

$$K_{ij} = \operatorname{erfc}\left(\frac{r_{ij}^*}{\alpha^*}\right) + \frac{2}{\sqrt{\pi}}\,\frac{r_{ij}^*}{\alpha^*}\exp\left(-r_{ij}^{*\,2}/\alpha^{*\,2}\right) \tag{2.26}$$

$$M_{ij} = 3\,\operatorname{erfc}\left(\frac{r_{ij}^*}{\alpha^*}\right) + \frac{6}{\sqrt{\pi}}\frac{r_{ij}^*}{\alpha^*}\exp\left(-r_{ij}^{*\,2}/\alpha^{*\,2}\right) + \frac{4}{\sqrt{\pi}}\frac{r_{ij}^{*\,3}}{\alpha^{*\,3}}\exp\left(-r_{ij}^{*\,2}/\alpha^{*\,2}\right). \tag{2.27}$$

In Eqs. (2.24) and (2.25), $\hat{\boldsymbol{\mu}}_i$ and $\hat{\mathbf{r}}_{ij}$ denote unit vectors [...]. The applicability of the general LMF approach to homogeneous systems with electrostatic pair potentials has been shown in previous studies of Weeks and colleagues[99–102].

For homogeneous mixtures of ions and dipoles interacting with short-ranged pair potentials according to Eqs. (2.22), (2.24) and (2.25), Rodgers and Weeks[102] developed the analytical long-range contribution to internal energy

$$\beta\frac{U^{\mathrm{lr}}}{N} = -\frac{1}{\alpha^*\sqrt{\pi}}xq^{*\,2} - \frac{2}{3}\frac{1}{\alpha^{*\,3}\sqrt{\pi}}(1-x)\mu^{*\,2} + \frac{1}{2\alpha^{*\,3}\pi^{\frac{3}{2}}\rho^*}\frac{\varepsilon-1}{\varepsilon} \tag{2.28}$$

that is based on LMF theory. [...] ε is the static dielectric constant of the solution. In contrast to the primitive model, where precise knowledge of ε is crucial, Eq. (2.28) is much less sensitive to ε. For the systems studied in this work, ε is large, and the assumption of infinite dielectric constant does not significantly influence the results of Eq. (2.28). Thus, as discussed and shown in Refs. 1 and 102 {as well as Sec. 2.6}, factor $(\varepsilon-1)/\varepsilon$ can be assumed as unity here without introducing a severe error.

Damping the coulomb potential according to Eq. (2.22) to make it converge faster is well known from simulation methods such as Ewald summation[103], Wolf summation[104], the Zahn method[105] or the damped shifted force method[106]. The term to correct for this damping given by Rodgers and Weeks, Eq. (2.28), is a correction to the ensemble averaged energy. Thus, it can directly be employed as Helmholtz energy contribution. The equality $U^{\mathrm{lr}} = A^{\mathrm{lr}}$ is justified by considering the microscopic definition of Helmholtz energy,

$$A = -\frac{1}{\beta}\ln\left[\frac{1}{N!\,\Lambda^{3N}}\int\exp\left(-\beta U(\mathbf{r}^N)\right)\mathrm{d}\mathbf{r}^N\right] \tag{2.29}$$

[...] Inserting $U(\mathbf{r}^N) = U^{\mathrm{sr}}(\mathbf{r}^N) + U^{\mathrm{lr}}$ into Eq. (2.29) yields

$$\begin{aligned} A &= -\frac{1}{\beta}\ln\left[\frac{1}{N!\,\Lambda^{3N}}\int \exp\left(-\beta(U^{\mathrm{sr}}(\mathbf{r}^N)+U^{\mathrm{lr}})\right)\mathrm{d}\mathbf{r}^N\right] \\ &= \underbrace{-\frac{1}{\beta}\ln\left[\frac{1}{N!\,\Lambda^{3N}}\int \exp\left(-\beta U^{\mathrm{sr}}(\mathbf{r}^N)\right)\mathrm{d}\mathbf{r}^N\right]}_{\equiv A^{\mathrm{sr}}} + U^{\mathrm{lr}}. \end{aligned} \tag{2.30}$$

which shows that the long-ranged Helmholtz energy contribution is an intermolecular potential energy. That is in accordance with intuition, because the structure of the fluid (i.e. the pair correlation function) and thus the entropic contribution from the intermolecular potential is determined by the short-ranged part of the potential - for a properly chosen division of the potential, the long-ranged part has no entropic contribution. In dimensionless form relative to the hard sphere fluid, we get

$$\underbrace{\beta\frac{A-A^{\mathrm{hs}}}{N}}_{=a^{\mathrm{res}}} = \underbrace{\beta\frac{A^{\mathrm{sr}}-A^{\mathrm{hs}}}{N}}_{=a^{\mathrm{sr}}} + \underbrace{\beta\frac{A^{\mathrm{lr}}}{N}}_{=a^{\mathrm{lr}}} \tag{2.31}$$

where the index 'hs' indicates the hard sphere contribution, i.e. A^{hs} is the Helmholtz energy of the pure hard sphere fluid. The index 'res' denotes the residual part with respect to the hard sphere fluid in this entire manuscript. The long-range contribution a^{lr} is identical to the correction term given in Eq. (2.28).
Eq. (2.30) and (2.31) are only valid if the long-ranged contribution is not a function of the molecular positions $\mathbf{r}^N$, and thus, if the conditions given by Eq. (2.19) and (2.20) are fulfilled. To ensure this α^* has to be chosen carefully. Therefore, in Sec. 3, we present a way for determining suitable values of α^* using molecular simulations.

2.4 A perturbation expansion in combination with LMF theory

When considering nonprimitive model electrolyte solutions with high-temperature expansion as introduced [...] {in Sec. 2.2}, one faces diverging correlation integrals, and the main challenge for perturbation theories of such models is to overcome this problem.
In our perturbation approach[1], we employ the division of Helmholtz energy according to Eqs. (2.30) and (2.31). Then, the perturbation expansion can be formed in terms of the short-ranged Helmholtz energy contribution A^{sr} only, and the short-ranged potentials from Eq. (2.22), (2.24) and (2.25) are relevant in the expansion. Using this

procedure, all correlation integrals converge.
{Applying the short-ranged potentials to Eq. (2.17),} the short-range contribution for a third-order perturbation theory is, at the outset, simply $a^{\rm sr} = a_2^{\rm sr} + a_3^{\rm sr}$ (for the model system regarded here, the first order term, $a_1^{\rm sr}$, vanishes), where the second order is

$$a_2^{\rm sr} = a_{cc}^{\rm sr} + a_{cd}^{\rm sr} + a_{dd}^{\rm sr} \tag{2.32}$$

with

$$a_{cc}^{\rm sr} = -\frac{1}{4}\rho^*\beta^2 x^2 \int g^{\rm hs}(12)\left(u_{cc,12}^{\rm sr}\right)^2 \, {\rm d}\mathbf{r}_{12}^* \tag{2.33}$$

$$a_{cd}^{\rm sr} = -\frac{1}{2}\rho^*\beta^2 x(1-x) \int g^{\rm hs}(12)\left\langle\left(u_{cd,12}^{\rm sr}\right)^2\right\rangle_{\hat{\boldsymbol{\mu}}_i} {\rm d}\mathbf{r}_{12}^* \tag{2.34}$$

$$a_{dd}^{\rm sr} = -\frac{1}{4}\rho^*\beta^2 (1-x)^2 \int g^{\rm hs}(12)\left\langle\left(u_{dd,12}^{\rm sr}\right)^2\right\rangle_{\hat{\boldsymbol{\mu}}_i} {\rm d}\mathbf{r}_{12}^* \tag{2.35}$$

and for the third order terms we get

$$a_3^{\rm sr} = a_{ccc}^{\rm sr} + a_{ccd}^{\rm sr} + a_{cdd}^{\rm sr} + a_{ddd}^{\rm sr} \tag{2.36}$$

where

$$a_{ccc}^{\rm sr} = \frac{1}{6}{\rho^*}^2\beta^3 x^3 \int g^{\rm hs}(123) u_{cc,12}^{\rm sr} u_{cc,13}^{\rm sr} u_{cc,23}^{\rm sr} {\rm d}\mathbf{r}_{12}^* {\rm d}\mathbf{r}_{13}^* \tag{2.37}$$

$$a_{ccd}^{\rm sr} = \frac{1}{2}{\rho^*}^2\beta^3 x^2(1-x) \times \int g^{\rm hs}(123)\left\langle u_{cd,12}^{\rm sr} u_{cd,13}^{\rm sr} u_{cc,23}^{\rm sr}\right\rangle_{\hat{\boldsymbol{\mu}}_i} {\rm d}\mathbf{r}_{12}^* {\rm d}\mathbf{r}_{13}^* \tag{2.38}$$

$$a_{cdd}^{\rm sr} = \frac{1}{2}{\rho^*}^2\beta^3 x(1-x)^2 \times \int g^{\rm hs}(123)\left\langle u_{dd,12}^{\rm sr} u_{cd,13}^{\rm sr} u_{cd,23}^{\rm sr}\right\rangle_{\hat{\boldsymbol{\mu}}_i} {\rm d}\mathbf{r}_{12}^* {\rm d}\mathbf{r}_{13}^* \tag{2.39}$$

$$a_{ddd}^{\rm sr} = \frac{1}{6}{\rho^*}^2\beta^3 (1-x)^3 \times \int g^{\rm hs}(123)\left\langle u_{dd,12}^{\rm sr} u_{dd,13}^{\rm sr} u_{dd,23}^{\rm sr}\right\rangle_{\hat{\boldsymbol{\mu}}_i} {\rm d}\mathbf{r}_{12}^* {\rm d}\mathbf{r}_{13}^*. \tag{2.40}$$

Here, $\langle ... \rangle_{\hat{\boldsymbol{\mu}}_i}$ denotes unweighted averaging of orientations of the dipolar particles and $g^{\rm hs}(12)$ and $g^{\rm hs}(123)$ are the two- and three-particle correlation functions of the hard sphere fluid. {The orientational averaged potentials given below have also been given in the first publication, Ref. 1. For the perturbation terms of second order, those

potentials are

$$\beta^2 \left\langle \left(u^{\mathrm{sr}}_{cd,12}\right)^2 \right\rangle_{\hat{\boldsymbol{\mu}}_i} = \frac{1}{3} \frac{q_1^{*\,2} \mu_2^{*\,2}}{r_{12}^{*\,4}} K_{12}^2 \tag{2.41}$$

$$\beta^2 \left\langle \left(u^{\mathrm{sr}}_{dd,12}\right)^2 \right\rangle_{\hat{\boldsymbol{\mu}}_i} = \frac{1}{9} \frac{\mu_1^{*\,2} \mu_2^{*\,2}}{r_{12}^{*\,6}} \left(M_{12}^2 - 2M_{12}K_{12} + 3K_{12}^2\right) \tag{2.42}$$

and those of third order terms are given as

$$\beta^3 \left\langle u^{\mathrm{sr}}_{cd,12} u^{\mathrm{sr}}_{cd,13} u^{\mathrm{sr}}_{cc,23} \right\rangle_{\hat{\boldsymbol{\mu}}_i} = \frac{1}{3} \frac{\mu_1^{*\,2} q_2^{*\,2} q_3^{*\,2}}{r_{12}^{*\,2} r_{13}^{*\,2} r_{23}^{*}} K_{12} K_{13} \cos\omega_1 \ \mathrm{erfc}\left(\frac{r_{23}^*}{\alpha^*}\right) \tag{2.43}$$

$$\beta^3 \left\langle u^{\mathrm{sr}}_{dd,12} u^{\mathrm{sr}}_{cd,13} u^{\mathrm{sr}}_{cd,23} \right\rangle_{\hat{\boldsymbol{\mu}}_i} = \frac{1}{9} \frac{\mu_1^{*\,2} \mu_2^{*\,2} q_3^{*\,2}}{r_{12}^{*\,3} r_{13}^{*\,2} r_{23}^{*\,2}} K_{13} K_{23} \left(M_{12} \cos\omega_1 \cos\omega_2 - K_{12} \cos(\omega_1 + \omega_2)\right) \tag{2.44}$$

$$\begin{aligned} \beta^3 \left\langle u^{\mathrm{sr}}_{dd,12} u^{\mathrm{sr}}_{dd,13} u^{\mathrm{sr}}_{dd,23} \right\rangle_{\hat{\boldsymbol{\mu}}_i} = {} & \frac{1}{27} \frac{\mu_1^{*\,2} \mu_2^{*\,2} \mu_3^{*\,2}}{r_{12}^{*\,3} r_{13}^{*\,3} r_{23}^{*\,3}} \\ & \times \left(-M_{23}K_{12}K_{13} - M_{13}K_{12}K_{23} - M_{12}K_{13}K_{23} + 3K_{12}K_{13}K_{23}\right. \\ & + M_{12}M_{13}K_{23} \cos^2\omega_1 + M_{12}M_{23}K_{13} \cos^2\omega_2 + M_{13}M_{23}K_{12} \cos^2\omega_3 \\ & \left. + M_{12}M_{13}M_{23} \cos\omega_1 \cos\omega_2 \cos\omega_3\right) \end{aligned} \tag{2.45}$$

Here, ω_i denote the interior angles of the triangle formed by the three particles and K_{ij} and M_{ij} are given by Eq. (2.26) and (2.27). For $\alpha^* \to \infty$, $K_{ij} = 1$ and $M_{ij} = 3$. Then, the damped pair potentials approach the full (original) electrostatic potentials given by Eq. (2.9) to (2.11). For those potential functions, the orientational averaging has been performed by Rasaiah and Stell[107]. For the full electrostatic potentials, the orientational averaged potentials given above are thus identical to the ones given by those authors, except for $\beta^3 \left\langle u^{\mathrm{sr}}_{dd,12} u^{\mathrm{sr}}_{cd,13} u^{\mathrm{sr}}_{cd,23} \right\rangle_{\hat{\boldsymbol{\mu}}_i}$. For this term, Rasaiah and Stell gave a wrong prefactor of $2/9$ instead of $1/9$.}

Inserting the orientational averaged potentials [...] {given by Eq. (2.41) to (2.45) into

the general approach}, we get the final expressions for our perturbation theory

$$a_{cc}^{\mathrm{sr}} = -\pi\rho^* x^2 q^{*\,4}\; I_{cc}(\rho^*, \alpha^*) \tag{2.46}$$

$$a_{cd}^{\mathrm{sr}} = -\frac{2}{3}\pi\rho^* x(1-x) q^{*\,2}\mu^{*\,2}\; I_{cd}(\rho^*, \alpha^*) \tag{2.47}$$

$$a_{dd}^{\mathrm{sr}} = -\frac{1}{9}\pi\rho^* (1-x)^2 \mu^{*\,4}\; I_{dd}(\rho^*, \alpha^*) \tag{2.48}$$

$$a_{ccc}^{\mathrm{sr}} = \frac{4}{3}\pi^2\rho^{*\,2} x^3 q^{*\,6}\; I_{ccc}(\rho^*, \alpha^*) \tag{2.49}$$

$$a_{ccd}^{\mathrm{sr}} = \frac{4}{3}\pi^2\rho^{*\,2} x^2(1-x) q^{*\,4}\mu^{*\,2}\; I_{ccd}(\rho^*, \alpha^*) \tag{2.50}$$

$$a_{cdd}^{\mathrm{sr}} = \frac{4}{9}\pi^2\rho^{*\,2} x(1-x)^2 q^{*\,2}\mu^{*\,4}\; I_{cdd}(\rho^*, \alpha^*) \tag{2.51}$$

$$a_{ddd}^{\mathrm{sr}} = \frac{4}{81}\pi^2\rho^{*\,2}(1-x)^3 \mu^{*\,6}\; I_{ddd}(\rho^*, \alpha^*). \tag{2.52}$$

In the above equations, $I_{ij(k)}$ represent the correlation integrals that only depend on the dimensionless density ρ^* and the damping parameter α^*. Those integrals can be solved numerically, given that appropriate expressions for $g^{\mathrm{hs}}(12)$ and $g^{\mathrm{hs}}(123)$ are available. In Sec. 2.5 we describe our procedure for obtaining numerical results. Those results are given [...] {as supplementary material of the second publication, Ref. 2.}
Since the Taylor expansion of the short-ranged potentials does not converge using third order, in [...] {the first publication, Ref. 1,} we followed the suggestion of Rushbrooke, Stell, and Høye[108] in applying the Padé approximation

$$a^{\mathrm{sr}} = \frac{a_2^{\mathrm{sr}}}{1 - a_3^{\mathrm{sr}}/a_2^{\mathrm{sr}}} \tag{2.53}$$

which is used for the short-ranged Helmholtz energy contribution in Eq. (2.31). [...]
A Padé approximation is essential for bringing the results of the third order theory even to the correct order of magnitude. However, Eq. (2.53) leads to the problem that the different contributions to the Helmholtz energy are not purely additive as they are in a basic Taylor expansion. Terms with a low absolute value, like a_{dd} and a_{ddd}, are dominated by terms of high absolute value, such as a_{cc} and a_{ccc}, at high ion concentrations. To avoid this problem, we suggest rearranging the Taylor expansion as

$$\begin{aligned} a^{\mathrm{res}} =& a_{cc}^{\mathrm{sr}} + a_{ccc}^{\mathrm{sr}} \\ &+ a_{dd}^{\mathrm{sr}} + a_{ddd}^{\mathrm{sr}} \\ &+ \underbrace{a_2^{\mathrm{sr}} - a_{cc}^{\mathrm{sr}} - a_{dd}^{\mathrm{sr}}}_{=a_{cd}^{\mathrm{sr}}} + \underbrace{a_3^{\mathrm{sr}} - a_{ccc}^{\mathrm{sr}} - a_{ddd}^{\mathrm{sr}}}_{\equiv a_{3,cd}^{\mathrm{sr}}} + a^{\mathrm{lr}} \end{aligned} \tag{2.54}$$

and forming a modified Padé approximation

$$a^{\mathrm{sr}}_{\mathrm{mod}} = \frac{a^{\mathrm{sr}}_{cc}}{1 - a^{\mathrm{sr}}_{ccc}/a^{\mathrm{sr}}_{cc}} + \frac{a^{\mathrm{sr}}_{dd}}{1 - a^{\mathrm{sr}}_{ddd}/a^{\mathrm{sr}}_{dd}} + \frac{a^{\mathrm{sr}}_{cd}}{1 - a^{\mathrm{sr}}_{3,cd}/a^{\mathrm{sr}}_{cd}}. \tag{2.55}$$

The term $a^{\mathrm{sr}}_{3,cd}$, defined in Eq. (2.54), collects the ion-dipole cross contributions, as $a^{\mathrm{sr}}_{3,cd} = a^{\mathrm{sr}}_{cdd} + a^{\mathrm{sr}}_{ccd}$. Similarly rearranged Padé approximations have also been used by other authors[35,36,53,54,58,59]. As will be shown in Sec. 3.4, substituting Eq. (2.53) with Eq. (2.55) significantly improves the results of the theory without changing the basic perturbation equations. [...]

2.5 Numerical solution of the correlation integrals

[...] The evaluation of numerical results for the now converging correlation integrals requires an appropriate description for the three-particle correlation function $g^{\mathrm{hs}}(123)$. The most accurate correlation functions are those obtained by computer simulations as presented, e.g., by Bildstein and Kahl[109] or by Müller and Gubbins[110]. An alternative to this elaborate method for obtaining $g^{\mathrm{hs}}(123)$ are analytical or empirical approaches some of which have been compared in Ref. 111. For example, the integral equation method proposed by Attard[112] has proven to give good results[109]. In this work, we use the Kirkwood superposition approximation[81]

$$g(123) = g(12)g(13)g(23). \tag{2.56}$$

The superposition approximation is known to be less accurate compared to other methods, especially at high densities[109], but is has the advantage of a much simpler form than other approaches. [...]

{The procedure for numerical calculation of the correlation integrals has been given in the second publication, Ref. 2. For the hard sphere pair correlation functions, data from molecular simulation was used. For densities between $\rho^* = 0.2$ and 1, very precise data for $g^{\mathrm{hs}}(r)$ has been given by Kolafa et al.[113], and thus this data was employed for that density regime. For densities lower than $\rho^* = 0.2$, data obtained from our own simulations was used. Numerical solutions for the different correlation integrals for densities $0 \leq \rho^* \leq 1.0$ and damping parameters $0.2 \leq \alpha^* \leq 5.0$ are given as supplementary material of the second publication, Ref. 2. In the first publication, Ref. 1, we gave solutions for those integrals obtained with $g^{\mathrm{hs}}(r)$ from Percus-Yevick theory[114]. I parametrized analytical ansatz functions to those numerical solutions. The functions turned out to be moderately accurate and caused problems especially for small α^*,

where the values of the integrals are close to zero. In that region, some of the functions became negative because of a too rough adjustment, and the resulting Helmholtz energy obtained by Padé approximations were not reasonable. Therefore, I decided to give tabulated values of the numerical solutions in the second publication, Ref. 2 and use cubic spline interpolation instead of analytical functions.}

Fig. 2.1a and 2.1b show how the different correlation integrals $I_{ij(k)}$ vary with the parameter α^* for a density of $\rho^* = 0.68$[1]. Parameter α^* defines the division of the potential according to Eq. (2.21). As can be seen, for large values of α^* and thus for vanishing damping, the correlation integrals I_{cd}, I_{dd}, and I_{ddd} approach a limiting value. For larger values of α^* than the ones covered in Fig. 2.1b, this is also the case for I_{cdd}. These correlation integrals approach finite values even for the original (undamped) potential, i.e., for $\alpha^* \to \infty$. In contrast I_{cc}, I_{ccc} and I_{ccd} diverge for the original (undamped) potential and it is these correlation integrals that require special techniques like resummation in HBT theory or decomposition of the potentials as done in this work. In the limit of $\alpha^* \to \infty$ and $x = 0$, the only remaining terms in [...] {the third order perturbation expansion} are the undamped dipolar terms. In this limit, our theory reduces to the one presented by Rushbrooke, Stell and Høye[108] for the dipolar hard sphere fluid. [...]

[1] The Figures shown in the original publication, Ref. 1, differ from the figures shown here: the correlation integrals shown here are based on data obtained with $g^{\mathrm{hs}}(12)$ from molecular simulations, i.e. the figures show the $I_{ij(k)}$ given as supplementary material of the second publication, Ref. 2. This data was generated after Ref. 1 had been published.

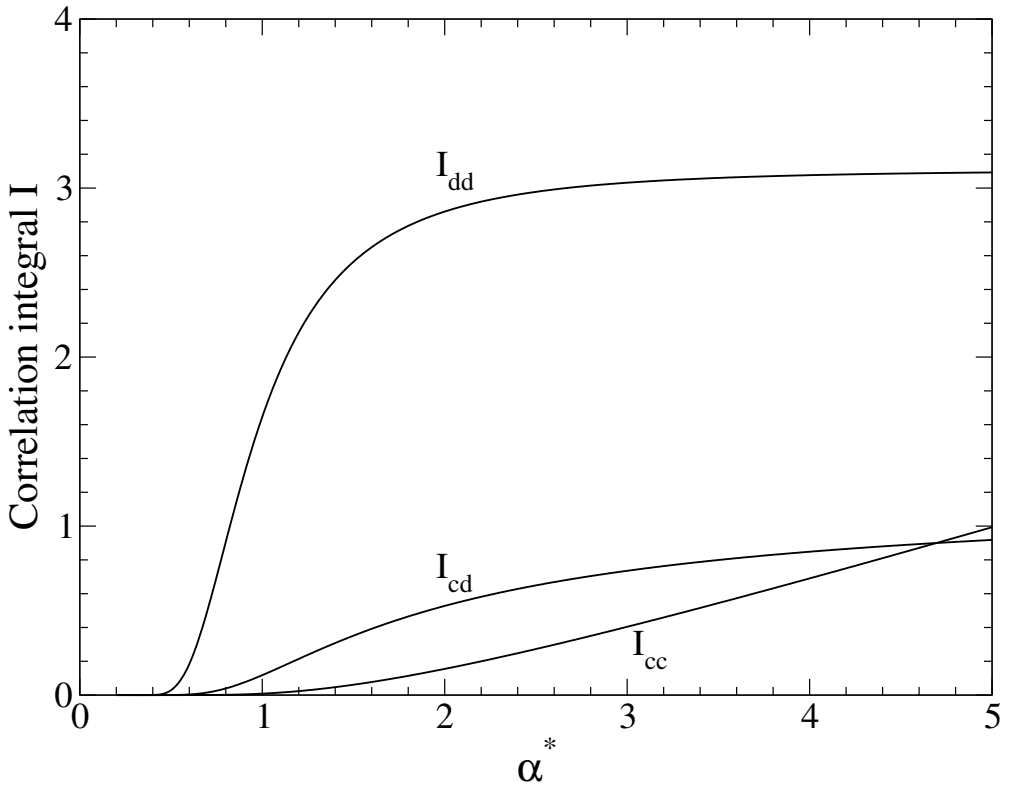

(a) 2nd order terms

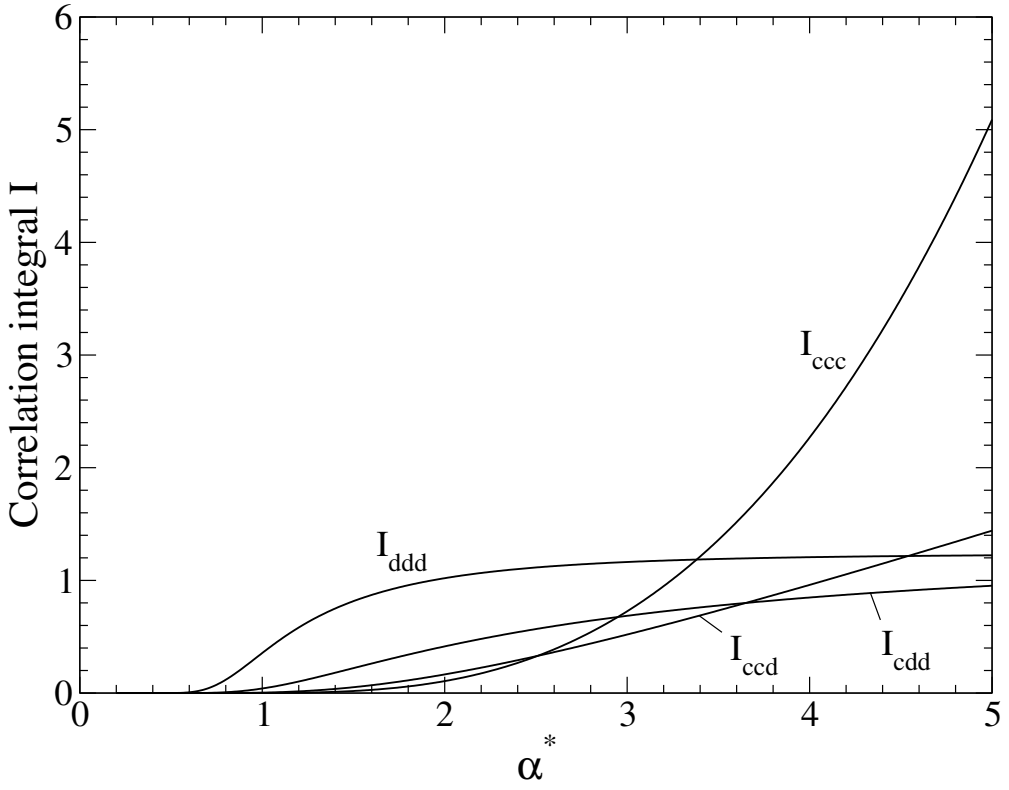

(b) 3rd order terms

Fig. 2.1: Correlation integrals at a constant density of $\rho^* = 0.68$.

2.6 Influence of the static dielectric constant on the results of the theory

By applying LMF theory to the perturbation expansion, our fluid theory depends on the static dielectric constant ε, as the long ranged Helmholtz energy contribution a^{lr} given by Eq. (2.28) is a function of $(\varepsilon-1)/\varepsilon$. As opposed to a primitive model, however, the sensitivity of our theoretical approach towards ε is small, as demonstrated in this section.

Outside of this section, we assume infinite ε, and thus $(\varepsilon-1)/\varepsilon = 1$ in this entire work. In order to assess the impact of this assumption on a^{lr}, we determined ε for varying dipole moment, ionic charge and ion concentration at a constant liquid-like density of $\rho^* = 0.6786$ in molecular simulations. The details on the simulation technique are given in Ref. 1.

As an alternative to the simple approximation employed in this work, one can also employ other ways for determining ε. A theoretical approach that has been presented by Tani et al.[115] is tested against the simulation data here. From perturbation theory for the pure dipolar hard sphere fluid, they obtained the simple expression

$$\varepsilon_{\mathrm{th}} = 1 + 3y + 3y^2 + 3y^3 \left(\frac{9 I_{dd\Delta}}{16\pi^2} - 1 \right) \tag{2.57}$$

with

$$y = \frac{4}{9} \pi {\mu^*}^2 \rho^*. \tag{2.58}$$

In the above equation, $I_{dd\Delta}$ is a correlation integral that is given in Ref. 115. In their work, Tani et al. showed that Eq. (2.57) gives fairly good results for the dipolar hard sphere fluid. Later, Henderson et al.[51] suggested using the approach also for roughly estimating the dielectric constant of model electrolyte solutions. They simply replaced the total density ρ^* in Eq. (2.58) with the density of the dipolar species, i.e. they suggested replacing y in Eq. (2.57) with

$$\tilde{y} = \frac{4}{9} \pi {\mu^*}^2 \rho^* (1 - x). \tag{2.59}$$

By doing this, the effect of decreasing number of dipolar particles with increasing ion concentration is accounted for, but the effect of the ionic species on ε is neglected. Therefore, Henderson et al. pointed out that the approach might be a crude approximation. Nonetheless, we here follow their suggestion and employ Eq. (2.57) with y

replaced by $\tilde{y}$ from Eq. (2.59).

In Tab. 2.1, the results of Eq. (2.57), denoted as ε_{th}, are compared to results from molecular simulations, denoted as ε_{sim}, for three different combinations of $\mu^{*\,2}$ and $q^{*\,2}$ and varying ion mole fraction x. A graphical representation of parts of this data is given in Fig. 2.2. The data confirms that the theoretical approach works very well for the pure dipolar fluid. However, significant deviation from the simulation data can be observed already for quite low ion concentrations x.

Both, theory and simulations show that ε is large for the systems with large dipole

Tab. 2.1: Static dielectric constant for three systems at a constant total density of $\rho^* = 0.6786$ from molecular simulations (ε_{sim}) and from the theoretical approach given by Eq. (2.57) (ε_{th}). A graphical representation of the data for ε_{sim} has been published in the first publication, Ref. 1.

x	ε_{sim}	ε_{th}
	$\mu^{*\,2} = 0.5;\ q^{*\,2} = 32$	
0	3.11 ± 0.03	3.15
0.032	2.99 ± 0.02	3.06
0.064	2.88 ± 0.03	2.97
0.12	2.72 ± 0.04	2.81
0.176	2.53 ± 0.02	2.66
	$\mu^{*\,2} = 2.5;\ q^{*\,2} = 160$	
0	32.6 ± 4.8	31.9
0.032	20.3 ± 1.7	30.0
0.064	13.2 ± 0.8	28.1
0.12	10.6 ± 1.4	25.1
0.176	8.1 ± 1.3	22.2
	$\mu^{*\,2} = 4.0;\ q^{*\,2} = 160$	
0	85.4 ± 22.9	84.1
0.032	50.0 ± 13.8	78.4
0.064	30.4 ± 4.8	72.9
0.12	23.3 ± 5.2	63.9
0.176	14.7 ± 3.2	55.7

moments of $\mu^{*\,2} = 2.5$ and 4.0 at low ion concentrations x. With increasing x, the simulations reveal a rapid decrease of ε, and the lowest value of those systems is $\varepsilon = 8.079$ which corresponds to $(\varepsilon - 1)/\varepsilon = 0.876$. For the system with $\mu^{*\,2} = 0.5$, ε is in a range between 2.53 and 3.11, resulting in the lowest value of $(\varepsilon - 1)/\varepsilon = 0.605$.

The simulation data, the theory given by Eq. (2.57) and the basic assumption $\varepsilon = \infty$ allow us to calculate a^{lr} in three different ways. The most exact results are obtained by determining $a^{\text{lr}}_{\text{sim}}$, the long range contribution calculated using ε_{sim}. With those values as reference data, we can assess a^{lr}_{∞}, the long ranged contribution assuming $\varepsilon = \infty$

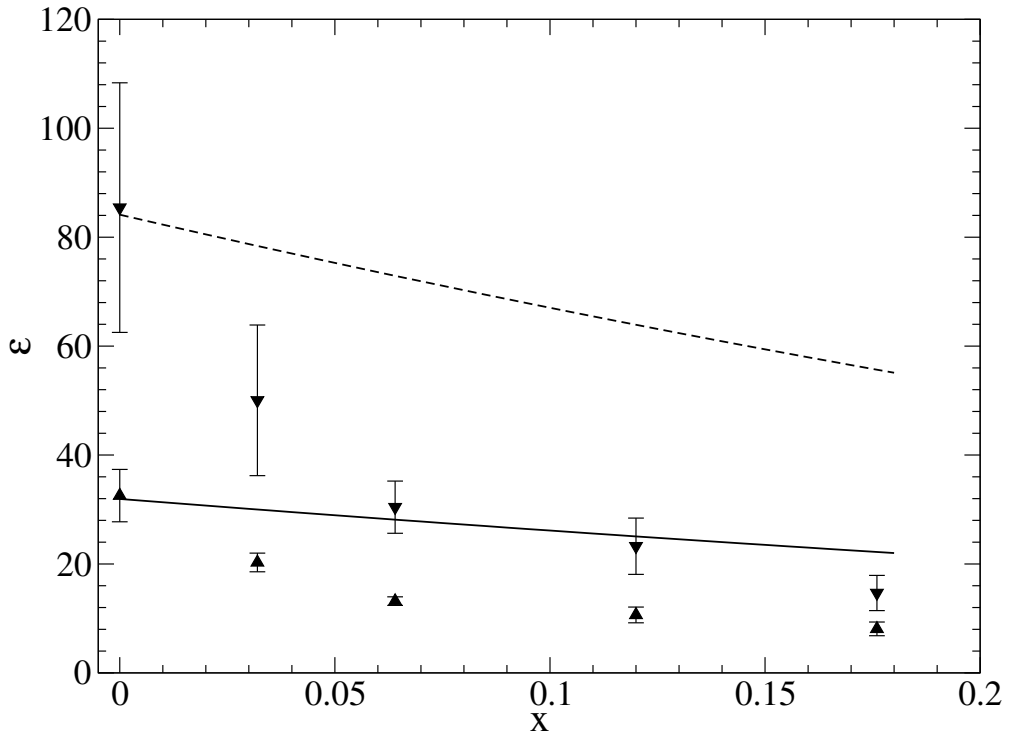

Fig. 2.2: Static dielectric constant over ion concentration for two of the regarded systems with $\rho^* = 0.6786$: ▼ ε_{sim} for ${\mu^*}^2 = 4.0$ and ${q^*}^2 = 160$; − − − ε_{th} for ${\mu^*}^2 = 4.0$ and ${q^*}^2 = 160$; ▲ ε_{sim} for ${\mu^*}^2 = 2.5$ and ${q^*}^2 = 160$; —— ε_{th} for ${\mu^*}^2 = 2.5$ and ${q^*}^2 = 160$;

and $a^{\text{lr}}_{\text{th}}$ with ε_{th} from Eq. (2.57). For this, we calculated the relative deviation of a^{lr}_{∞} and $a^{\text{lr}}_{\text{th}}$ from the reference $a^{\text{lr}}_{\text{sim}}$, denoted as $\delta a^{\text{lr}}_{\infty}$ and $\delta a^{\text{lr}}_{\text{th}}$, respectively. In Tab. 2.2, those relative deviations are summarized for the model solutions regarded here for an exemplary value of $\alpha^* = 1.5$ (as is shown in Sec. 3.4, this is a reasonable value of α^* for the given liquid-like density of $\rho^* = 0.6786$).

The data given in Tab. 2.2 shows that the assumption of infinite dielectric constant causes the largest error in a^{lr} for $x = 0$, the pure dipolar fluid, with a large deviation of over 40 % for ${\mu^*}^2 = 0.5$. For the two systems with ${\mu^*}^2 \geq 2.5$, the deviations are much lower in that limit. With increasing ion concentration, the error caused in a^{lr} by assuming infinite ε decreases for all systems, although the approximation itself becomes more inaccurate. This is caused by the fact that for increasing x, the contribution of the ions, i.e. the first term in Eq. (2.28), gains more and more impact on a^{lr} and the influence of the dielectric constant on a^{lr} decreases.

The above consideration, however, has shown that Eq. (2.57) is most accurate in the region of low ion concentrations, and thus in the region where ε has the largest impact on a^{lr}. As can be seen from the data given in Tab. 2.2, employing the ansatz of Tani et al., Eq. (2.57), significantly lowers the deviation from the exact $a^{\text{lr}}_{\text{sim}}$ especially for

Tab. 2.2: Relative deviations $\delta a_{\infty}^{\mathrm{lr}}$ and $\delta a_{\mathrm{th}}^{\mathrm{lr}}$.

x	$\delta a_{\infty}^{\mathrm{lr}}$ / %	$\delta a_{\mathrm{th}}^{\mathrm{lr}}$ / %
$\mu^{*\,2} = 0.5$; $q^{*\,2} = 32$		
0	43.3	0.560
0.032	3.175	0.070
0.064	1.705	0.047
0.12	0.983	0.033
0.176	0.724	0.035
$\mu^{*\,2} = 2.5$; $q^{*\,2} = 160$		
0	0.501	−0.010
0.032	0.090	0.029
0.064	0.073	0.039
0.12	0.050	0.029
0.176	0.045	0.029
$\mu^{*\,2} = 4.0$; $q^{*\,2} = 160$		
0	0.113	−0.002
0.032	0.034	0.012
0.064	0.030	0.018
0.12	0.022	0.014
0.176	0.024	0.018

low x. The same conclusion has been recently drawn by Theiss and Gross[116] who carried out a similar analysis as part of a work in which they present a fourth order perturbation theory for dipolar hard spheres. In their work, the same a^{lr} as given in this work is employed for the limit of $x = 0$.

The above considerations show that for large dipole moments, assuming $\varepsilon = \infty$ does not introduce a significant error to the theory. In the following, we only consider liquid-like densities and dipole moments $\mu^{*\,2} \geq 2.5$ and therefore assume infinite ε. However, the study also shows that for low dipole moments, this is not a good assumption. In such cases, more realistic values, e.g. determined by Eq. (2.57) should be used.

2.7 Validation of Kirkwood superposition approximation by MC simulations

Before assessing the new third order perturbation approach, the accuracy of the third order perturbation terms themselves has to be ensured. For their numerical evaluation, Kirkwood superposition approximation (KSA) has been employed, as is discussed in Sec. 2.5. In this section, a method for determining the correlation integrals I_{ijk} in MC simulations is presented. Using the simulation results, it is shown that KSA has

negligible influence on the theory.

2.7.1 Correlation integrals from molecular simulations

The correlation integrals formulated in Eq. (2.46) to (2.52) can be sampled in MC simulations. In this section, we derive expressions for calculating the third order correlation integrals in terms of canonical ensemble averages of the hard sphere fluid. We explain the route to this ensemble average expression in detail for one correlation integral, i.e. for I_{ccd}. The same scheme is analogously applied to the remaining integrals.
For deriving a suitable expression, it is helpful to start with the third order terms of the basic perturbation expansion, i.e. with the terms given in Eqs. (2.37) to (2.40). For the ion-ion-dipole term, Eq. (2.38), the required orientational averaged three-particle potential is [...] {given by Eq. (2.43).} The remaining orientational averaged potentials required for the rest of the terms are given [...] {by Eqs. (2.44) and (2.45)}. Inserting Eq. (2.43) into Eq. (2.38) and additionally replacing the three-particle correlation function $g^{\mathrm{hs}}(123)$ with its definition

$$g^{\mathrm{hs}}(123) = \frac{N(N-1)(N-2)}{{\rho^*}^3 {Z^*}^{\mathrm{hs}}} \int \exp\left(-\beta U^{\mathrm{hs}}\right) \mathrm{d}\mathbf{r}^{*\,N>3} \tag{2.60}$$

(where ${Z^*}^{\mathrm{hs}}$ is the configuration integral of the hard sphere fluid) yields

$$\begin{aligned} a_{ccd}^{\mathrm{sr}} &= \frac{1}{6}{\rho^*}^2 x^2 (1-x) {q^*}^4 {\mu^*}^2 (N-1)(N-2) \frac{1}{{Z^*}^{\mathrm{hs}}} \\ &\quad \times \int \underbrace{\frac{K_{12}K_{13}\cos\omega_1 \ \mathrm{erfc}\left(r_{23}^*/\alpha^*\right)}{{r_{12}^*}^2 {r_{13}^*}^2 r_{23}^*}}_{\equiv \phi_{123}^{ccd}} \ \exp\left(-\beta U^{\mathrm{hs}}\right) \mathrm{d}\mathbf{r}^{*\,N} \qquad (2.61) \\ &= \frac{1}{6}{\rho^*}^2 x^2 (1-x) {q^*}^4 {\mu^*}^2 (N-1)(N-2) \left\langle \phi_{123}^{ccd} \right\rangle_{NVT,\mathrm{hs}} \qquad (2.62) \end{aligned}$$

where we took advantage of monovalent ions ($|q_i^*| = q^*$) and regard only one dipolar solvent species ($\mu_i^* = \mu^*$). Additionally, for brevity, we write the argument of the integral, and thus the term that has to be sampled, as ϕ_{123}^{ccd}. The angular brackets $\langle ... \rangle_{NVT,\mathrm{hs}}$ denote the canonical ensemble average in the hard sphere fluid.
By requiring equality of Eq. (2.62) with Eq. (2.50), we get

$$I_{ccd}^{\mathrm{sim}}(\rho^*, \alpha^*) = \frac{1}{8} \frac{(N-1)(N-2)}{\pi^2 {\rho^*}^2} \left\langle \phi_{123}^{ccd} \right\rangle_{NVT,\mathrm{hs}} . \tag{2.63}$$

For getting reasonable statistics, it is not useful to select one particle triplet and sample ϕ_{123}^{ccd} of this triplet only. We can simply substitute ϕ_{123}^{ccd} with the average of a given number of triplets, $1/N_{tr}\sum_{m=1}^{N_{tr}}\phi_{ijk,m}^{ccd}$ where i,j,k are selected randomly and N_{tr} is the number of triplets regarded. We select a fixed number N_{tr} instead of regarding all possible triplets since it dramatically reduces computation time (but gives less accurate statistical averages). The final expression for I_{ccd}^{sim} from molecular simulations in NVT ensemble is thus

$$I_{ccd}^{\mathrm{sim}}(\rho^*,\alpha^*)=\frac{1}{8}\frac{(N-1)(N-2)}{\pi^2{\rho^*}^2}\left\langle\frac{1}{N_{tr}}\sum_{m=1}^{N_{tr}}\phi_{ijk,m}^{ccd}\right\rangle_{NVT,\mathrm{hs}}. \tag{2.64}$$

By repeating the procedure described above for the remaining terms of third order, we see that the equations for all correlation integrals are identical to Eq. (2.64), except for different ϕ_{ijk}. Those are[2]

$$\phi_{ijk}^{ccc}=\frac{\mathrm{erfc}(r_{ij}^*/\alpha^*)\mathrm{erfc}(r_{ik}^*/\alpha^*)\mathrm{erfc}(r_{jk}^*/\alpha^*)}{r_{ij}^*r_{ik}^*r_{jk}^*} \tag{2.65}$$

$$\phi_{ijk}^{cdd}=\frac{K_{ik}K_{jk}\left(M_{ij}\cos\omega_i\cos\omega_j-K_{ij}\cos(\omega_i+\omega_j)\right)}{{r_{ij}^*}^3{r_{ik}^*}^2{r_{jk}^*}^2} \tag{2.66}$$

$$\begin{aligned}\phi_{ijk}^{ddd}=\frac{1}{{r_{ij}^*}^3{r_{ik}^*}^3{r_{jk}^*}^3}\,(&-M_{jk}K_{ij}K_{ik}-M_{ik}K_{ij}K_{jk}\\&-M_{ij}K_{ik}K_{jk}+3\,K_{ij}K_{ik}K_{jk}\\&+M_{ij}M_{ik}K_{jk}\cos^2\omega_i\\&+M_{ij}M_{jk}K_{ik}\cos^2\omega_j\\&+M_{ik}M_{jk}K_{ij}\cos^2\omega_k\\&+M_{ij}M_{ik}M_{jk}\cos\omega_i\cos\omega_j\cos\omega_k)\end{aligned} \tag{2.67}$$

where K_{ij} and M_{ij} are defined by Eqs. (2.26) and (2.27) and $\omega_{i,j,k}$ are the interior angles of the triangle formed by the three particles. For sampling I_{ijk}, we carried out NVT MC simulations of the hard sphere fluid for different particle numbers N between 200 and 19000. The damping parameter was kept at a constant value of $\alpha^*=1.5$ and we considered two different densities, $\rho^*=0.6786$ and $\rho^*=0.8$. The systems were equilibrated for 10000 MC cycles. We then sampled all of the ϕ_{ijk} every 10 cycles for a total of 50000 cycles. The number of particle triples N_{tr} was chosen to be $1\cdot10^7$ in all simulations, independent from the total number of particles. The cutoff was set to $0.25\cdot L$, where L is the length of the simulation box.

[2] in the originally published manuscript, Ref. 2, the brackets in Eq. (2.67) are missing due to a misprint.

Fig. 2.3 shows one representative correlation integral, I_{ccd}, versus the particle number for $\rho^* = 0.6786$ and $\alpha^* = 1.5$. Each data point is the average of five independent simulations. The statistical uncertainty is the standard deviation of those five simulations. It can be seen that the simulated I_{ccd}^{sim} approaches a limiting value already for quite low particle numbers. This value is in excellent agreement with the results from numerical integration [...]. Similar behavior can also be observed for the remaining correlation integrals that are not shown here. From our simulation study, the values of I_{ijk}^{sim} used for calculating δI_{ijk} in Tab. 2.3 were obtained by taking the average of the simulated values of all simulations with $N \geq 7000$.

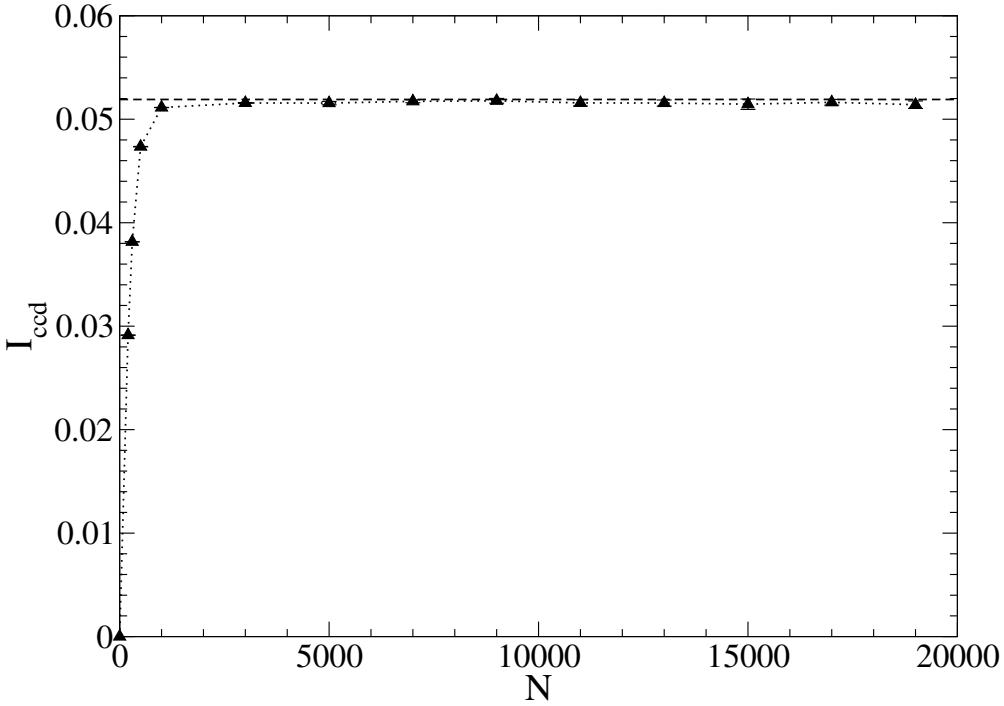

Fig. 2.3: I_{ccd} versus particle number for $\rho^* = 0.6786$ and $\alpha^* = 1.5$: ▲ results from molecular simulations, I_{ccd}^{sim}; – – – result of numerical integration using Kirkwood superposition approximation, Eq. (2.56), for $g^{\mathrm{hs}}(123)$.

2.7.2 Influence of KSA on the results of the perturbation theory

As mentioned in Sec. 2.5, we use Kirkwood superposition approximation (KSA)[81] [...] for approximating the three-particle correlation function of the hard sphere fluid [...] because of its simple form. In doing so we follow other theories for polar fluids[42,51,108,117,118].

In the studies of Barker et al.[119,120] and Tani et al.[115], the validity of KSA for I_{ddd} in the limit of $\alpha^* \to \infty$ (undamped potentials) has already been tested by comparison

with molecular simulation data. In their work, they found good agreement between numerically calculated and simulated values. Beyond only dipolar fluids, the impact of using Eq. (2.56) in theories for electrolyte solutions is unknown. To ensure that KSA does not introduce significant errors to the theory, we computed I_{ijk} in MC simulations. [...]

In Tab. 2.3, I_{ijk} from numerical integration are compared to the simulation results. As can be seen, the deviation between both methods is in the order of one percent or lower for typical liquid phase densities and a damping parameter of $\alpha^* = 1.5$ (which is a reasonable choice of α^*, as will be shown in [...] Sec. 3.4.2).

The Padé approximation of the third order theory further damps the errors of I_{ijk} in

Tab. 2.3: Relative deviation δI_{ijk} between the value from numerical integration (using Kirkwood superposition approximation) and simulated value for $\alpha^* = 1.5$.

ρ^*	δI_{ccc} / %	δI_{ccd} / %	δI_{cdd} / %	δI_{ddd} / %
0.6786	0.52	0.61	1.22	1.24
0.8	0.27	0.26	0.46	−0.35

the calculation of a^{sr}. Tab. 2.4 shows the errors in Helmholtz energy caused by Kirkwood's superposition approximation for different choices of q^*, μ^* and ion mole fraction x. This comparison clearly reveals that the errors in a^{sr} are well below one percent, so that KSA does not introduce severe errors to the theory.

Tab. 2.4: Relative errors δa^{sr} and $\delta a^{\mathrm{sr}}_{\mathrm{mod}}$ of the perturbation theory caused by using Kirkwood superposition approximation in numerical calculation of I_{ijk}.

x	δa^{sr} / % (Eq. (2.53))	$\delta a^{\mathrm{sr}}_{\mathrm{mod}}$ / % (Eq. (2.55))
$\rho^* = 0.6786$; $\mu^{*\,2} = 4.0$; $q^{*\,2} = 160$		
0	−0.67	−0.67
0.032	−0.71	−0.66
0.064	−0.62	−0.63
0.12	−0.55	−0.59
0.176	−0.53	−0.56
$\rho^* = 0.8$; $\mu^{*\,2} = 2.5$; $q^{*\,2} = 100$		
0	0.17	0.17
0.032	−0.20	0.02
0.064	−0.24	−0.04
0.12	−0.26	−0.09
0.176	−0.26	−0.13

3 Evaluation of the perturbation theory by comparison with MC simulation data

Parts of this chapter are literal quotes from the second publication, Ref. 2.
The origin of the sections is as follows:

- *Section 3.1 has not been published previously.*
- *Sections 3.2, 3.3, 3.4 and 3.5 including all subsections are literal quotes from the second publication, Ref. 2, where the sections have been published with identical headings as used in this work.*

3.1 Preliminary remark

In the theory presented in the previous chapter, the intermolecular pair potential is decomposed into a short- and a long-ranged part. For obtaining expressions for the corresponding Helmholtz energy contributions a^{sr} and a^{lr}, some basic approximations were made.
The short-ranged part is described by a Padé approximated third order Taylor expansion. For the calculation of numerical results of the correlation integrals, Kirkwood superposition approximation was employed.
The long-range contribution a^{lr} is captured in a mean field manner by a term resulting from LMF theory. Furthermore, the expression for a^{lr} depends on the static dielectric constant that is assumed to be infinity.
In the previous chapter, it has been shown that neither the Kirkwood superposition approximation nor the assumption of infinite dielectric constant causes severe errors in the corresponding expressions for a^{sr} and a^{lr}. In this chapter, the accuracy of the Padé approximated third order Taylor expansion for a^{sr} as well as the accuracy of the long-range contribution term, Eq. (2.28), is assessed by comparison with data from molecular simulations. For this, the (exact) total residual Helmholtz energy a^{res} as well as the short-ranged part a^{sr} are calculated with different thermodynamic integration schemes in MC simulations. Using the resulting data, the exact long-ranged contribution can be determined as $a^{\mathrm{lr}} = a^{\mathrm{sr}} - a^{\mathrm{res}}$. The simulation results are thus used to individually assess the theoretical expressions for a^{sr} and a^{lr}.

3.2 Thermodynamic integration methods in molecular simulations

Thermodynamic integration is a standard method for calculating Helmholtz energies relative to any arbitrary reference point or reference system. It is obtained by integrating a suitable Helmholtz energy derivative from the chosen reference state to the desired state.
In this section, we present two different Helmholtz energy derivatives for thermodynamic integration in molecular simulations. One of those methods significantly reduces our simulation effort for calculating the Helmholtz energy contribution arising from the short-ranged part of the electrostatic pair potential. We note that other efficient methods exist for sampling Helmholtz energies (see, e.g., Ref. 121).

3.2.1 Total Helmholtz energy from λ-integration

The most common thermodynamic integration method in molecular simulations is one where the intermolecular pair potential u_{ij} between two particles i and j is split into a reference part u_{ij}^{ref} and a residual part u_{ij}^{res} according to

$$u_{ij} = u_{ij}^{\mathrm{ref}} + \lambda \cdot u_{ij}^{\mathrm{res}} \tag{3.1}$$

where λ is a coupling parameter between 0 and 1 for the reference fluid and for the target fluid, respectively. In our study, we use the hard sphere fluid as reference part, $u_{ij}^{\mathrm{ref}} = u_{ij}^{\mathrm{hs}}$ and the electrostatic potential as residual part, $u_{ij}^{\mathrm{res}} = u_{ij}^{\mathrm{es}}$.
With this definition, the Helmholtz energy can be written as

$$A - A^{\mathrm{hs}} = \int_0^1 \left(\frac{\partial A}{\partial \lambda}\right) \mathrm{d}\lambda. \tag{3.2}$$

The partial derivative of A with respect to λ is obtained from the partition function as average of the total electrostatic energy $\langle \sum_i \sum_{j>i} u_{ij}^{\mathrm{es}} \rangle_{NVT,\lambda}$ calculated in a system of particles interacting with scaled pair potentials defined by Eq. (3.1). The residual Helmholtz energy from λ-integration is

$$a^{\mathrm{res}} = \int_0^1 \frac{1}{N} \left\langle \sum_i \sum_{j>i} \beta u_{ij}^{\mathrm{es}} \right\rangle_{NVT,\lambda} \mathrm{d}\lambda. \tag{3.3}$$

We calculated the argument of the integral in Eq. (3.3) for 20 equidistant values of λ between 0.05 and 1. For the model system we use, the argument is zero for $\lambda = 0$ which gives us an additional value.
The integrand of Eq. (3.3) over λ is strictly monotonic as shown in [...] {Fig. 3.1[1]}. Simple trapezoidal rule for numerical integration is sufficiently accurate. Adding two additional supporting points in the steepest region between $\lambda = 0$ and 0.05 changed the results only within statistical uncertainty (for a state point that is not included in this study, but similar to the ones regarded here). Thus, increasing the number of supporting points does not significantly change the results of numerical integration.

[1] Fig. 3.1 was not part of the original publication, Ref. 2. It is given in the appendix of the first publication, Ref. 1.

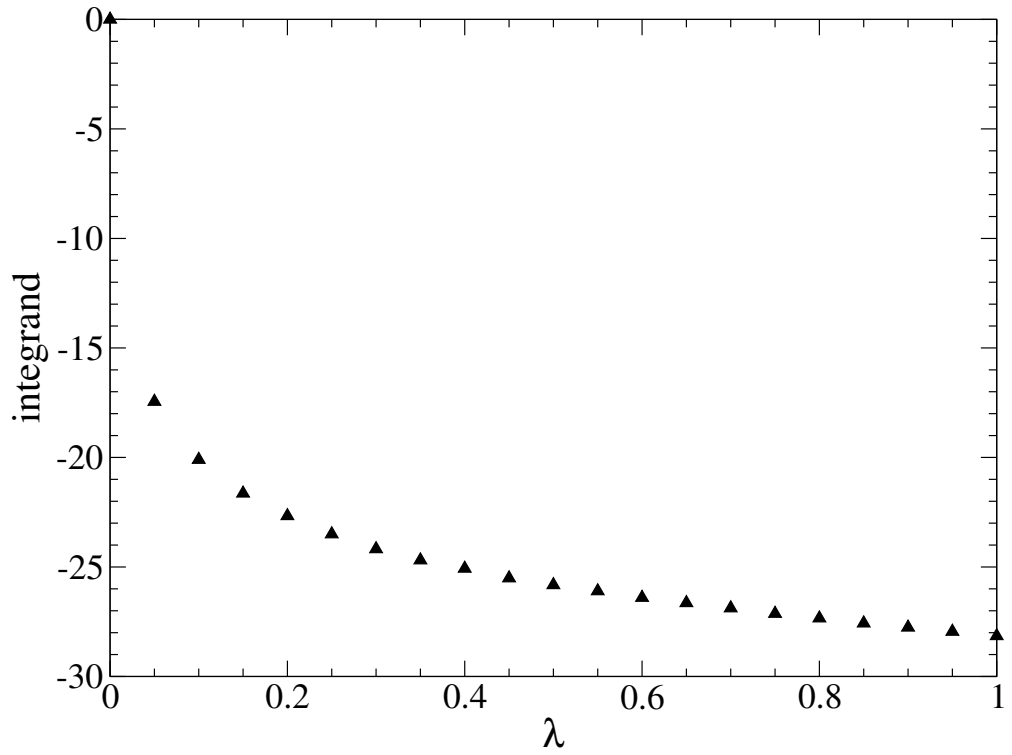

Fig. 3.1: Integrand in Eq. (3.3) versus λ for $\rho^* = 0.6786$, $\mu^{*\,2} = 4.0$, $q^{*\,2} = 160$, $x = 0.176$. Error bars are within symbol size.

3.2.2 Short-ranged contribution to Helmholtz energy from α-integration

An important objective of this study is to assess the short-ranged contribution a^{sr} and the long-ranged part a^{lr} of the Helmholtz energy. An individual evaluation of the underlying perturbation theory (a^{sr}) and the correction term of Weeks and coworkers[98,102] (a^{lr}) is not only valuable in itself, the analysis will also reveal a reasonable value (or range) for the damping parameter α^*. What is needed are molecular simulations for the short-ranged Helmholtz energy a^{sr}. As a simulation technique, in principle, we could apply the standard λ-integration scheme, sampling only the short-ranged electrostatic potentials in Eq. (3.3) instead of the total electrostatic potential. With this approach, each data point would require 20 single simulations, and the computational effort for calculating $a^{\mathrm{sr}}(\alpha^*)$ for a variety of different systems would be high.

The simulation effort can be considerably reduced by considering α^* instead of λ as the integration path variable and using the derivative of the Helmholtz energy with respect to α^* instead of λ for the thermodynamic integration. The short-ranged part

of the pair potential is

$$\beta u_{ij}^{\mathrm{sr}} = \beta u_{ij}^{\mathrm{hs}} + \beta u_{cc,ij}^{\mathrm{sr}} = \beta u_{ij}^{\mathrm{hs}} + \frac{q_i^* q_j^*}{r_{ij}^*} \cdot \mathrm{erfc}\left(\frac{r_{ij}^*}{\alpha^*}\right). \tag{3.4}$$

In the simulations, point dipoles are modeled by two point charges, as is explained in Sec. 3.3 below. Thus, in contrast to the perturbation theory, all short-ranged electrostatic interactions are described as (short-ranged) charge-charge potentials, without the need to distinguish between charge-charge, charge-dipole and dipole-dipole interactions. For $\alpha^* \to 0$, the complementary error function $\mathrm{erfc}(r_{ij}^*/\alpha^*)$ is zero, and the short-ranged part of the Helmholtz energy as a function of α^* can be obtained from

$$A^{\mathrm{sr}} - A^{\mathrm{hs}} = \int_0^{\alpha^*} \left(\frac{\partial A^{\mathrm{sr}}}{\partial \tilde{\alpha}^*}\right) \mathrm{d}\tilde{\alpha}^*. \tag{3.5}$$

The required partial derivative is

$$\left(\frac{\partial A^{\mathrm{sr}}}{\partial \tilde{\alpha}^*}\right) = \frac{1}{\tilde{Z}_{\tilde{\alpha}^*}} \int \left(\sum_i \sum_{j>i} \frac{\partial u_{ij}^{\mathrm{sr}}}{\partial \tilde{\alpha}^*}\right) \exp\left(-\beta U^{\mathrm{sr}}(\tilde{\alpha}^*, \mathbf{r}^N)\right) \mathrm{d}\mathbf{r}^N \tag{3.6}$$

with

$$\frac{\partial u_{ij}^{\mathrm{sr}}}{\partial \tilde{\alpha}} = \frac{q_i^* q_j^*}{\tilde{\alpha}^{*\,2}} \frac{2}{\sqrt{\pi}} \exp\left(-\frac{r_{ij}^{*\,2}}{\tilde{\alpha}^{*\,2}}\right) \tag{3.7}$$

From Eq. (3.5) – (3.7), it follows that the short-ranged contribution to the Helmholtz energy from α^*-integration can be determined in the NVT ensemble from

$$\begin{aligned} a^{\mathrm{sr}} &= \beta \frac{A^{\mathrm{sr}} - A^{\mathrm{hs}}}{N} \\ &= \int_0^{\alpha^*} \left\langle \frac{1}{N} \sum_i \sum_{j>i} \frac{q_i^* q_j^*}{\tilde{\alpha}^{*\,2}} \frac{2}{\sqrt{\pi}} \exp\left(-\frac{r_{ij}^{*\,2}}{\tilde{\alpha}^{*\,2}}\right) \right\rangle_{NVT,\tilde{\alpha}^*} \mathrm{d}\tilde{\alpha}^* \end{aligned} \tag{3.8}$$

Using Eq. (3.8), each additional data point $a^{\mathrm{sr}}(\alpha^*)$ in a series of increasing α^*-values can be calculated with only one single simulation (by integrating over the previous $a^{\mathrm{sr}}(\alpha^*)$ results).

Since this approach for thermodynamic integration has not been tested or applied so far, we carefully analyzed the accuracy of this method. Fig. 3.2 shows the argument of the integral in Eq. (3.8) over the parameter α^* for particle numbers of $N = 1000$ and $N = 2000$ for the same density, with accordingly increased simulation box volume (for a representative state point). We first regard the left-hand side of Fig. 3.2, where one

observes, the argument first decreases and has a minimum before increasing smoothly. We realize it is essential to have a sufficiently fine α^*-grid in the region of α^* lower than 1. A sufficient number of supporting points is important because errors propagate with increasing α^* when using the α-integration scheme. We therefore chose $\Delta\alpha^* = 0.05$ for $\alpha^* \leq 1$. For $\alpha^* > 1$, we increased $\Delta\alpha^*$ to 0.1. For the numerical integration, we integrated cubic splines adjusted to the simulation data.

When regarding the right-hand region of Fig. 3.2 we observe the argument of Eq. (3.8)

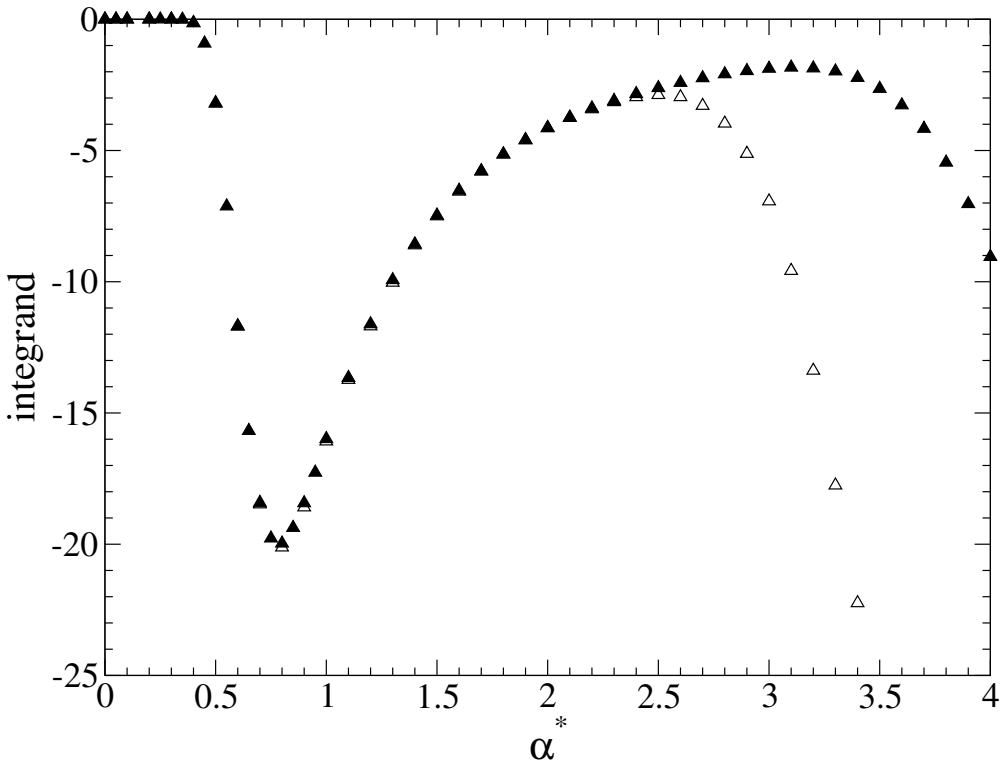

Fig. 3.2: Integrand in Eq. (3.8) versus α^* for $\rho^* = 0.6786$, $\mu^{*\,2} = 4.0$, $q^{*\,2} = 160$, $x = 0.176$: $\triangle$ $N = 1000$ particles; $\blacktriangle$ $N = 2000$ particles. Error bars are within symbol size.

to be system size dependent. The tail of the (grid-)curve in Fig. 3.2 must converge to zero in order to allow the convergence of a^{sr} to a^{res} for $\alpha^* \to \infty$. The system-size dependent 'run-away' of the (grid-)curve is caused by the increasing range of the $u_{ij}^{\mathrm{sr}}(\alpha^*)$ potential with increasing α^*, while restricting a constant cutoff radius for evaluating the potential at half the length of the simulation box. Our study requires analyzing the short- and long-ranged Helmholtz energy only to values $\alpha^* < 3$. It is therefore sufficient to obtain correct values for the integrand in Eq. (3.8) for $\alpha^* \leq 3$, and thus to simulate systems with N=2000 particles.

3.3 Simulation details

All of the simulations were carried out in an NVT ensemble with a total of $N = 1000$ particles for the λ-integration and $N = 2000$ particles for the α-integration. For pure dipolar fluids (with $x = 0$), we equilibrated for at least $5 \cdot 10^4$ MC cycles and considered $5 \cdot 10^4$ cycles for sampling (where one cycle comprises N MC moves) for both thermodynamic integration methods. The systems containing ions required longer simulations. Those systems were equilibrated for 10^5 cycles. Subsequently, we sampled the desired quantities for 10^5 cycles for λ-integration and for $5 \cdot 10^4$ cycles for the α-integration scheme.

For the λ-integration, we used standard Ewald summation[103] as it is described in detail e.g. in Ref. 122 or Ref. 123 with an Ewald parameter of 5.6 and 7 k-vectors in each spatial direction.

In all simulations we used the 'ion extended dipole model', in which the dipoles are modeled with two point charges of the same magnitude with opposite signs, separated by a small distance $d = 0.1 \cdot \sigma$. The dipole moments were defined by adjusting the magnitude of the point charges. We validated this model by comparing our results to literature data of internal energies of Caillol et al.[124] and Eggebrecht and Ozler[58] who both used point dipoles in their simulations. In Ref. 1, a slightly more detailed discussion of the literature concerning the ion extended dipole model is given.

In accordance with the study of Eggebrecht and Ozler[58], we also studied ion-dipolar mixtures at a reduced density of $\rho^* = 0.6786$. In addition we conducted simulations for $\rho^* = 0.8$, as a significantly higher liquid density. We vary the ionic mole fraction in 5 steps.

3.4 Results

The two simulation techniques described above allow us to determine comprehensive results for the total electrostatic Helmholtz energy contribution a^{res} in ion-dipole systems, as well as for only the short-ranged part of the electrostatic Helmholtz energy contribution a^{sr}.

In this section, we first discuss the different Helmholtz energy contributions obtained from molecular simulations. We then use the simulation data to evaluate the long-range correction term a^{lr} given by Eq. (2.28). Finally, we analyze and evaluate the third order perturbation theory for the short-ranged Helmholtz energy described in Sec. 2.4.

3.4.1 Helmholtz energy contributions from molecular simulations

Fig. 3.3 shows a^{res} as well as a^{sr} for a fixed $\alpha^* = 1.5$ with increasing ion concentration for one of the systems studied in this work. Both, a^{res} and a^{sr} decrease nearly linear with ion concentration. [...] The difference between both values, a^{res} and a^{sr}, however, increases rapidly with increasing ion concentration. For the pure dipolar fluid, at $x = 0$, the short-ranged contribution covers 91 % of the total electrostatic Helmholtz energy, whereas the value is only 55 % for the state point with $x = 0.176$. That is in accordance with intuition, because dipolar interactions are effectively more short-ranged leading to relatively small contribution from a^{lr}. In Sec. 3.4.2 we will show that $\alpha^* = 1.5$ is indeed a meaningful value for α^*.

The contribution of the long-ranged part of the electrostatic potential to the total

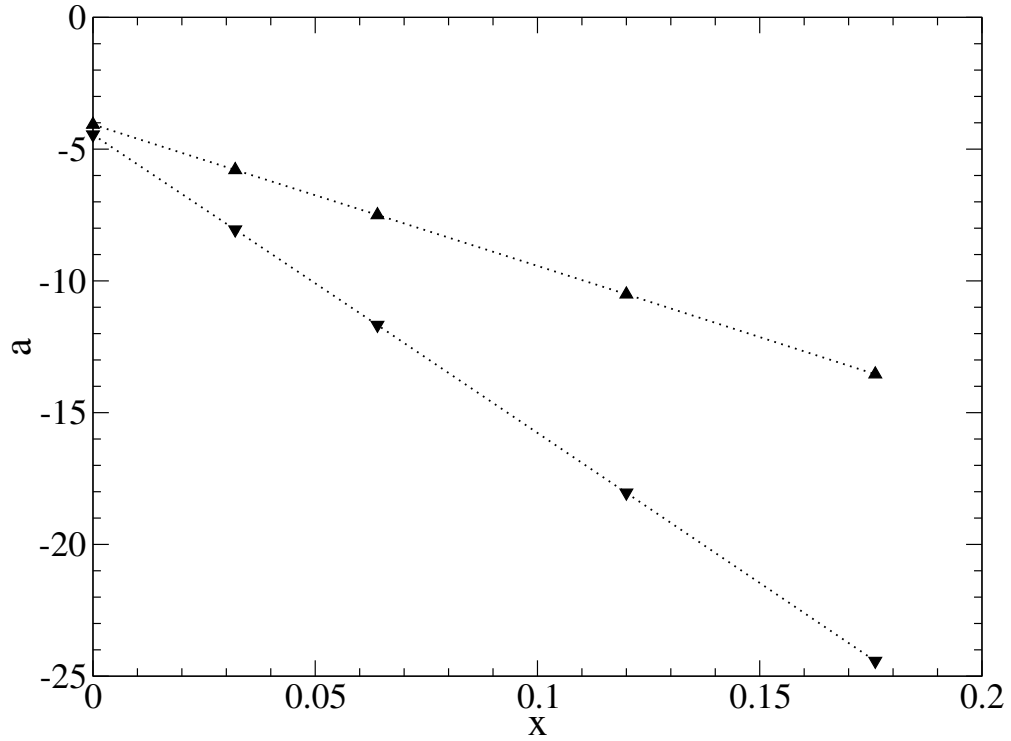

Fig. 3.3: Helmholtz energy over ion concentration x for $\rho^* = 0.6786$, $\mu^{*\,2} = 4.0$, $q^{*\,2} = 160$: ▲ short-range contribution a^{sr} for $\alpha^* = 1.5$ from simulations with α-integration; ▼ total residual Helmholtz energy a^{res} from simulation with λ-integration. Error bars are within symbol size.

Helmholtz energy can be obtained from our simulation data as

$$a^{\mathrm{lr}}_{\mathrm{sim}} = a^{\mathrm{res}}_{\lambda} - a^{\mathrm{sr}}_{\alpha}. \tag{3.9}$$

The indices 'λ' and 'α' in this equation are only indicative of the simulation technique used for obtaining the value of a^{res} and a^{sr}, respectively.

In Fig. 3.4 we analyze the short-ranged and long-ranged contributions to the Helmholtz energy from molecular simulations for varying damping parameter α^* . The state point corresponds to the largest ion concentration x of Fig. 3.3. The short-ranged part, starting at zero for $\alpha^* = 0$, decreases for increasing α^*. The long-ranged contribution $a^{\mathrm{lr}}_{\mathrm{sim}}$ starts at a^{res} for low values of α^* and increases with rising α^*. The remarkable feature is that both, the short- and the long-ranged part contribute significantly to the Helmholtz energy within the entire range of α^* shown here. A sufficiently accurate description of both contributions is thus essential for a reliable calculation of a^{res}.

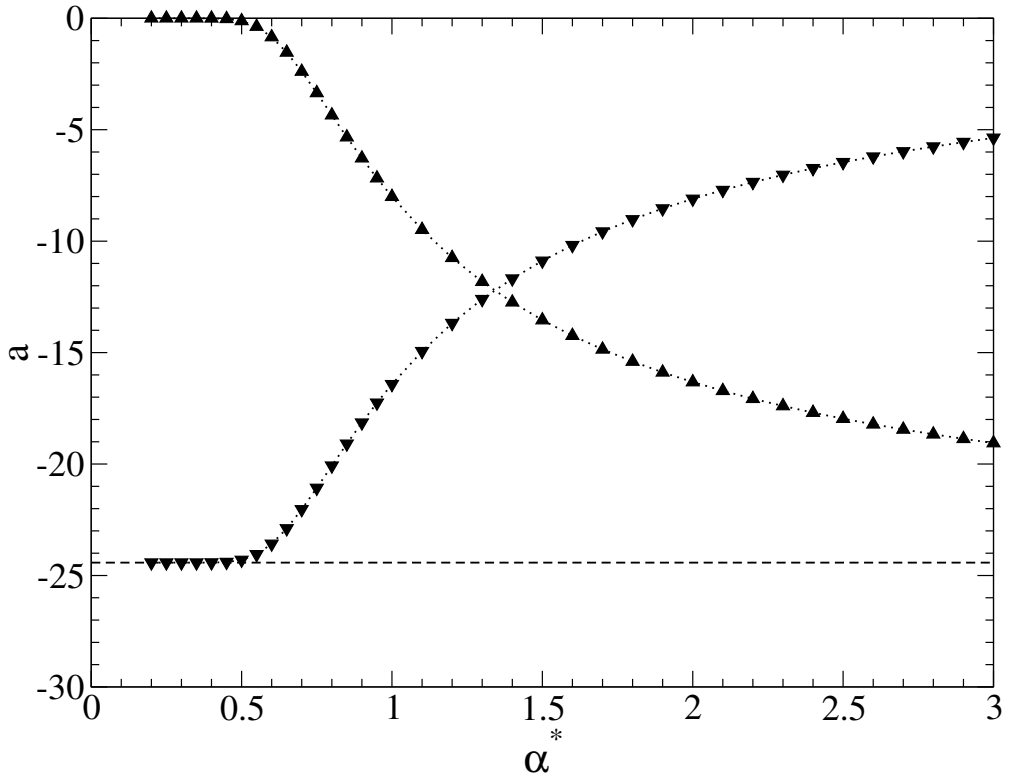

Fig. 3.4: Contributions to Helmholtz energy for varying α^* for $\rho^* = 0.6786$, $\mu^{*\,2} = 4.0$, $q^{*\,2} = 160$, $x = 0.176$: ▲ short-range contribution a^{sr} from simulations with α-integration; ▼ long-range contribution $a^{\mathrm{lr}}_{\mathrm{sim}}$ from simulations; −−− total residual Helmholtz energy a^{res} from simulation with λ-integration. Error bars are within symbol / line size.

3.4.2 Evaluation of the long-range term a^{lr}

For evaluating the analytical correction term of Rodgers and Weeks, Eq. (2.28), we can now compare this term with with simulation results for $a^{\mathrm{lr}}_{\mathrm{sim}}$. In Fig. 3.5, this is

done for the same state point as shown in Fig. 3.4. For very low values of α^*, the analytical term shows non-physical behavior as it diverges towards $-\infty$. With increasing α^*, however, a^{lr} approaches the simulation data. For any $1.5 \leq \alpha^* \leq 3$, it is within statistical uncertainties of the simulation data.

In order to assess Eq. (2.28) for various ion concentrations, we choose a different

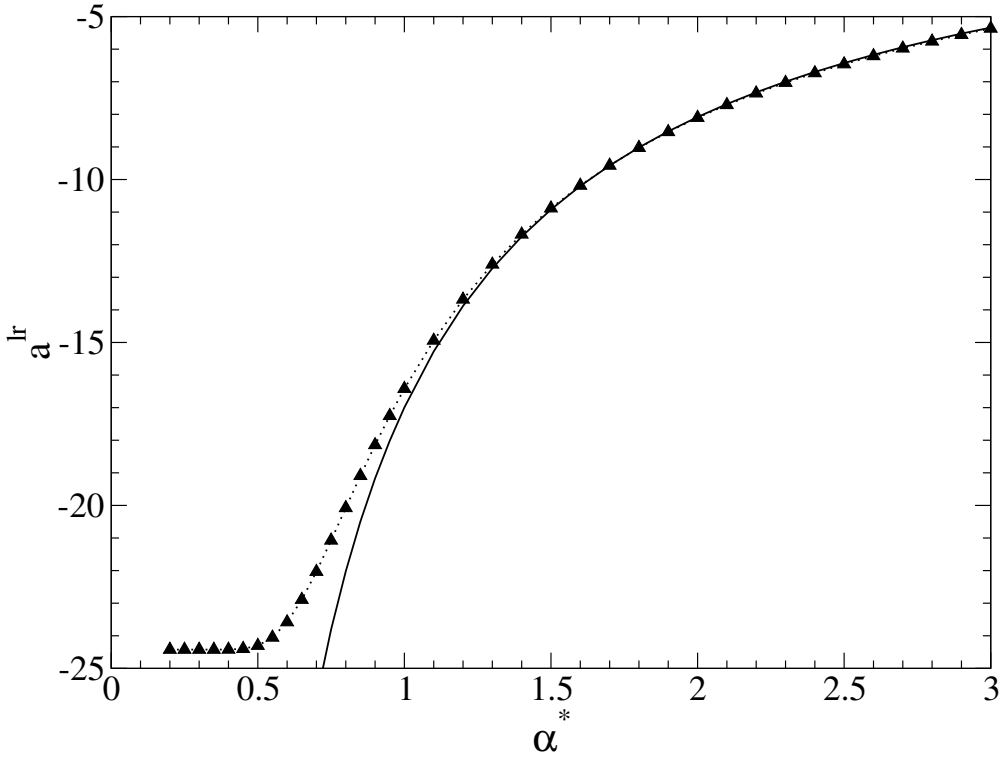

Fig. 3.5: Comparison of long-ranged Helmholtz energy contributions for $\rho^* = 0.6786$, $\mu^{*\,2} = 4.0$, $q^{*\,2} = 160$, $x = 0.176$: ▲ long-range contribution from molecular simulations, $a^{\mathrm{lr}}_{\mathrm{sim}}$; —— long-range correction a^{lr} of Rodgers and Weeks[102], Eq. (2.28). Error bars are within symbol size.

representation in Fig. 3.6. We add the quasi-exact short-ranged contribution a^{sr}_{α} obtained from molecular simulations to a^{lr} for two system-densities and at different ion concentrations x. As can be seen, a^{res} (and thus a^{lr}) is for all conditions in good agreement with the reference data a^{res} for $\alpha^* \geq 1.5$ (for liquid densities). A similar behavior was also observed by Rodgers and Weeks[102], however, in internal energy rather than in Helmholtz energy. They tested their correction term in molecular simulations of SPC/E water[125], using damped electrostatic pair potentials, applying Eq. (2.28) as a long-range contribution to the internal energy. For all state points we studied, the errors introduced by the expression a^{lr} of Rodgers and Weeks are well below 1 % for any $\alpha^* \geq 1.5$. We thus choose $\alpha^* = 1.5$ as the lowest possible value for which employing short-ranged pair potentials according to Eqs. (2.22), (2.24) and (2.25) together

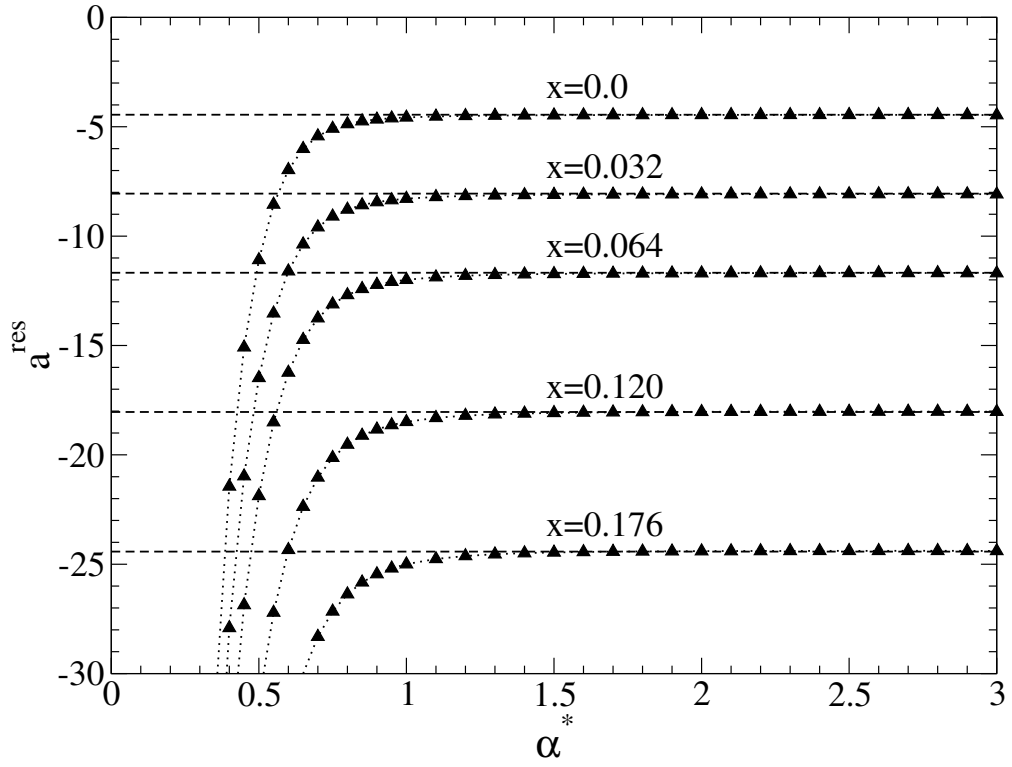

(a) $\rho^* = 0.6786$, $\mu^{*\,2} = 4.0$, $q^{*\,2} = 160$

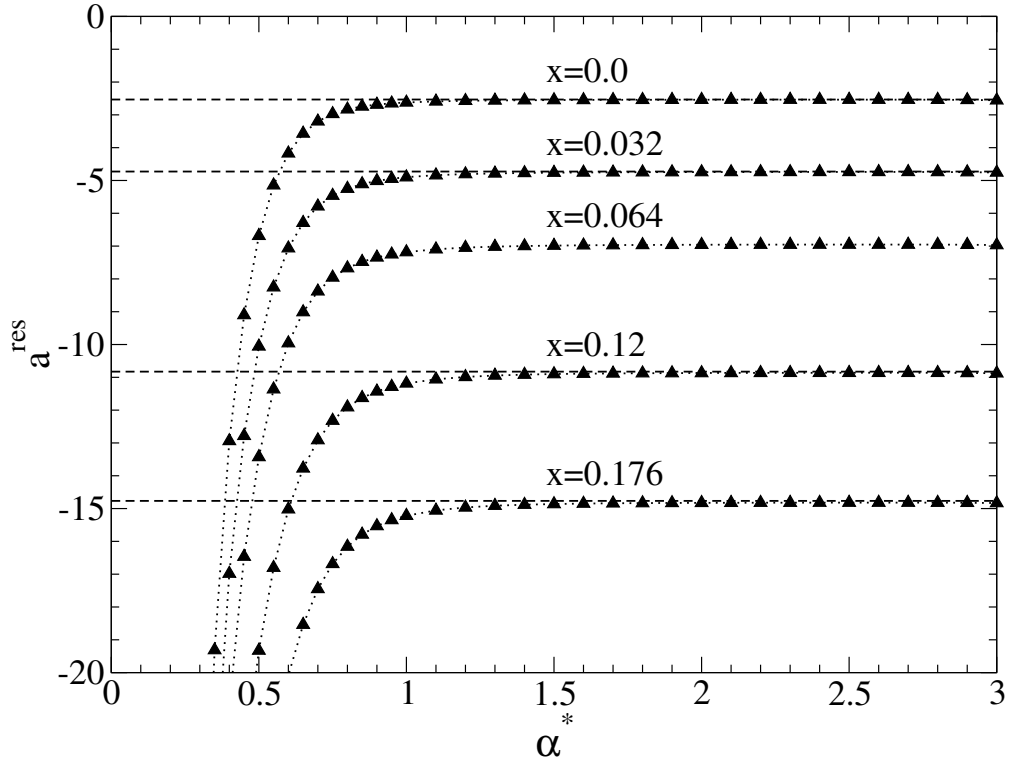

(b) $\rho^* = 0.8$, $\mu^{*\,2} = 2.5$, $q^{*\,2} = 100$

Fig. 3.6: Assessing a^{lr} for two different system-densities and for various ion mole fractions: ▲ $a^{\mathrm{res}} = a^{\mathrm{sr}} + a^{\mathrm{lr}}$ using the a^{lr}-expression of Rodgers and Weeks[102], Eq. (2.28); − − − a^{res} from λ-integration. Error bars are within symbol / line size.

with the expression for a^{lr} of Rodgers and Weeks gives sufficiently accurate results. The work of Weeks and coworkers shows that this choice of α^* also represents fluid structure, $g(r)$, of ionic model fluids for liquid-like densities[99,100]. It is important to note that this value might be different for systems that are significantly different from the ones considered in this work.

As a lower bound of α^* for the basic LMF, Weeks and coworkers[99,100,126,127] specified the nearest neighbor distance, $\alpha^*_{\mathrm{min}} = (2 \cdot \rho^*)^{-1/3}$. This requirement corresponds to $\alpha^*_{\mathrm{min}} = 0.903$ for $\rho^* = 0.6786$ and $\alpha^*_{\mathrm{min}} = 0.855$ for $\rho^* = 0.8$. This lower bound is not violated using a value of 1.5 for the densities we studied. Reasonable values for α^* to gain accurate thermodynamic results are, however, much larger than nearest neighbor distance, as has also been highlighted by Rodgers et al.[102,127]

An upper bound for α^* only exists when LMF approach is applied in molecular simulations. These errors, however, are not native in the long-range correction; they occur due to truncation of the short-ranged potential, as discussed in Sec. 3.2.2.

3.4.3 Evaluation of third order perturbation theory

Having validated the basic approach of our fluid theory, we can now use the simulation data directly for comparison with the theory.

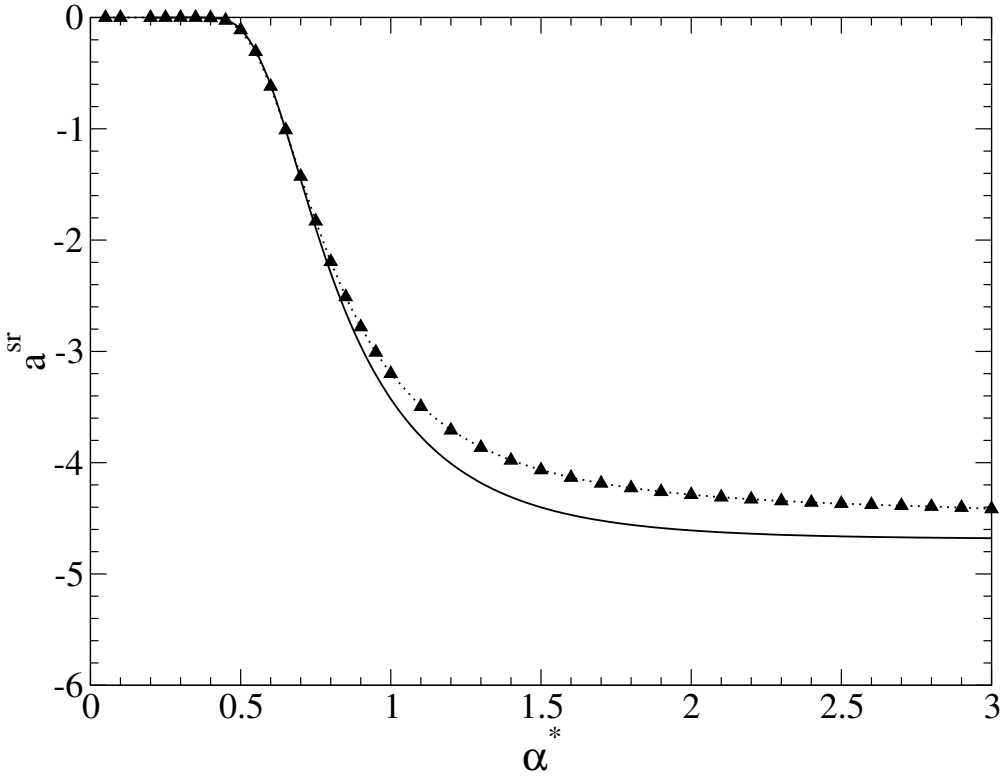

(a) $x = 0$ (pure dipolar fluid)

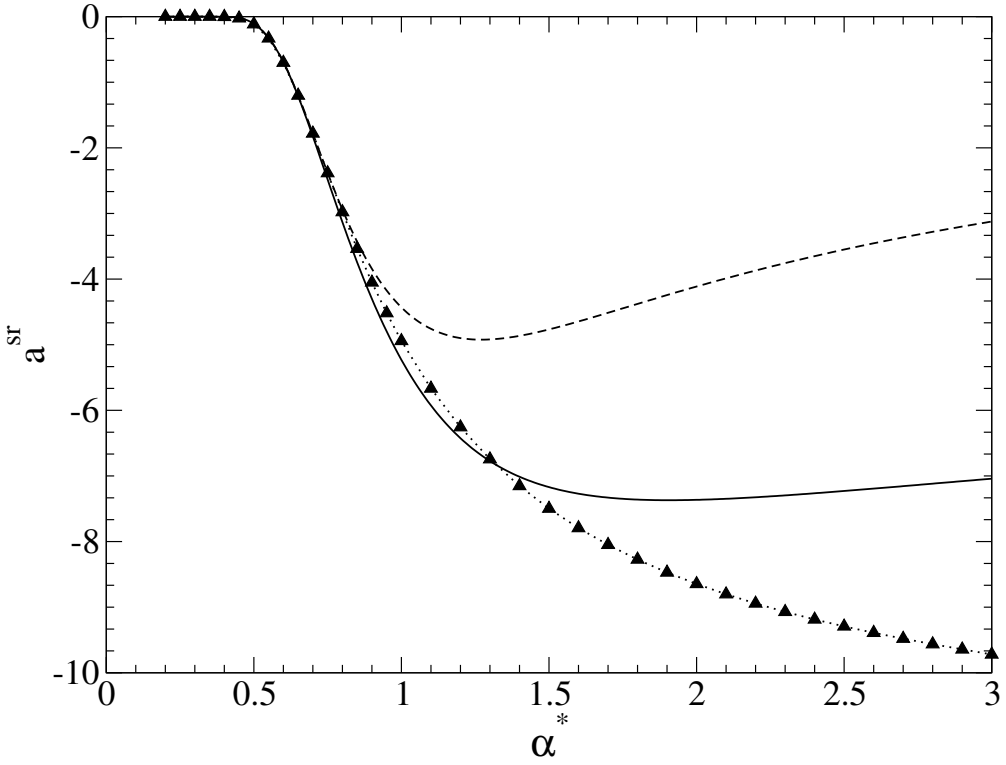

(b) $x = 0.064$

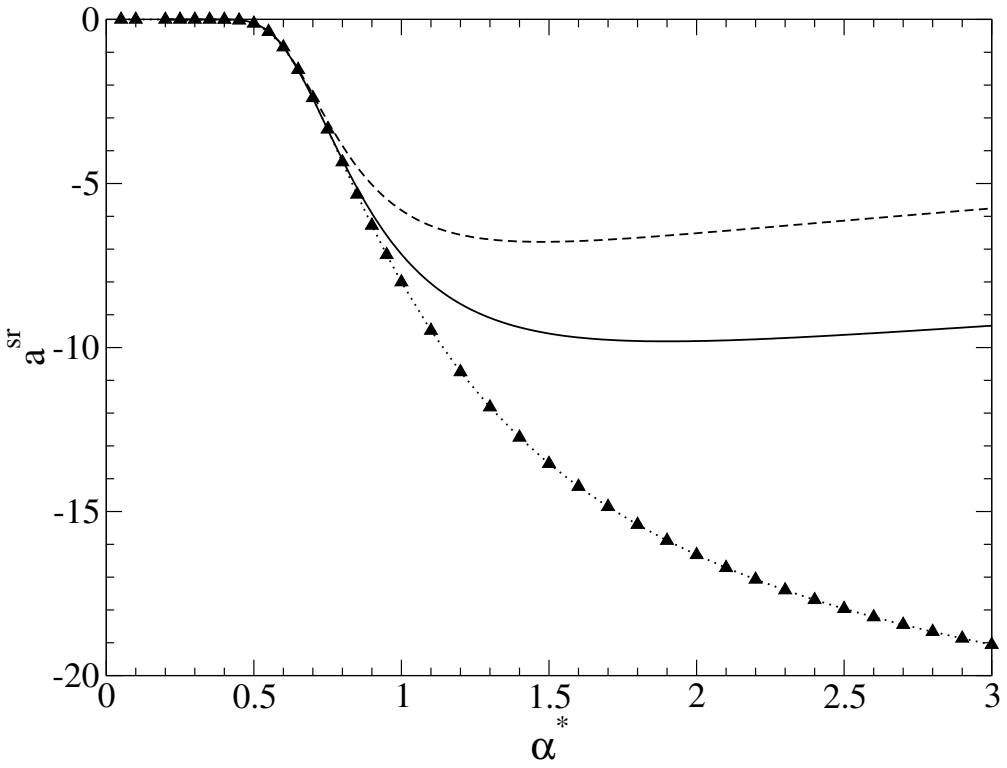

(c) $x = 0.176$

Fig. 3.7: Short-ranged Helmholtz energy: comparison of simulation data with the results of the perturbation theory for $\rho^* = 0.6786$, $\mu^{*\,2} = 4.0$, $q^{*\,2} = 160$: ▲ a^{sr} from molecular simulation; – – – a^{sr} from standard Padé approximation, Eq. (2.53); —— $a^{\mathrm{sr}}_{\mathrm{mod}}$ from modified Padé approximation, Eq. (2.55). Error bars are within symbol size.

In Fig. 3.7, the two variants of the Padé approximations for the third order theory introduced above are compared to results of molecular simulations. Fig. 3.7a shows the case of a pure dipolar fluid with $x = 0$. In that case, both Padé approximations from Eq. (2.53) and Eq. (2.55) are identical. For $\alpha^* \to \infty$ and $x = 0$, our theory approaches the one of Rushbrooke et al.[108] for the dipolar hard sphere fluid. For all state points containing ions (Fig. 3.7b and 3.7c), the modified Padé approximation given by Eq. (2.55) clearly gives much better results than the original one, Eq. (2.53). Both approximations match the simulated short-ranged contribution to Helmholtz energy well for low values of α^*. This is understood, because the perturbation expansion converges faster with decreasing α^*, and consequently the Padé approximated third order expansion gives the best results for low values of α^*. Unfortunately, also the theory with the new variant of the Padé approximation starts to deviate significantly from the reference simulation data for values of α^* outside of $\alpha^* < 0.9$. This conflicts with the analysis of the long-ranged part of the Helmholtz energy from the previous section, which is valid only for $\alpha^* \geq 1.5$. The deviations of theory from results of molecular

simulations further increase for higher ion concentrations.
There are two levels of approximation in the third order theory we are here studying. First, the perturbation expansion is truncated after the term of third order and rearranged in a Padé approximation, and secondly, the three-particle distribution function in the third order term is approximated with a Kirkwood superposition approximation. In Sec. 2.7, it is shown that errors caused by Kirkwood superposition approximation are below one percent. Thus, we conclude that for non-primitive model electrolyte solutions and to a lesser extent also for purely dipolar fluids, third order perturbation theory written as a Padé approximant is not sufficient.
There are two obvious approaches to improve the representation of the theory. First, we can formulate an effective third order theory in which we adjust the correlation integrals $I_{ij(k)}$ of the third order perturbation terms to molecular simulation data. The second approach is to formulate a theory of fourth order. The fourth order term requires numerical values of four-particle correlation integrals. Those six dimensional integrals contain four-particle correlation functions, and numerical solution with sufficient accuracy is demanding. Alternatively, one can either sample them in MC simulations as we did with the third order integrals in this work or one can adjust the fourth order theory to simulation data of a^{res}.
All of the suggested procedures can be carried out at a constant value of α^*. Removing the dependance on α^* significantly reduces the complexity of the theory. Our analysis suggests $\alpha^* = 1.5$ as a suitable value.

3.5 Conclusions

[...] The analytical LMF-term of Rodgers and Weeks[102] describing the long-range contribution of the electrostatic potential was found to be in excellent agreement to results from molecular simulations for a damping parameter $\alpha^* \geq 1.5$ for the liquid-like systems we studied. This finding confirms the approach of decomposing the electrostatic potential into a damped, short-range part, for which we formulate a perturbation theory and into a long-range part, is very promising for electrolyte solutions. For perturbation theories, the approach overcomes the problem of diverging correlation integrals and improves convergence of the perturbation expansion.
By comparison of the short-ranged contribution of perturbation theory with simulation data, we gained detailed information about the shortcomings of the theory. We showed that a modified Padé approximation according to Eq. (2.55), in which the charge-charge, the dipole-dipole and the charge-dipole terms are Padé approximated separately, can significantly improve the theory without changing the basic terms of

the perturbation expansion. However, even then, third order Taylor expansion gives good results only for low values of α^*. From this observation, we conclude that one should either formulate effective third order terms or one has to extend the theory to fourth order.

4 Chemical potential of nonprimitive model electrolyte solutions from molecular simulations

Parts of this chapter are literal quotes from the third publication, Ref. 3.
The origin of the sections is as follows:

- *Section 4.1 has not been published previously.*
- *Section 4.2, 4.3 and 4.4 including all subsections are literal quotes from the third publication, Ref. 3, where the sections have been published with identical headings as used in this work.*

4.1 Preliminary remark

For electrolyte solutions, it is convenient to give the chemical potential as mean ionic chemical potential $\mu_\pm$ (or, equivalently, the mean ionic activity coefficient $\gamma_\pm$). Here, the index '$\pm$' indicates a pair of ions, and thus in this notation the number of ion pairs is defined as $N_\pm = N_+ = N_-$. This differs from the description used in previous sections, where the ionic mole fraction x was defined as mole fraction of ions, $x = x_+ + x_-$, and accordingly the number of ions was defined as $N_I = N_+ + N_-$. In this section, it is crucial to carefully distinguish between the two notations. Henceforth, the index 'I' is used whenever I refer to the number of ions and index '$\pm$' is used to indicate quantities defined based on ion pairs.
The difference in notations also means that care has to be taken when evaluating chemical potential from the perturbation expansion presented above. The mean ionic chemical potential can be obtained as partial derivative of Helmholtz energy with respect to ion pairs, i.e. as

$$\mu_\pm(T, \rho, x_I) = \left(\frac{\partial A}{\partial N_\pm}\right)_{T,V,N_{j\neq I}} . \tag{4.1}$$

When evaluating the partial derivative of A with respect to the number of ions from the perturbation theory, one would calculate the chemical potential as

$$\mu_I(T, \rho, x_I) = \left(\frac{\partial A}{\partial N_I}\right)_{T,V,N_{j\neq I}} \tag{4.2}$$

due to the definition of the number of ions employed. Obviously, $N_I = 2 \cdot N_\pm$, and the mean ionic chemical potential can be easily converted from the theory as $\mu_\pm = 2 \cdot \mu_I$.

4.2 Simulation methods

We determine the chemical potential by sampling the transition probabilities between neighboring macrostates in Monte Carlo (MC) simulations. In this section, we describe how the chemical potential is estimated from those probabilities and we discuss different methods for their computation. A system size study is performed to ensure that finite size effects are negligible for the results of this study.

4.2.1 Chemical potential from transition probabilities

In molecular simulations, the mean ionic chemical potential at given density ρ, temperature T and ion concentration x_I can be calculated via

$$\begin{aligned}\mu_{\pm}(T,\rho,x_I) &= \left(\frac{\partial A}{\partial N_{\pm}}\right)_{T,V,N_{j\neq I}} \\ &\approx (A_{N+1} - A_N) = -\frac{1}{\beta}\ln\frac{Q_{N+1}}{Q_N}\end{aligned} \tag{4.3}$$

where A is the Helmholtz energy and Q is the partition function. Index 'N' indicates the N-particle system and index '$N+1$' refers to the N-particle system with an additional *pair* of ions. We use the formulation of $\mu_{\pm}$ in terms of ion pairs since we use standard Ewald summation, and thus have to ensure electroneutrality of the system at any time of the simulation.

From Eq. (4.3), it follows that the chemical potential relative to the ideal gas, denoted as residual part $\beta\mu_{\pm}^{\mathrm{res}}$ is

$$\beta\mu_{\pm}^{\mathrm{res}} = \beta\left(\mu_{\pm} - \mu_{\pm}^{\mathrm{ig}}\right) = -\ln\frac{Z_{N+1}}{Z_N} \tag{4.4}$$

where Z is the configuration integral and $\mu_{\pm}^{\mathrm{ig}}$ is the ideal gas chemical potential of the mixture. The ratio of partition functions in Eq. (4.4) can be calculated in different ways in molecular simulations.

The most common approach is Widom test particle method[75]. The prerequisite for the applicability of this approach is that the configurations in the N-particle system are a subset of the important region of the $(N+1)$-particle system. A very clear and detailed account of this prerequisite is given by Kofke and Cummings[128]. For high densities, for example, Widom test particle method is known to give wrong results because the test particle always overlaps with other particles in the system. Then, none of the tested $(N+1)$-particle configurations are part of the $(N+1)$-important configurational space.

For nonprimitive model electrolyte solutions, problems occur even for low densities because there is a very distinct structure surrounding ions, with very pronounced ordering of the dipolar particles or formation of highly ordered ion clusters. Therefore, inserting test particles without considering their surrounding structure does not resemble the $(N+1)$-important configurational space. This problem can be overcome by subdividing the region between the N- and the $(N+1)$-particle ensemble into subensembles in which the test particles (and thus, their corresponding surrounding structure) are

partially present. Then, the chemical potential can be written as

$$\beta\mu_{\pm}^{\mathrm{res}} = -\ln\left(\frac{Z_{N+\kappa_1}}{Z_{N+\kappa_0}}\cdot\frac{Z_{N+\kappa_2}}{Z_{N+\kappa_1}}\cdot\ldots\cdot\frac{Z_{N+\kappa_n}}{Z_{N+\kappa_{n-1}}}\right) \tag{4.5}$$

where for $\kappa_0 = 0$ the test particles are ideal gas particles and for $\kappa_n = 1$ the test particles are fully present. The κ_i between those values simply scale the potential parameter(s) of the test particle(s), e.g. the hard sphere diameter or the charge of the ions are scaled. By choosing κ_i properly, sufficient phase space (configurational space) overlaps towards the neighboring subensemble.
Various methods exist for calculating $Z_{N+\kappa_i}/Z_{N+\kappa_{i-1}}$ in simulations, and an overview of some common techniques is given e.g. in Ref. 128.
For the model electrolyte system regarded, it is useful to first separate the hard sphere contribution to the chemical potential according to

$$\beta\mu_{\pm}^{\mathrm{res}} = \beta\Delta\mu^{\mathrm{2hs}} + \beta\Delta\mu^{\mathrm{c}} \tag{4.6}$$

with

$$\beta\Delta\mu^{\mathrm{2hs}} = -\ln\left(\frac{Z_{N+\mathrm{2hs}}}{Z_N}\right) \tag{4.7}$$

$$\beta\Delta\mu^{\mathrm{c}} = -\ln\left(\frac{Z_{N+\kappa_1}}{Z_{N+\mathrm{2hs}}}\cdot\ldots\cdot\frac{Z_{N+\kappa_n}}{Z_{N+\kappa_{n-1}}}\right) \tag{4.8}$$

where the index '$N+2$hs' indicates the system of N particles plus two uncharged hard spheres, $\Delta\mu^{\mathrm{2hs}}$ is the chemical potential contribution of two uncharged hard spheres and $\Delta\mu^{\mathrm{c}}$ is the chemical potential arising from the charges. For large systems, $\Delta\mu^{\mathrm{2hs}}$ equals twice the chemical potential of one hard sphere, $\Delta\mu^{\mathrm{2hs}} \approx 2\cdot\Delta\mu^{\mathrm{hs}}$.
Separating the hard sphere contribution from the electrostatic part yields the advantage that $\Delta\mu^{\mathrm{hs}}$ can be calculated by standard Widom test particle method with very little statistical uncertainty for the densities studied in this work. We now focus on the more demanding calculation of the electrostatic part defined by Eq. (4.8), where κ_0 now denotes the system of N particles with two additional (uncharged) hard sphere particles.
The methods we use for the estimation of $\Delta\mu^{\mathrm{c}}$ are based on the calculation of the transition probabilities between the different states κ_i. The ratios of the partition functions are then replaced according to

$$\frac{Z_{N+\kappa_i}}{Z_{N+\kappa_{i-1}}} = \frac{P(\kappa_i)}{P(\kappa_{i-1})} \tag{4.9}$$

where $P(\kappa_i)$ and $P(\kappa_{i-1})$ denote the probabilities of finding the system in the macroscopic state $(N + \kappa_i)$ and $(N + \kappa_{i-1})$, respectively. In this work, we use capital letters for the macrostate probabilities and small letters for microstate probabilities. Further, we indicate subensembles by κ_i instead of $(N + \kappa_i)$.
Considering detailed balance for the macroscopic probabilities,

$$P(\kappa_i) \cdot T(\kappa_i \to \kappa_{i-1}) = P(\kappa_{i-1}) \cdot T(\kappa_{i-1} \to \kappa_i) \tag{4.10}$$

one can rewrite Eq. (4.9) as

$$\frac{Z_{N+\kappa_i}}{Z_{N+\kappa_{i-1}}} = \frac{T(\kappa_{i-1} \to \kappa_i)}{T(\kappa_i \to \kappa_{i-1})}. \tag{4.11}$$

with $T(\kappa_{i-1} \to \kappa_i)$ and $T(\kappa_i \to \kappa_{i-1})$ as transition probabilities from subensemble κ_{i-1} to κ_i and vice versa. Substituting Eq. (4.11) into Eq. (4.8) yields

$$\begin{aligned} \beta\Delta\mu^{\mathrm{c}} = -\ln \Bigg(& \frac{T(\kappa_0 \to \kappa_1)}{T(\kappa_1 \to \kappa_0)} \cdot \frac{T(\kappa_1 \to \kappa_2)}{T(\kappa_2 \to \kappa_1)} \\ & \times \ldots \cdot \frac{T(\kappa_{n-1} \to \kappa_n)}{T(\kappa_n \to \kappa_{n-1})} \Bigg) \end{aligned} \tag{4.12}$$

where for κ_0 the labeled (test) particles are two uncharged hard spheres. For evaluating the transition probabilities, we used two different methods.

Multistage sampling method

A very simple way to obtain the transition probabilities is simulating every subensemble κ_i in one single simulation. The transition probabilities to the neighboring subensembles κ_{i+1} and κ_{i-1}, henceforth jointly referred to as κ_j, are calculated by performing trial moves $\kappa_i \to \kappa_j$. From those trial moves, the macroscopic transition probabilities are obtained as

$$T(\kappa_i \to \kappa_j) = \langle t(\kappa_i \to \kappa_j) \rangle \,, \tag{4.13}$$

$$t(\kappa_i \to \kappa_j) = \min \left[1, \; \frac{p(\kappa_j)}{p(\kappa_i)} \right] \tag{4.14}$$

where $\langle ... \rangle$ denotes the canonical ensemble average, $t(\kappa_i \to \kappa_j)$ are the microscopic transition probabilities and $p(\kappa_{i,j}) = \exp(-\beta U(\kappa_{i,j}))$ are the probabilities of the microstates. In this work, we refer to this method as multistage sampling method.
It is a simple way of estimating the transition probabilities, but requires considerable simulation effort. We compared the method to the expanded ensemble transition ma-

trix method.

Expanded ensemble method

A computationally efficient method is the expanded ensemble[95,96] transition matrix (EETM) method[129–131]. In this work, we use the EETM method combined with Wang-Landau[97] approach as suggested by Shell et al.[132]. That approach was recently applied to electrolyte solutions by Paluch et al.[92,93].
The advantage of the EETM method is that all subensembles are sampled in one single simulation. This is achieved by not only performing subensemble changes $\kappa_i \to \kappa_j$ as trial moves, but also accepting them with a biased probability

$$t_b(\kappa_i \to \kappa_j) = \min\left[1,\ \frac{\exp(\eta_j)}{\exp(\eta_i)}\frac{p(\kappa_j)}{p(\kappa_i)}\right] \tag{4.15}$$

where $\eta_{i,j}$ are biasing weights of the different states $\kappa_{i,j}$.
The transition probabilities in this method are obtained from a collection matrix C that is collected as follows: If a move $\kappa_i \to \kappa_j$ is performed, the matrix is updated according to

$$C(\kappa_i, \kappa_i \to \kappa_j) \ \Rightarrow\ C(\kappa_i, \kappa_i \to \kappa_j) + t(\kappa_i \to \kappa_j) \tag{4.16}$$

$$C(\kappa_i, \kappa_i \to \kappa_i) \ \Rightarrow\ C(\kappa_i, \kappa_i \to \kappa_i) + 1 - t(\kappa_i \to \kappa_j) \tag{4.17}$$

where $t(\kappa_i \to \kappa_j)$ are the unbiased microscopic transition probabilities defined by Eq. (4.14). This matrix update is performed regardless if the move is accepted or not. If any other MC move is performed, the matrix update is

$$C(\kappa_i, \kappa_i \to \kappa_i) \ \Rightarrow\ C(\kappa_i, \kappa_i \to \kappa_i) + 1. \tag{4.18}$$

From this collection matrix, the desired macroscopic transition probabilities are calculated as

$$T(\kappa_i \to \kappa_j) = \frac{C(\kappa_i, \kappa_i \to \kappa_j)}{\sum_k C(\kappa_i, \kappa_i \to \kappa_k)}. \tag{4.19}$$

As can be seen from Eq. (4.16) to (4.19), the collection matrix C, and thus the transition probabilities $T(\kappa_i \to \kappa_j)$, are independent from the weight factors η_i. However, those weight factors are important for ensuring well-balanced sampling of all subensembles κ_i.

The bias potential can be chosen according to the problem at hand. We choose $\exp(\eta_j)/\exp(\eta_i) = P(\kappa_i)/P(\kappa_j)$ ensuring equal average acceptance ratios for trial moves towards other subensembles, because then $\exp(\eta_j)p(\kappa_j)/\exp(\eta_i)p(\kappa_i)$ (in Eq. (4.15)) is on average constant for all i and j. From detailed balance, Eq. (4.10), then follows

$$\frac{\exp(\eta_j)}{\exp(\eta_i)} = \frac{P(\kappa_i)}{P(\kappa_j)} = \frac{T(\kappa_j \to \kappa_i)}{T(\kappa_i \to \kappa_j)}. \tag{4.20}$$

Since only the ratios $\exp(\eta_j)/\exp(\eta_i)$ are required, one can arbitrarily set $\eta_0 = 0$ and obtain all other weight factors from

$$\eta_{i+1} = \eta_i + \ln \frac{T(\kappa_{i+1} \to \kappa_i)}{T(\kappa_i \to \kappa_{i+1})}. \tag{4.21}$$

for $0 \leq i \leq (n-1)$.
Employing Eq. (4.21) requires knowledge of the transition probabilities, which are of course unknown at the beginning of the simulation. Therefore, during equilibration of the simulations, we use a Wang-Landau scheme instead of Eq. (4.21) for obtaining the weight factors η_i. In the Wang-Landau scheme we initialize all η_i with zero and update any current state κ_i after every MC move according to

$$\eta_i \;\Rightarrow\; \eta_i - \gamma \tag{4.22}$$

where γ is a constant greater than 0. When every state κ_i has been visited at least 10,000 times, we lower γ by a constant factor τ,

$$\gamma \;\Rightarrow\; \tau \cdot \gamma \tag{4.23}$$

In this work, we started with $\gamma = 0.01$ and used $\tau = 0.2$. A sufficiently precise guess of the weight factors was then obtained very efficiently. We used the Wang-Landau procedure during the entire equilibration of the EETM simulations. In the production phase, the weight factors were obtained from Eq. (4.21). We started sampling a collection matrix C_w when $\gamma \leq 10^{-4}$. By combining the Wang-Landau with transition matrix scheme, we benefit from the advantages of both methods: while the Wang-Landau approach is known to give a good first estimate of the weight factors very efficiently, the transition matrix scheme converges faster and gives more accurate results. A more detailed discussion on that topic has been given, for example, by Shell et al.[132] and Maerzke et al.[133].

4.2.2 Finite size effects

We use the standard Ewald summation[103] for calculating the electrostatic interactions. The key feature of this method is that a system much larger than the one that simulated is mimicked by assuming that the simulation box is surrounded by periodic images of itself. The total electrostatic potential of one point charge is the sum of pair interactions with all other charges in the original box and with all image charges located in the image boxes, including its own images. For a detailed derivation and discussion of Ewald sum, see e.g. Refs. 123 and 122.

The concept of considering a labeled (test) ion pair infinitely often in their periodic images is in certain contradiction with Eq. (4.3) that requires adding a single pair of ions to the N-particle system. Using Ewald summation, we implicitly add a pair of ions to the simulation box as well as to every periodic image of the original box. Hence, we do not add one single pair of ions, but rather increase the ion pair density $\rho_\pm = N_\pm/V$ by $\Delta\rho_\pm = 1/V$ where V is the volume of the simulation box. However, Eq. (4.3) can be rewritten as

$$\begin{aligned}\mu_\pm(T,\rho,x_I) &= \left(\frac{\partial A}{\partial N_\pm}\right)_{T,V,N_{j\neq I}} = \frac{1}{V}\left(\frac{\partial A}{\partial \rho_\pm}\right)_{T,V,\rho_{j\neq I}} \\ &\approx (A_{\rho_\pm+\Delta\rho_\pm} - A_{\rho_\pm}.)\end{aligned} \tag{4.24}$$

From this, it can be seen that Ewald summation changes the increment of the numerical derivative from $\Delta N_\pm = 1$ to $\Delta\rho_\pm = 1/V$, but is a valid technique to use for our study. For infinitely large systems, Eq. (4.3) and Eq. (4.24) give identical results. However, when using systems of only a few hundred to thousand particles, the effects of system size on chemical potential need to be investigated carefully.

The system size study presented here involves both, the multistage sampling method described in Sec. 4.2.1 as well as the EETM scheme discussed in Sec. 4.2.1. Additionally, we tested a possible route to mimic an infinitely large system in which the test particles do not affect each other in any way. For this, we carried out simulations (using multistage sampling) omitting all of the test particle to test particle interactions in the trial moves ($\kappa_i \to \kappa_j$). This way, the *direct* influence of the test particle interactions on chemical potential is eliminated. It is important to note that by omitting those direct interactions, not all of their influence on each other is eliminated. Omitting particular interactions in Ewald summation is not entirely straightforward. Therefore, we give details of our implementation in Appendix D.

For testing the system size dependence of different procedures for calculating the chemical potential, we picked one exemplary state point and estimated the chemical potential

for varying particle numbers between 500 and 1500. In Fig. 4.1, the chemical potential contribution of the charges $\beta\Delta\mu^c$ obtained by the different methods is shown, for the inverse particle number $1/N$ as an abscissis. It can be seen that both, the multistage sampling approach and the EETM method show no significant system size dependence when standard Ewald summation is used. Furthermore, the results of those methods are in very good agreement. The chemical potentials are, within statistical uncertainty, identical for all N except for $N = 500$. In contrast, the multistage sampling method where the test particle interactions are omitted gives results very different from the other methods, with a pronounced system size dependence. For an infinitely large system ($1/N \to 0$), the results of all approaches should of course be identical. From this study we conclude that omitting the test particle interactions is not a good way of mimicking an infinitely large system.
Further, we conclude that standard Ewald summation is well suited for the multistage sampling approach as well as for the EETM method. The calculated chemical potentials do not show a pronounced system size dependence even for moderate number of particles. For the state point considered so far, 500 particles are sufficient for avoiding pronounced finite size effects. Because this finding should to some extent depend on the state point (e.g. ion concentration or ionic charge) we decided to perform all simulations with 1000 particles and using the standard Ewald sum.

4.2.3 Simulation details

The Ewald damping parameter was set to 5.6, and we used 7 k-vectors in each spacial direction.
The dipoles of the solute were modeled by two point charges of the same magnitude with opposite signs, separated by a distance of $0.1 \cdot \sigma$. The desired dipole moment μ^{*2} was adjusted by adjusting the strength of those point charges. Our previous work[1,2] confirmed that this set-up resembles point dipoles without measurable deviation. All simulations were carried out with a total of 1000 particles.
For all simulations (multistage sampling and EETM), we used 61 subensembles leading to 61 values of κ_i ranging from 0 to 1. For obtaining good statistical averages, we aimed for (approximately) constant ratios $T(\kappa_j \to \kappa_i)/T(\kappa_i \to \kappa_j)$. From Eq. (4.12), it can be seen that this is equivalent to equal contributions to chemical potential of all ratios $T(\kappa_j \to \kappa_i)/T(\kappa_i \to \kappa_j)$, and Eq. (4.21) shows that this also means constant steps in the weight factors, i.e. $\eta_{i+1} - \eta_i \approx$ const. We observed that constant steps in the weight factors can roughly be achieved by discretizing κ_i according to a square

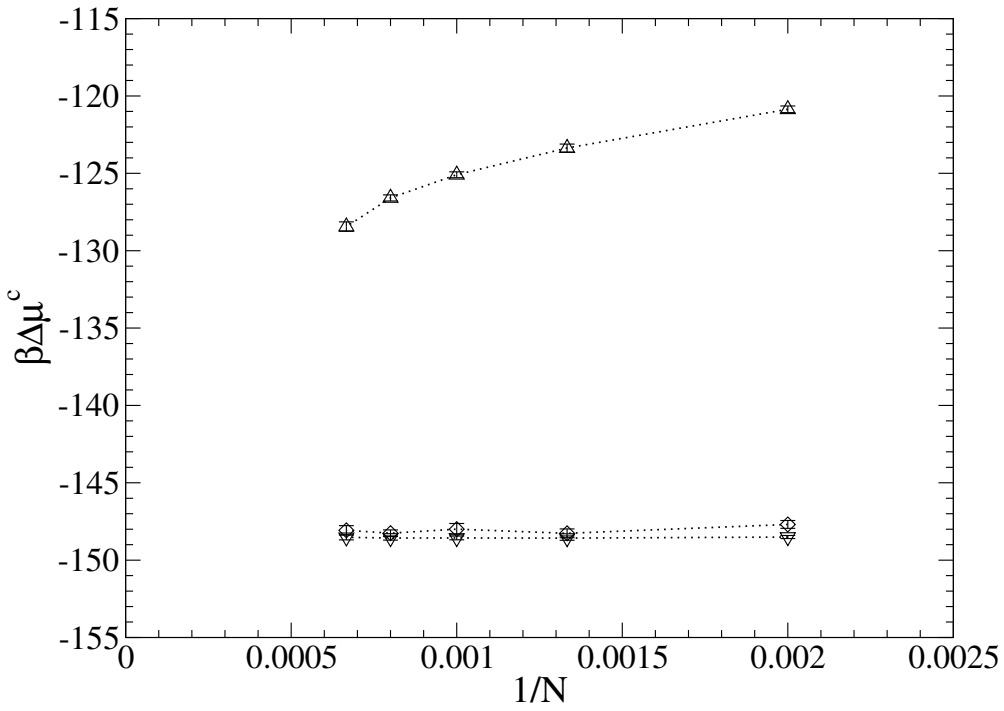

Fig. 4.1: System size dependence of the different methods for $\rho^* = 0.6786$, $\mu^{*2} = 4.0$, $q^{*2} = 100$, $x_I = 0.032$: $\triangle$ multistage sampling method without images; $\triangledown$ standard multistage sampling approach; $\diamond$ EETM method.

root function, according to $\kappa_i = \sqrt{\tilde{\kappa}_i}$ with $\tilde{\kappa}_i$ chosen equidistant between 0 and 1.
Besides translational and rotational MC moves, we also performed particle swap moves where two particles were interchanged in some cases. For those moves, we ensured equal probability of selecting any species. We first selected the species of the first particle with a probability of $1/N_{\mathrm{sp}}$, where N_{sp} is the number of species. Then, we randomly selected a particle of that species. The same procedure was repeated for picking the second particle. When swap moves were performed in simulations involving test particles, each of the two test particles was considered as an own species.
For estimating statistical uncertainty, the simulations were subdivided into 10 blocks. For every block, one individual chemical potential was estimated. The statistical uncertainty given in this work is the 95% confidence interval calculated from those 10 values.

Pre-equilibration

Equilibration of some of the systems we simulated is very demanding. Appendix C shows how maliciously slow some systems relax to an equilibrated state, due to the formation of charge clusters. For the sampling of the total chemical potential, we had to carry out at least two simulations, one for the hard sphere contribution and one

for the electrostatic part. For the multistage sampling method, even more simulations were required. To save computation time, we equilibrated all the N-particle systems of interest once and used those equilibrated systems to initialize simulations for sampling chemical potentials. We refer to the equilibration of the N-particle systems as pre-equilibration.

At the beginning of pre-equilibration runs, all particles were arranged on a cubic lattice configuration. Then, 10^6 particle swaps were performed without performing displacement or rotation moves. After this, a normal NVT simulation without particle swaps was carried out.

For all state points with an ion concentration $x_I < 0.064$, pre-equilibration was performed for $5 \cdot 10^5$ MC cycles. For $x_I \geq 0.064$, the N-particle systems were pre-equilibrated for $1.5 \cdot 10^6$ cycles. We define one MC cycle as N MC moves.

Hard sphere contribution

The contribution of two uncharged hard spheres defined by Eq. (4.6) was estimated by calculating the chemical potential of one hard sphere using a standard Widom test particle method and employing the relation $\beta\Delta\mu^{\mathrm{2hs}} \approx 2\beta\Delta\mu^{\mathrm{hs}}$.

Starting from pre-equilibrated systems, N trial test particle insertions were performed after every cycle for a total of 10^5cycles. For those simulations, no additional equilibration was carried out before sampling.

Multistage sampling method

For simulations with the multistage sampling approach, we carried out 61 independent simulations, one for each κ_i. At the beginning of each simulation, the two additional test particles were inserted into the pre-equilibrated N-particle systems (according to their Boltzmann weights). Then, 10^6 particle swaps were carried out without performing thermal moves. Afterwards, the systems were equilibrated for 10^5 cycles. After equilibration, the desired transition probabilities were sampled for $2 \cdot 10^5$ cycles. Trial moves $\kappa_i \rightarrow \kappa_j$ were performed after each cycle.

Expanded ensemble transition matrix method

Like the simulations with multistage sampling, the simulations with EETM sampling were also initiated by inserting two test particles into the pre-equilibrated N-particle systems, followed by equilibration for 10^5 cycles. During the equilibration period, we used the Wang-Landau method for estimating the weight factors η_i (Sec. 4.2.1). When $\gamma \leq 10^{-4}$, we started collecting a transition matrix C_w for subsequent weight factor

estimation from transition probabilities according to Eq. (4.21).
After equilibration, the weight factors were calculated from C_w and Eq. (4.21) instead of Wang-Landau method. We kept on sampling C_w for the entire simulation and updated the weight factors every 1000 cycles. Simultaneously, for estimating the chemical potential, a second transition matrix C_μ was sampled for a total of 10^6 MC cycles. We collected a second transition matrix, because for block averaging the chemical potential in 10 independent blocks, $\beta\Delta\mu_{\mathrm{c}}$ was calculated at the end of each block and the second transition matrix C_μ was zeroed afterwards.
During the entire EETM simulations, 10 % of the MC moves were trial subensemble changes ($\kappa_i \rightarrow \kappa_j$), 5 % were trial particle swaps and the rest were translational or rotational NVT moves.

4.3 Results

Before presenting our simulation results, we reemphasize that we observed very slow equilibration behavior for some state points. All state points in Tab. 4.1 marked with a '†' were, despite all effort, possibly not entirely equilibrated after pre-equilibration. Slow equilibration behavior as well as its impact on the data given in Tab. 4.1 is discussed in detail in Appendix C.
We carried out a series of simulations with constant density $\rho^* = 0.6786$. The results are summarized in Tab. 4.1. For this density, we separately varied ion mole fraction x_I, dipole moment μ^{*2} and ionic charge q^{*2}, in order to single out the appropriate parameter dependencies.
A first comparison between results from multistage sampling and from the EETM method was shown in section 4.2.2 in the context of studying the finite size effects. We further compare both sampling schemes by comparing values for the chemical potential from both methods for a system of $\mu^{*2} = 4.0$ and $q^{*2} = 100$ and for varying x_I. Tab. 4.1 confirms that both methods agree very convincingly for the entire concentration range. The deviation between the methods is below 1% for all considered state points, but the statistical uncertainty of the multistage sampling method is slightly smaller compared to the EETM method. The advantage of multistage sampling method is put into perspective, however, by the fact that calculating one value of $\beta\Delta\mu^{\mathrm{c}}$ through the multistage sampling approach requires more than 10 times the CPU time of a corresponding EETM simulation. We therefore conclude that the EETM method is superior to the multistage sampling approach due to the much higher efficiency. The rest of the data we present was obtained using EETM sampling.

Tab. 4.1: Results for the ionic chemical potential of hard dipoles and hard ions at a constant density, $\rho^* = 0.6786$. The sampling methods, multistage sampling (MS) or EETM, determine the electrostatic part only. Identical hard-sphere contributions were used for sampling methods. For state points marked with '†' we found particularly slow equilibration behavior, see Appendix C. The numbers in brackets give the uncertainty of the last digit(s).

x_I	$2\beta\Delta\mu^{\mathrm{hs}}$	$\beta\Delta\mu^{\mathrm{c}}$	$\beta\mu_{\pm}^{\mathrm{res}}$
$\mu^{*2} = 4.0$; $q^{*2} = 100$; EETM method			
0.016	11.32 (5)	−147.92 (17)	−136.60 (22)
0.032	11.21 (7)	−148.00 (37)	−136.79 (43)
0.064	11.07 (6)	−148.05 (29)	−136.98 (35)
0.096	10.87 (5)	−149.00 (47)	−138.14 (52)
0.128	10.64 (5)	−149.67 (30)	−139.03 (36)
0.160†	10.42 (4)	−149.68 (42)	−139.26 (46)
0.192†	10.26 (4)	−150.20 (49)	−139.94 (54)
$\mu^{*2} = 4.0$; $q^{*2} = 100$; MS method			
0.016	11.32 (5)	−148.26 (10)	−136.95 (14)
0.032	11.21 (7)	−148.57 (12)	−137.36 (19)
0.064	11.07 (6)	−149.31 (25)	−138.23 (31)
0.096	10.87 (5)	−149.42 (19)	−138.55 (23)
0.128	10.64 (5)	−149.98 (21)	−139.34 (26)
0.160†	10.42 (4)	−150.42 (27)	−140.00 (31)
$\mu^{*2} = 2.5$; $q^{*2} = 100$; EETM method			
0.016	12.33 (5)	−142.15 (19)	−129.82 (24)
0.032	12.20 (4)	−142.79 (17)	−130.59 (21)
0.064	11.98 (3)	−145.21 (57)	−133.23 (60)
0.096	11.79 (4)	−145.56 (35)	−133.78 (39)
0.128†	11.55 (4)	−146.72 (64)	−135.17 (68)
$\mu^{*2} = 4.0$; $q^{*2} = 160$; EETM method			
0.016	11.23 (5)	−237.98 (35)	−226.75 (40)
0.032	11.09 (9)	−238.77 (48)	−227.68 (57)
0.064	10.83 (5)	−238.78 (40)	−227.95 (45)
0.096	10.58 (6)	−239.93 (132)	−229.35 (138)
0.128	10.30 (9)	−240.12 (37)	−229.82 (47)
0.160†	10.01 (9)	−240.74 (59)	−230.73 (68)
0.192†	9.69 (9)	−242.98 (129)	−233.29 (138)

Fig. 4.2 gives a graphical representation of the total chemical potential $\beta\mu_{\pm}^{\mathrm{res}}$ with varying ion mole fraction x_I for constant density $\rho^* = 0.6786$, dipole moment $\mu^{*2} = 4.0$ and ionic charge $q^{*2} = 100$. The diagram shows results of two additional calculation series: one for a system with increased ionic charge ($q^{*2} = 160$) and one system with decreased dipole moment ($\mu^{*2} = 2.5$). All of the data series show an approximately linear course

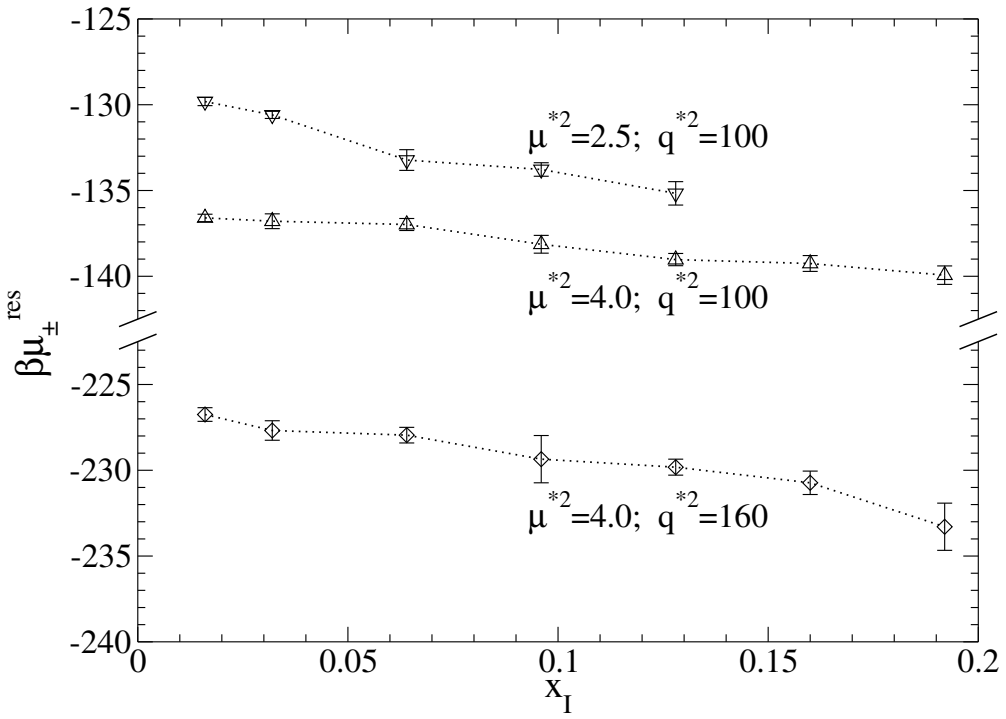

Fig. 4.2: Residual chemical potential $\beta\mu_{\pm}^{\mathrm{res}}$ for varying ion mole fraction x_I at a constant density $\rho^* = 0.6786$.

of chemical potential with changing x_I. Additionally it can be seen that the chemical potential only slightly decreases with increasing ion concentration. This observation is in agreement with previous studies that found nearly linear behavior of Helmholtz energy with varying ion concentration[1,2,55]. The results presented in Fig. 4.2 show that a significant variation of $\mu^{*2} = 4.0$ by 37.5% changes the chemical potential by only about 4 to 5%. Whereas increasing the charge by 60% (from $q^{*2} = 100$ to 160) at fixed $\mu^{*2} = 4.0$ leads to a pronounced decrease of chemical potential of about 65%. Thus, as expected, the chemical potential is dominated by the permanent charges q^{*2}. We proceeded with analyzing a variation of the total density ρ^* at fixed $\mu^{*2} = 4.0$ and $q^{*2} = 100$. We investigated total densities of $\rho^* = 0.6$ and 0.8 and determined the chemical potential for a number of different ion mole fractions x_I. The results are summarized in Tab. 4.2.

In Fig. 4.3 visualizes how the chemical potential changes with total density ρ^* for $\mu^{*2} = 4.0$, $q^{*2} = 100$ and for two different ion mole fractions, $x_I = 0.016$ and 0.128,

Tab. 4.2: Results for the ionic chemical potential for systems with dipole moment $\mu^{*2} = 4.0$, ionic charge $q^{*2} = 100$ obtained from the EETM method. The numbers in brackets give the uncertainty of the last digit(s).

x_I	$2\beta\Delta\mu^{\mathrm{hs}}$	$\beta\Delta\mu^{\mathrm{c}}$	$\beta\mu_{\pm}^{\mathrm{res}}$
$\rho^* = 0.6$			
0.016	8.66 (3)	−145.59 (22)	−136.93 (25)
0.032	8.58 (4)	−145.66 (10)	−137.09 (14)
0.064	8.41 (3)	−146.52 (38)	−138.11 (41)
0.096	8.25 (3)	−146.27 (27)	−138.02 (31)
0.128	8.04 (2)	−147.40 (47)	−139.37 (49)
$\rho^* = 0.8$			
0.016	8.66 (3)	−145.59 (22)	−136.93 (25)
0.032	8.58 (4)	−145.66 (10)	−137.09 (14)
0.064	8.41 (3)	−146.52 (38)	−138.11 (41)
0.096	8.25 (3)	−146.27 (27)	−138.02 (31)
0.128	8.04 (2)	−147.40 (47)	−139.37 (49)

respectively. The diagram shows the total chemical potential, $\beta\mu_{\pm}^{\mathrm{res}}$, but also only the electrostatic part of the chemical potential, $\Delta\mu^{\mathrm{c}}$. Whereas $\Delta\mu^{\mathrm{c}}$ decreases with increasing density, the total chemical potential increases. That is caused by the rapidly increasing hard sphere contribution. It can be concluded that the magnitude of chemical potential is determined by the electrostatic interactions. The slope of $\beta\mu_{\pm}^{\mathrm{res}}$ in direction of varying ρ^*, however, is mainly determined by the repulsive hard sphere interactions.

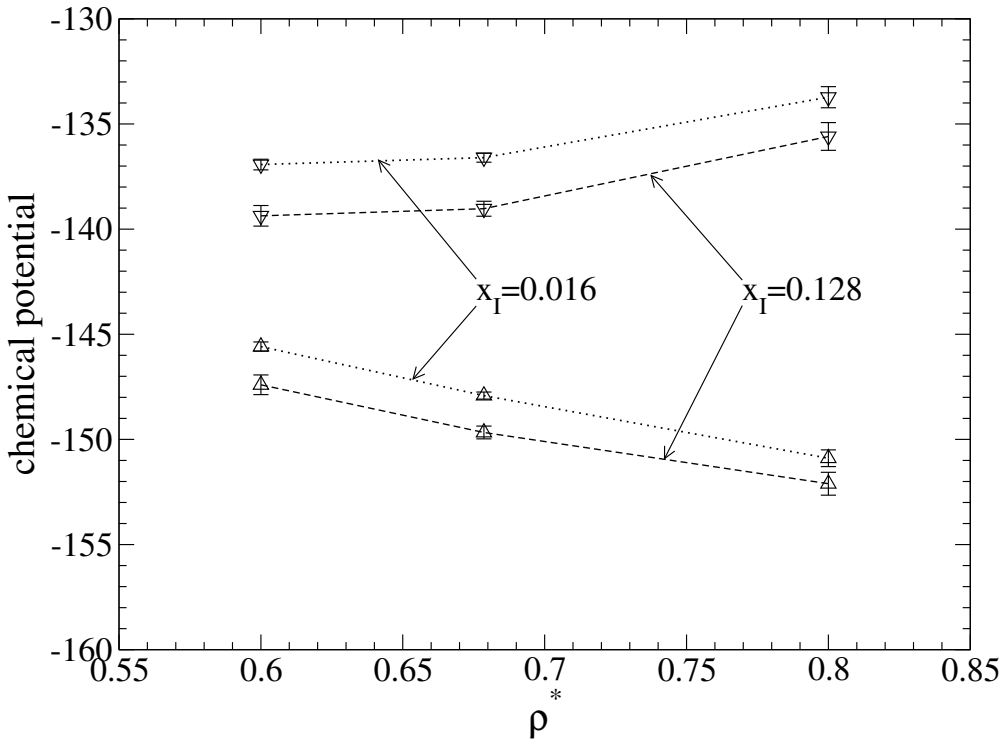

Fig. 4.3: Chemical potential contributions for varying density for $\mu^{*2} = 4.0$, $q^{*2} = 100$: $\triangle$ electrostatic contribution $\beta\Delta\mu^{c}$; $\triangledown$ residual chemical potential $\beta\mu_{\pm}^{res}$

4.4 Conclusions

This work provides values for ionic chemical potentials for the restricted nonprimitive model of electrolyte solutions consisting of hard sphere dipoles and hard-sphere cations and anions. We investigated systems with varying charge, dipole moment, ion mole fraction and density. The electrostatic part of the chemical potential, $\beta\Delta\mu^{c}$, was calculated from the transition probabilities of neighboring macrostates. Those probabilities were obtained from two different methods, i.e. multistage sampling and expanded ensemble transition matrix (EETM) sampling. We showed that both methods give almost identical results, with the EETM method being superior due to higher computational efficiency.

We carefully analyzed finite size effects of two different approaches for mimicking an infinitely large system when using Ewald summation for the electrostatic interactions. We showed that employing standard Ewald summation is a suitable method for determining the chemical potential from transition probabilities.

5 Summary

In this work, a new framework for formulating a perturbation theory for nonprimitive model electrolyte solutions has been developed. The diverging correlation integrals appearing in native perturbation expansions have been avoided by splitting the intermolecular pair potential into a short- and a long-ranged term. I developed a perturbation theory in terms of short-ranged potentials that yields converging correlation integrals. The Helmholtz energy for the long-ranged pair potential is captured in an analytical term derived from local molecular field (LMF) theory.

Monte Carlo (MC) molecular simulation method has been used for distinct computation of quantities of model electrolyte solutions. With the simulation data, assumptions that were made when deriving and applying the theory, i.e. Kirkwood superposition approximation and the assumption of infinite static dielectric constant, were assessed and I found them to be sufficiently justified.

By computing total Helmholtz energies for model electrolyte solutions consisting of dipolar hard spheres and charged hard spheres and by computing the contribution to Helmholtz energy arising from the short-ranged part of the electrostatic pair potentials, the basic framework and the applicability of LMF theory to the model system has been validated. The work showed that parameter α^* that defines the split between the short- and long-ranged part of the potential needs to be equal or larger than 1.5 for obtaining accurate results from LMF approach.

By comparing the third order perturbation theory with the MC data, the main deficiency of the theory, i.e. the limitation to order three, could be revealed. It was shown that the Padé-approximated theory for electrolyte solutions is only satisfyingly accurate for low values of α^* (well below $\alpha^* = 1.5$). This leaves a conflict with the finding that α^* should be at least 1.5 for LMF theory to be sufficiently accurate. I therefore conclude that the short-ranged contribution to Helmholtz energy, i.e. the perturbation expansion, needs to be modified. This can be either achieved by evaluating higher order terms or by forming an effective third order theory e.g. by adjusting the values of the correlation integrals to MC data.

In order to validate Kirkwood superposition approximation, a method for computing correlation integrals in MC simulations has been implemented successfully. Some further optimization of this method with respect to computation time can lead to efficient estimations of the fourth order terms of the perturbation theory.

In addition to developing a new fluid theory for electrolyte solutions, comprehensive simulation data for nonprimitive model electrolyte solutions is presented in this work. This data can be used for assessing and refining the presented theory as well as other fluid theories that employ the same molecular model.

References

[1] F. Drunsel, W. Zmpitas, J. Gross, A new perturbation theory for electrolyte solutions, J. Chem. Phys. 141 (2014) 054103.

[2] F. Drunsel, J. Gross, Theory of model electrolyte solutions: Assessing the short- and long-ranged contributions by molecular simulations, Fluid Phase Equilib. 430 (2016) 195.

[3] F. Drunsel, J. Gross, Chemical potential of model electrolyte solutions consisting of hard sphere ions and hard dipoles from molecular simulations, Fluid Phase Equilib. 429 (2016) 205.

[4] J.-P. Hansen, I. R. McDonald, Theory of simple liquids, Elsevier, 1990.

[5] C. Gray, K. Gubbins, Theory of Molecular Fluids: Vol. 1: Fundamentals, Clarendon Press, 1984.

[6] R. W. Zwanzig, High-temperature equation of state by a perturbation method. I. Nonpolar gases, J. Chem. Phys. 22 (1954) 1420.

[7] J. A. Barker, D. Henderson, Perturbation theory and equation of state for fluids. II. A successful theory of liquids, J. Chem. Phys. 47 (1967) 4714.

[8] J. A. Barker, D. Henderson, What is "liquid"? Understanding the states of matter, Rev. Mod. Phys. 48 (1976) 587.

[9] D. Chandler, J. D. Weeks, Equilibrium structure of simple liquids, Phys. Rev. Lett. 25 (1970) 149.

[10] H. C. Andersen, D. Chandler, Mode expansion in equilibrium statistical mechanics. III. Optimized convergence and application to ionic solution theory, J. Chem. Phys. 55 (1971) 1497.

[11] J. D. Weeks, D. Chandler, H. C. Andersen, Role of repulsive forces in determining the equilibrium structure of simple liquids, J. Chem. Phys. 54 (1971) 5237.

[12] T. van Westen, J. Gross, A critical evaluation of perturbation theories by Monte Carlo simulation of the first four perturbation terms in a Helmholtz energy expansion for the Lennard-Jones fluid, J. Chem. Phys. 147 (2017) 014503.

[13] A. Mulero, Theory and Simulation of Hard–Sphere Fluids and Related Systems, Springer, Berlin, Heidelberg, 2008.

[14] N. F. Carnahan, K. E. Starling, Equation of state for nonattracting rigid spheres, J. Chem. Phys. 51 (1969) 635.

[15] A. Mulero, C. Galán, M. Parra, F. Cuadros, Equations of State for Hard Spheres and Hard Disks. In: Mulero A. (eds), Theory and Simulation of Hard-Sphere Fluids and Related Systems. Lecture Notes in Physics, volume 753, Springer, Berlin, Heidelberg, 2008.

[16] J. R. Loehe, M. D. Donohue, Recent advances in modeling thermodynamic properties of aqueous strong electrolyte systems, AIChE J. 43 (1997) 180.

[17] Y. Li, Recent advances in the use of statistical mechanics to establish molecular thermodynamic

models for electrolyte solutions, Tsinghua Sci. Technol. 9 (2004) 444.

[18] L. L. Lee, Molecular Thermdynamics of Electrolyte Solutions, World Scientific Publishing Co. Pte. Ltd., 2008.

[19] W. Raatschen, A. H. Harvey, J. M. Prausnitz, Equation of state for solutions of electrolytes in mixed solvents, Fluid Phase Equilib. 38 (1987) 19.

[20] H.-G. Simon, H. Kistenmacher, J. M. Prausnitz, D. Vortmeyer, An equation of state for systems containing electrolytes and nonelectrolytes, Chem. Eng. Process 29 (1991) 139.

[21] J. Wu, J. M. Prausnitz, Phase equilibria for systems containing hydrocarbons, water, and salt: An extended peng–robinson equation of state, Ind. Eng. Chem. Res. 37 (1998) 1634.

[22] J. A. Myers, S. I. Sandler, R. H. Wood, An equation of state for electrolyte solutions covering wide ranges of temperature, pressure, and composition, Ind. Eng. Chem. Res. 41 (2002) 3282.

[23] R. Inchekel, J.-C. de Hemptinne, W. Fürst, The simultaneous representation of dielectric constant, volume and activity coefficients using an electrolyte equation of state, Fluid Phase Equilib. 271 (2008) 19.

[24] B. Maribo-Mogensen, G. M. Kontogeorgis, K. Thomsen, Comparison of the Debye-Hückel and the Mean Spherical Approximation theories for electrolyte solutions, Ind. Eng. Chem. Res. 51 (2012) 5353.

[25] L. Ornstein, F. Zernike, Accidental deviations of density and opalescence at the critical point of a single substance, Proc. Akad. Sci. (Amsterdam) 17 (1914) 793.

[26] J. P. Valleau, L. K. Cohen, D. N. Card, Primitive model electrolytes. II. The symmetrical electrolyte, J. Chem. Phys. 72 (1980) 5942.

[27] J. S. Høye, E. Lomba, G. Stell, Analysis of the hypernetted chain equation for ionic fluids, Mol. Phys. 79 (1993) 523.

[28] L. Blum, Mean spherical model for asymmetric electrolytes: I. Method of solution, Mol. Phys. 30 (1975) 1529.

[29] L. Blum, J. Høye, Mean spherical model for asymmetric electrolytes. 2. Thermodynamic properties and the pair correlation function, J. Phys. Chem. 81 (1977) 1311.

[30] P. Debye, E. Hückel, Zur Theorie der Elektrolyte. I. Gefrierpunktserniedrigung und verwandte Erscheinungen, Physikalische Zeitschrift 24 (1923) 185.

[31] E. Waisman, J. L. Lebowitz, Mean spherical model integral equation for charged hard spheres I. Method of solution, J. Chem. Phys. 56 (1972) 3086.

[32] E. Waisman, J. L. Lebowitz, Mean spherical model integral equation for charged hard spheres. II. Results, J. Chem. Phys. 56 (1972) 3093.

[33] Y. Lin, K. Thomsen, J.-C. de Hemptinne, Multicomponent equations of state for electrolytes, AIChE J. 53 (2007) 989.

[34] C. Li, Y. Li, J. Lu, L. Yang, Study of the ionic activity coefficients in aqueous electrolytes by the non-primitive Mean Spherical Approximation equation, Fluid Phase Equilib. 124 (1996) 99.

[35] W. Liu, Y. Li, J. Lu, Comparison of perturbation theory and Mean Spherical Approximation based on molecular simulation data, Chin. J. Chem. Eng. 1 (1999) 10.

[36] W.-B. Liu, Z.-P. Liu, Y.-G. Li, J.-F. Lu, Comparison of perturbation theory and Mean Spherical Approximation for polar fluids and ion–dipole mixtures based on molecular simulation data, Fluid Phase Equilib. 178 (2001) 45.

[37] R. Triolo, J. R. Grigera, L. Blum, Simple electrolytes in the Mean Spherical Approximation, J. Phys. Chem. 80 (1976) 1858.

[38] R. Triolo, L. Blum, M. A. Floriano, Simple electrolytes in the Mean Spherical Approximation. III. A workable model for aqueous solutions, J. Chem. Phys. 67 (1977) 5956.

[39] R. Triolo, L. Blum, M. A. Floriano, Simple electrolytes in the Mean Spherical Approximation. 2. Study of a refined model, J. Phys. Chem. 82 (1978) 1368.

[40] J.-F. Lu, Y.-X. Yu, Y.-G. Li, Modification and application of the Mean Spherical Approximation method, Fluid Phase Equilib. 85 (1993) 81.

[41] G. Stell, J. L. Lebowitz, Equilibrium properties of a system of charged particles, J. Chem. Phys. 48 (1968) 3706.

[42] B. Larsen, J. Rasaiah, G. Stell, Thermodynamic perturbation theory for multipolar and ionic liquids, Mol. Phys. 33 (1977) 987.

[43] K.-Y. Chan, Comparison of a primitive model perturbation theory with experimental data of simple electrolytes, J. Phys. Chem. 94 (1990) 8472.

[44] L. Blum, Solution of a model for the solvent–electrolyte interactions in the Mean Spherical Approximation, J. Chem. Phys. 61 (1974) 2129.

[45] S. A. Adelman, J. M. Deutch, Exact solution of the mean spherical model for strong electrolytes in polar solvents, J. Chem. Phys. 60 (1974) 3935.

[46] D. Wei, L. Blum, The Mean Spherical Approximation for an arbitrary mixture of ions in a dipolar solvent: Approximate solution, pair correlation functions, and thermodynamics, J. Chem. Phys. 87 (1987) 2999.

[47] L. Blum, D. Wei, Analytical solution of the Mean Spherical Approximation for an arbitrary mixture of ions in a dipolar solvent, J. Chem. Phys. 87 (1987) 555.

[48] Z.-P. Liu, Y.-G. Li, J.-F. Lu, Low-density expansion of the solution of Mean Spherical Approximation for ion–dipole mixtures, J. Phys. Chem. B 106 (2002) 5266.

[49] N. Seyfkar, C. Ghotbi, V. Taghikhani, G. Azimi, Application of the non-primitive MSA-based models in predicting the activity and the osmotic coefficients of aqueous electrolyte solutions, Fluid Phase Equilib. 221 (2004) 189.

[50] S. Herzog, J. Gross, W. Arlt, Equation of state for aqueous electrolyte systems based on the semirestricted non-primitive Mean Spherical Approximation, Fluid Phase Equilib. 297 (2010) 23.

[51] D. Henderson, L. Blum, A. Tani, Equation of state of ionic fluids, ACS Symp. Ser. 300 (1986) 281.

[52] K.-Y. Chan, K. E. Gubbins, D. Henderson, L. Blum, Monte carlo and simple theoretical calculations for ion-dipole mixtures, Mol. Phys. 66 (1989) 299.

[53] J. Wu, J. Lu, Y. Li, A new perturbation method for electrolyte solutions based on MSA, Fluid Phase Equilib. 101 (1994) 121.

[54] K.-Y. Chan, Ion–dipole perturbation theory applied to simple electrolytes, J. Phys. Chem. 95 (1991) 7465.

[55] J. Eggebrecht, P. Ozler, Multipolar electrolyte solution models. I. Computer simulation of the charged and dipolar hard sphere mixture, J. Chem. Phys. 93 (1990) 2004.

[56] J. Eggebrecht, G. H. Peters, Multipolar electrolyte solution models. II. Monte carlo convergence and size dependence, J. Chem. Phys. 98 (1993) 1539.

[57] G. Peters, J. Eggebrecht, Multipolar electrolyte solution models. III. Free energy of the charged and dipolar hard sphere mixture, J. Chem. Phys. 98 (1993) 1546.

[58] J. Eggebrecht, P. Ozler, Multipolar electrolyte solution models. IV. Thermodynamic perturba-

tion theory, J. Chem. Phys. 98 (1993) 1552.

[59] W. Cong, Y. Li, J. Lu, A study of a nonprimitive model for electrolyte solutions based on perturbation theory, J. Solution Chem. 25 (1996) 1213.

[60] D. N. Card, J. P. Valleau, Monte Carlo study of the thermodynamics of electrolyte solutions, J. Chem. Phys. 52 (1970) 6232.

[61] W. van Megen, I. Snook, The grand canonical ensemble Monte Carlo method applied to electrolyte solutions, Mol. Phys. 39 (1980) 1043.

[62] J. P. Valleau, L. K. Cohen, Primitive model electrolytes. I. Grand canonical Monte Carlo computations, J. Chem. Phys. 72 (1980) 5935.

[63] P. Sloth, T. S. Sørensen, Monte Carlo simulations of single-ion chemical potentials. Preliminary results for the restricted primitive model, Chem. Phys. Lett. 143 (1988) 140.

[64] P. Sloth, T. S. Sørensen, Monte Carlo simulations of single ion chemical potentials. Results for the unrestricted primitive model, Chem. Phys. Lett. 146 (1988) 452.

[65] B. R. Svensson, C. E. Woodward, Widom's method for uniform and non-uniform electrolyte solutions, Mol. Phys. 64 (1988) 247.

[66] P. Sloth, T. S. Sørensen, Monte Carlo calculations of chemical potentials in ionic fluids by application of Widom's formula: Correction for finite-system effects, Chem. Phys. Lett. 173 (1990) 51.

[67] P. Sloth, T. S. Sørensen, Single-ion activity coefficients and structure of ionic fluids: results for the primitive model of electrolyte solutions, J. Phys. Chem. 94 (1990) 2116.

[68] B. Svensson, T. Åkesson, C. E. Woodward, On the simulation of thermodynamic and structural properties of simple liquids, J. Chem. Phys. 95 (1991) 2717.

[69] T. S. Sørensen, High precision canonical ensemble Monte Carlo simulations of very dilute, primitive z:z and 2:1 electrolytes and of moderately concentrated 1:1 electrolyte mixtures, Mol. Simulat. 11 (1993) 1.

[70] S. Hanassab, T. VanderNoot, Monte Carlo simulations of restricted primitive model (rpm) electrolytes in non-euclidean geometries, J. Electroanal. Chem. 528 (2002) 135.

[71] M. Lund, B. Jönsson, T. Pedersen, Activity coefficients in sea water using Monte Carlo simulations, Mar. Chem. 80 (2003) 95.

[72] S. Hanassab, T. VanderNoot, Monte Carlo simulations of primitive model (pm) electrolytes in non-euclidean geometries, Mol. Simulat. 30 (2004) 301.

[73] S. Lamperski, The individual and mean activity coefficients of an electrolyte from the inverse GCMC simulation, Mol. Simulat. 33 (2007) 1193.

[74] Z. Abbas, E. Ahlberg, S. Nordholm, Monte Carlo simulations of salt solutions: Exploring the validity of primitive models, J. Phys. Chem. B 113 (2009) 5905.

[75] B. Widom, Some topics in the theory of fluids, J. Chem. Phys. 39 (1963) 2808.

[76] I. Nezbeda, F. Moučka, W. R. Smith, Recent progress in molecular simulation of aqueous electrolytes: force fields, chemical potentials and solubility, Mol. Phys. 114 (2016) 1665.

[77] M. Ferrario, G. Ciccotti, E. Spohr, T. Cartailler, P. Turq, Solubility of KF in water by molecular dynamics using the kirkwood integration method, J. Chem. Phys. 117 (2002) 4947.

[78] E. Sanz, C. Vega, Solubility of KF and NaCl in water by molecular simulation, J. Chem. Phys. 126 (2007) 014507.

[79] J. L. Aragones, E. Sanz, C. Vega, Solubility of NaCl in water by molecular simulation revisited, J. Chem. Phys. 136 (2012) 244508.

[80] A. L. Benavides, J. L. Aragones, C. Vega, Consensus on the solubility of NaCl in water from computer simulations using the chemical potential route, J. Chem. Phys. 144 (2016) 124504.

[81] J. G. Kirkwood, Statistical mechanics of fluid mixtures, J. Chem. Phys. 3 (1935) 300.

[82] M. Lísal, W. R. Smith, J. Kolafa, Molecular simulations of aqueous electrolyte solubility: 1. The Expanded-Ensemble Osmotic Molecular Dynamics method for the solution phase, J. Phys Chem. B 109 (2005) 12956.

[83] F. Moučka, M. Lísal, J. Škvor, J. Jirsák, I. Nezbeda, W. R. Smith, Molecular simulation of aqueous electrolyte solubility. 2. Osmotic Ensemble Monte Carlo methodology for free energy and solubility calculations and application to NaCl, J. Phys. Chem. B 115 (2011) 7849.

[84] F. Moučka, M. Lísal, W. R. Smith, Molecular simulation of aqueous electrolyte solubility. 3. Alkali-halide salts and their mixtures in water and in hydrochloric acid, J. Phys. Chem. B 116 (2012) 5468.

[85] F. Moučka, I. Nezbeda, W. R. Smith, Molecular force fields for aqueous electrolytes: SPC/E-compatible charged LJ sphere models and their limitations, J. Chem. Phys. 138 (2013) 154102.

[86] F. Moučka, I. Nezbeda, W. R. Smith, Molecular simulation of aqueous electrolytes: Water chemical potential results and Gibbs-Duhem equation consistency tests, J. Chem. Phys. 139 (2013) 124505.

[87] F. Moučka, I. Nezbeda, W. R. Smith, Chemical potentials, activity coefficients, and solubility in aqueous NaCl solutions: Prediction by polarizable force fields, J. Chem. Theory Comput. 11 (2015) 1756.

[88] W. R. Smith, F. Moučka, I. Nezbeda, Osmotic pressure of aqueous electrolyte solutions via molecular simulations of chemical potentials: Application to NaCl, Fluid Phase Equilib. 407 (2016) 76.

[89] Z. Mester, A. Z. Panagiotopoulos, Mean ionic activity coefficients in aqueous NaCl solutions from molecular dynamics simulations, J. Chem. Phys. 142 (2015) 044507.

[90] Z. Mester, A. Z. Panagiotopoulos, Temperature-dependent solubilities and mean ionic activity coefficients of alkali halides in water from molecular dynamics simulations, J. Chem. Phys. 143 (2015) 044505.

[91] J. M. Young, C. Tietz, A. Z. Panagiotopoulos, Activity coefficients and solubility of CaCl2 from molecular simulations, J. Chem. Eng. Data 65 (2020) 337.

[92] A. S. Paluch, S. Jayaraman, J. K. Shah, E. J. Maginn, A method for computing the solubility limit of solids: Application to sodium chloride in water and alcohols, J. Chem. Phys. 133 (2010) 124504.

[93] A. S. Paluch, S. Jayaraman, J. K. Shah, E. J. Maginn, Erratum: A method for computing the solubility limit of solids: Application to sodium chloride in water and alcohols [J. Chem. Phys. 133, 124504 (2010)], J. Chem. Phys. 137 (2012) 039901.

[94] C. H. Bennett, Efficient estimation of free energy differences from Monte Carlo data, J. Comput. Phys. 22 (1976) 245.

[95] A. P. Lyubartsev, A. A. Martsinovski, S. V. Shevkunov, P. N. Vorontsov-Velyaminov, New approach to Monte Carlo calculation of the free energy: Method of expanded ensembles, J. Chem. Phys. 96 (1992) 1776.

[96] A. P. Lyubartsev, A. Laaksonen, P. N. Vorontsov-velyaminov, Determination of free energy from chemical potentials: Application of the Expanded Ensemble method, Mol. Simulat. 18 (1996) 43.

[97] D. Landau, F. Wang, Determining the density of states for classical statistical models by a flat-histogram random walk, Comput. Phys. Commun. 147 (2002) 674.

[98] J. D. Weeks, R. L. B. Selinger, J. Q. Broughton, Self–consistent treatment of repulsive and attractive forces in nonuniform liquids, Phys. Rev. Lett. 75 (1995) 2694.

[99] Y.-G. Chen, C. Kaur, J. D. Weeks, Connecting systems with short and long ranged interactions: Local molecular field theory for ionic fluids, J. Phys. Chem. B 108 (2004) 19874.

[100] N. A. Denesyuk, J. D. Weeks, A new approach for efficient simulation of Coulomb interactions in ionic fluids, J. Chem. Phys. 128 (2008) 124109.

[101] J. M. Rodgers, J. D. Weeks, Local molecular field theory for the treatment of electrostatics, J. Phys.: Condens. Matter 20 (2008) 494206.

[102] J. M. Rodgers, J. D. Weeks, Accurate thermodynamics for short–ranged truncations of Coulomb interactions in site–site molecular models, J. Chem. Phys. 131 (2009) 244108.

[103] P. P. Ewald, Die Berechnung optischer und elektrostatischer Gitterpotentiale, Ann. Phys. 369 (1921) 253.

[104] D. Wolf, P. Keblinski, S. R. Phillpot, J. Eggebrecht, Exact method for the simulation of Coulombic systems by spherically truncated, pairwise r^{-1} summation, J. Chem. Phys. 110 (1999) 8254.

[105] D. Zahn, B. Schilling, S. M. Kast, Enhancement of the wolf damped Coulomb potential: Static, dynamic, and dielectric properties of liquid water from molecular simulation, J. Phys. Chem. B 106 (2002) 10725.

[106] C. J. Fennell, J. D. Gezelter, Is the Ewald summation still necessary? Pairwise alternatives to the accepted standard for long-range electrostatics, J. Chem. Phys. 124 (2006) 234104.

[107] J. Rasaiah, G. Stell, Three-body free-energy terms and effective potentials in polar fluids and ionic solutions, Chem. Phys. Lett. 25 (1974) 519.

[108] G. S. Rushbrooke, G. Stell, J. S. Høye, Theory of polar liquids, Mol. Phys. 26 (1973) 1199.

[109] B. Bildstein, G. Kahl, Triplet correlation functions for hard–spheres: Computer simulation results, J. Chem. Phys. 100 (1994) 5882.

[110] E. A. Müller, K. E. Gubbins, Triplet correlation function for hard sphere systems, Mol. Phys. 80 (1993) 91.

[111] B. Bildstein, G. Kahl, Triplet correlation functions for hard spheres: Comparison of different approaches, Phys. Rev. E 47 (1993) 1712.

[112] P. Attard, Integral equations and closure relations for the bridge function and for the triplet correlation function, J. Chem. Phys. 93 (1990) 7301.

[113] J. Kolafa, S. Labik, A. Malijevsky, Radial distribution function of the hard sphere fluid, 18th IUPAC International Conference on Chemical Thermodynamics, August 17-21, Beijing, China, 2004.

[114] J. K. Percus, G. J. Yevick, Analysis of classical statistical mechanics by means of collective coordinates, Phys. Rev. 110 (1958) 1.

[115] A. Tani, D. Henderson, J. A. Barker, C. E. Hecht, Application of perturbation theory to the calculation of the dielectric constant of a dipolar hard sphere fluid, Mol. Phys. 48 (1983) 863.

[116] M. Theiss, J. Gross, A third and fourth order perturbation theory for dipolar hard spheres, J. Chem. Phys. 149 (2018) 044901.

[117] J. C. Rasaiah, B. Larsen, G. Stell, Thermodynamic perturbation theory for potentials of multipolar symmetry. I, J. Chem. Phys. 63 (1975) 722.

[118] G. Stell, J. C. Rasaiah, H. Narang, Thermodynamic perturbation theory for simple polar fluids. II, Mol. Phys. 27 (1974) 1393.

[119] J. A. Barker, D. Henderson, W. R. Smith, Three-body forces in dense systems, Phys. Rev. Lett. 21 (1968) 134.

[120] J. A. Barker, D. Henderson, W. R. Smith, Pair and triplet interactions in argon, Mol. Phys. 17 (1969) 579.

[121] S. Bruckner, S. Boresch, Efficiency of alchemical free energy simulations. I. A practical comparison of the exponential formula, thermodynamic integration, and Bennett's acceptance ratio method, J. Comput. Chem. 32 (2011) 1303.

[122] D. Frenkel, B. Smit, Understanding Molecular Simulation (2nd ed.), Academic Press, San Diego, 2002.

[123] M. P. Allen, D. J. Tildesley, Computer Simulation of Liquids, Clarendon Press, 1989.

[124] J. Caillol, D. Levesque, J. Weis, Monte Carlo simulation of an ion–dipole mixture, Mol. Phys. 69 (1990) 199.

[125] H. J. C. Berendsen, J. R. Grigera, T. P. Straatsma, The missing term in effective pair potentials, J. Phys. Chem. 91 (1987) 6269.

[126] Y.-G. Chen, J. D. Weeks, Local molecular field theory for effective attractions between like charged objects in systems with strong Coulomb interactions, Proc. Natl. Acad. Sci. USA 103 (2006) 7560.

[127] J. M. Rodgers, Z. Hu, J. D. Weeks, On the efficient and accurate short-ranged simulations of uniform polar molecular liquids, Mol. Phys. 109 (2011) 1195.

[128] D. A. Kofke, P. T. Cummings, Quantitative comparison and optimization of methods for evaluating the chemical potential by molecular simulation, Mol. Phys. 92 (1997) 973.

[129] M. Fitzgerald, R. R. Picard, R. N. Silver, Canonical transition probabilities for adaptive Metropolis simulation, Europhys. Lett. 46 (1999) 282.

[130] M. Fitzgerald, R. Picard, R. Silver, Monte Carlo transition dynamics and variance reduction, J. Stat. Phys. 98 (2000) 321.

[131] J. R. Errington, Direct calculation of liquid-vapor phase equilibria from transition matrix Monte Carlo simulation, J. Chem. Phys. 118 (2003) 9915.

[132] M. S. Shell, P. G. Debenedetti, A. Z. Panagiotopoulos, An improved Monte Carlo method for direct calculation of the density of states, J. Chem. Phys. 119 (2003) 9406.

[133] K. A. Maerzke, L. Gai, P. T. Cummings, C. McCabe, Simulating phase equilibria using Wang-Landau-Transition Matrix Monte Carlo, J. of Phys.: Conf. Ser. 487 (2014) 012002.

APPENDIX

All sections of the Appendix have been published as part of previous publications. The origin of the sections is as follows:

- *Appendix A is a literal quote from the first publication, Ref. 1, where the section was published as 'Appendix B: Inaccuracies in HBT Theory'*
- *Appendix B is a literal quote from the first publication, Ref. 1, where the section was published as 'A New Perturbation Theory for Electrolyte Solutions: Supplementary material'*
- *Appendix C is a literal quote from the third publication, Ref. 3, where the section was published as 'Appendix A: Equilibration of the systems'*
- *Appendix D is a literal quote from the third publication, Ref. 3, where the section was published as 'Appendix B: Removing the test particle to test particle interactions in Ewald summation'*
- *Appendix E is a literal quote from the second publication, Ref. 2, where the section was published as 'Appendix B: Tabulated simulation results'*

A Inaccuracies in HBT theory

At the start of this work, we analysed the HBT theory and found some inaccuracies not all of which are easy to correct. One error goes back to previous work of Rasaiah and Stell[107], who laid an important foundation to perturbation theory of electrostatic systems, but unfortunately gave the orientational averaged charge-dipole-dipole potential too large by a factor of two. This results in a wrong correlation for I_{cdd} in HBT theory. But, since it is a constant prefactor, one can easily correct this error by multiplying I_{cdd} with one half.

In Ref. 51 we further identified a inaccurate solution of the correlation integral

$$I''_{cc} = \int \left(g^{\mathrm{hs}}(r) - 1\right) r \, \mathrm{d}r. \tag{A.1}$$

We solved the integral for various densities using highly accurate values of $g^{\mathrm{hs}}(r)$ from molecular simulations by Kolafa et al.[113] and found the correlation given by Henderson et al.[51] to be inaccurate (possibly caused by a misprint). The correlation provided by Larsen et al.[42] on the other hand is in good agreement to the numerical results using $g^{\mathrm{hs}}(r)$ from the molecular simulations. Therefore, we simply considered the correlation for I_{cdd} from Larsen et al. in our calculations.

Having a close look at the mathematics used when resumming the diverging correlation integrals, we found the inaccurate approximation

$$\frac{1}{1-9y} \approx \left(1 - \frac{3}{2}y\right)^2, \tag{A.2}$$

where $y = 4/9 \cdot \pi\beta\mu^2\rho(1-x) = 4/9 \cdot \pi\mu^{*2}\rho^*(1-x)$. For the systems [...] {we considered in our first publication, Ref. 1}, y is in the range between 0.39 and 3.79. Figure A.1 shows that this is not a useful approximation for most values of y. One can speculate that this approximation was introduced in order to recover the Debye-Hückel limit for low ion concentrations. Since the approximation, Eq. (A.2), is crucial for the resummation, there is no easy way to correct it.

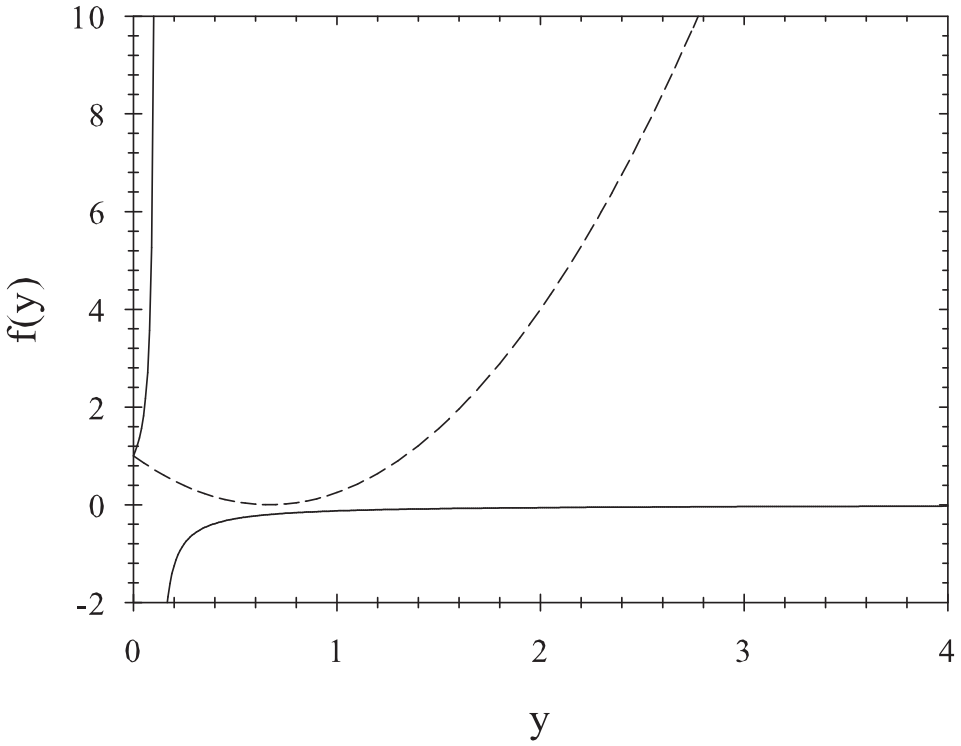

Fig. A.1: Approximation used in HBT theory. The solid line is the function $f(y) = 1/(1-9y)$, the dashed line denotes $f(y) = (1 - 3/2\ y)^2$.

B Derivation of third order perturbation theory

In this [...] {section}, we provide more detail on the derivation of the basic perturbation equation used in our work, i.e. we describe the route from Eq. (2.16) to Eq. (2.17) in the main document. The Eq. (2.17) is not entirely derived. Rather we give a detailed derivation of the 1st order term for pure substances and mixtures, then apply the proposed (damped) electrostatic potentials and show how some terms of the theory vanish for the model electrolyte solution. More briefly, we then derive the 2nd order contribution. From the exemplary derivation of the 1st and 2nd order term, one can easily derive the higher order perturbation theory. Doing so is lengthy, but straightforward.

The basic Taylor expansion around $\lambda = 0$, Eq. (2.16) in the main document, evaluated at $\lambda = 1$ writes

$$A - A^{\mathrm{ref}} = \left(\frac{\partial A}{\partial \lambda}\right)_{\lambda=0} + \frac{1}{2}\left(\frac{\partial^2 A}{\partial \lambda^2}\right)_{\lambda=0} + \frac{1}{6}\left(\frac{\partial^3 A}{\partial \lambda^3}\right)_{\lambda=0} \tag{B.1}$$

or in terms of the dimensionless residual Helmholtz energy relative to the hard sphere system

$$a^{\mathrm{res}} = \beta\frac{A - A^{\mathrm{hs}}}{N} = \underbrace{\frac{\beta}{N}\left(\frac{\partial A}{\partial \lambda}\right)_{\lambda=0}}_{\equiv a_1} + \underbrace{\frac{\beta}{2N}\left(\frac{\partial^2 A}{\partial \lambda^2}\right)_{\lambda=0}}_{\equiv a_2} + \underbrace{\frac{\beta}{6N}\left(\frac{\partial^3 A}{\partial \lambda^3}\right)_{\lambda=0}}_{\equiv a_3} \tag{B.2}$$

The partial derivatives are obtained using the Helmholtz energy definition

$$A_\lambda = -\frac{1}{\beta}\ln Q_\lambda \tag{B.3}$$

with the partition function

$$Q_\lambda = \frac{1}{N!\,\Lambda^{3N}} \underbrace{\int \exp\left(-\beta U(\widetilde{\mathbf{r}}^N, \lambda)\right) \mathrm{d}\widetilde{\mathbf{r}}^N}_{\equiv Z_\lambda} \tag{B.4}$$

1st order contribution

Pure substances

To obtain the first order, we can write

$$\begin{aligned} \frac{\partial A}{\partial \lambda} &= -\frac{1}{\beta}\frac{\partial \left(\ln Q_\lambda\right)}{\partial \lambda} = -\frac{1}{\beta}\frac{1}{Z_\lambda}\frac{\partial Z_\lambda}{\partial \lambda} \\ &= \frac{1}{Z_\lambda}\int \frac{\partial U(\widetilde{\mathbf{r}}^N, \lambda)}{\partial \lambda} \exp\left(-\beta U(\widetilde{\mathbf{r}}^N, \lambda)\right) \mathrm{d}\widetilde{\mathbf{r}}^N \end{aligned} \tag{B.5}$$

For pairwise additive potentials, from the definition given in Eq. (2.13) of the main document follows that

$$U(\widetilde{\mathbf{r}}^N, \lambda) = U^{\mathrm{ref}}(\widetilde{\mathbf{r}}^N) + \lambda \cdot W(\widetilde{\mathbf{r}}^N) \tag{B.6}$$

and thus

$$\frac{\partial U(\widetilde{\mathbf{r}}^N, \lambda)}{\partial \lambda} = W(\widetilde{\mathbf{r}}^N) \tag{B.7}$$

and

$$W(\widetilde{\mathbf{r}}^N) = \sum_i^N \sum_{j>i}^N w_{ij}(ij) \tag{B.8}$$

With this, Eq. (B.5) becomes

$$\frac{\partial A}{\partial \lambda} = \frac{1}{Z_\lambda}\int \sum_i^N \sum_{j>i}^N w_{ij}(ij) \exp\left(-\beta U(\widetilde{\mathbf{r}}^N, \lambda)\right) \mathrm{d}\widetilde{\mathbf{r}}^N \tag{B.9}$$

Since the integration is carried out over all (indistinguishable) particles, the integrals in Eq. (B.9) have the same contribution for all particle combinations i, j. Thus, we can simply count the number of identical contributions arising from the double sum $\sum_i^N \sum_{j>i}^N w_{ij}(ij)$, and in this (easy) case the result is $N(N-1)/2$. Writing the integral

for two arbitrary particles 1 and 2, Eq. (B.9) becomes

$$\frac{\partial A}{\partial \lambda} = \frac{1}{Z_\lambda} \frac{N(N-1)}{2} \int w_{12}(12) \exp\left(-\beta U(\widetilde{\mathbf{r}}^N, \lambda)\right) \mathrm{d}\widetilde{\mathbf{r}}^N \tag{B.10}$$

Finally, we can introduce the two particle correlation function, defined as

$$g_\lambda(12) = \frac{1}{Z_\lambda} \frac{N(N-1)}{\rho^2} \int \exp\left(-\beta U(\widetilde{\mathbf{r}}^N, \lambda)\right) \mathrm{d}\widetilde{\mathbf{r}}^{N>2} \tag{B.11}$$

where $\mathrm{d}\widetilde{\mathbf{r}}^{N>2}$ means that the integration runs over all N particles except particles 1 and 2. Using this correlation function, Eq. (B.10) can be written as

$$\begin{aligned} \frac{\partial A}{\partial \lambda} &= \frac{1}{2}\rho^2 \int w_{12}(12) \left[\frac{1}{Z_\lambda} \frac{N(N-1)}{\rho^2} \int \exp\left(-\beta U(\widetilde{\mathbf{r}}^N, \lambda)\right) \mathrm{d}\widetilde{\mathbf{r}}^{N>2} \right] \mathrm{d}\widetilde{\mathbf{r}}_1 \mathrm{d}\widetilde{\mathbf{r}}_2 \\ &= \frac{\rho^2}{2} \int w_{12}(12)\ g_\lambda(12)\ \mathrm{d}\widetilde{\mathbf{r}}_1 \mathrm{d}\widetilde{\mathbf{r}}_2 \end{aligned} \tag{B.12}$$

For $\lambda = 0$, $g_{\lambda=0}(12) = g^{\mathrm{hs}}(12)$, and consequently

$$\left(\frac{\partial A}{\partial \lambda}\right)_{\lambda=0} = \frac{\rho^2}{2} \int w_{12}(12)\ g^{\mathrm{hs}}(12)\ \mathrm{d}\widetilde{\mathbf{r}}_1 \mathrm{d}\widetilde{\mathbf{r}}_2 \tag{B.13}$$

As defined in the main document, the $\widetilde{\mathbf{r}}_i$ contain the spacial coordinates of particle i as well as its orientation $\boldsymbol{\omega}_i$. Since the hard sphere correlation function $g^{\mathrm{hs}}(12)$ is not a function of $\boldsymbol{\omega}_i$, the integrals $\mathrm{d}\boldsymbol{\omega}_1$ and $\mathrm{d}\boldsymbol{\omega}_2$ are carried out only over the potentials. This results in unweighted orientational averaged potentials, indicated by the angular brackets. Applying this to the above equation, we get

$$\begin{aligned} \left(\frac{\partial A}{\partial \lambda}\right)_{\lambda=0} &= \frac{\rho^2}{2} \int \langle w_{12}(12) \rangle\ g^{\mathrm{hs}}(12)\ \mathrm{d}\mathbf{r}_1 \mathrm{d}\mathbf{r}_2 \\ &= \frac{\rho^2}{2} V \int \langle w_{12}(12) \rangle\ g^{\mathrm{hs}}(12)\ \mathrm{d}\mathbf{r}_{12} \end{aligned} \tag{B.14}$$

where now $\mathbf{r}_1$ and $\mathbf{r}_2$ are position vectors and $\mathbf{r}_{12}$ is the distance vector without any information about the particle orientation. Finally, for the dimensionless 1st order contribution a_1 for pure substances, we get

$$a_1 = \frac{\beta}{N} \left(\frac{\partial A}{\partial \lambda}\right)_{\lambda=0} = \beta \frac{\rho}{2} \int \langle w_{12}(12) \rangle\ g^{\mathrm{hs}}(12)\ \mathrm{d}\mathbf{r}_{12} \tag{B.15}$$

Mixtures

The procedure to obtain a_1 for mixtures is quite similar to the route for pure substances. Eq. (B.8) for a mixture of C components writes

$$W(\widetilde{\mathbf{r}}^N) = \frac{1}{2}\sum_{\alpha}^{C}\sum_{\gamma}^{C}\sum_{i\alpha}^{N_\alpha}\sum_{\substack{j\gamma \\ i\alpha\neq j\gamma\ \forall\ \alpha=\gamma}}^{N_\gamma} w_{i\alpha j\gamma}(i\alpha\ j\gamma) \tag{B.16}$$

where $i\alpha$ denotes the i^{th} particle of component α and $j\gamma$ the j^{th} particle of component γ. N_α and N_γ are number of particles of components α and γ, respectively. The condition $i\alpha \neq j\gamma\ \forall\ \alpha = \gamma$ avoids that interactions of particles with themselves are included.

Analog to Eq. (B.9) for pure substances, we now get

$$\frac{\partial A}{\partial \lambda} = \frac{1}{2}\frac{1}{Z_\lambda}\int \sum_{\alpha}^{C}\sum_{\gamma}^{C}\sum_{i\alpha}^{N_\alpha}\sum_{\substack{j\gamma \\ i\alpha\neq j\gamma\ \forall\ \alpha=\gamma}}^{N_\gamma} w_{i\alpha j\gamma}(i\alpha\ j\gamma)\exp\left(-\beta U(\widetilde{\mathbf{r}}^N,\lambda)\right)\mathrm{d}\widetilde{\mathbf{r}}^N \tag{B.17}$$

For of a mixture, the particles between the different components are distinguishable and identical contributions to the integral in the above equation arise from identical combinations $i\alpha$ and $j\gamma$. Again, by counting the number of such identical contributions, we get $N_\alpha(N_\alpha - 1)$ identical contributions for $\alpha = \gamma$ and $N_\alpha \cdot N_\gamma$ ones otherwise. Thus,

$$\frac{\partial A}{\partial \lambda} = \frac{1}{2}\frac{1}{Z_\lambda}\sum_{\alpha}^{C}\sum_{\gamma}^{C} N_\alpha(N_\gamma - \delta_{\alpha\gamma})\int w_{1\alpha 2\gamma}(1\alpha\ 2\gamma)\exp\left(-\beta U(\widetilde{\mathbf{r}}^N,\lambda)\right)\mathrm{d}\widetilde{\mathbf{r}}^N \tag{B.18}$$

where we introduced the Kronecker delta, as $\delta_{\alpha\gamma} = 1$ for $\alpha = \gamma$ and $\delta_{\alpha\gamma} = 0$, otherwise. For mixtures, the two particle correlation function writes

$$g_{\lambda,1\alpha 2\gamma}(1\alpha\ 2\gamma) = \frac{N_\alpha(N_\gamma - \delta_{\alpha\gamma})}{\rho_\alpha \rho_\gamma}\frac{1}{Z_\lambda}\int \exp\left(-\beta U(\widetilde{\mathbf{r}}^N,\lambda)\right)\mathrm{d}\widetilde{\mathbf{r}}^{N^{\alpha\neq 1}}\mathrm{d}\widetilde{\mathbf{r}}^{N^{\gamma\neq 2}} \tag{B.19}$$

Applying Eq.(B.19) to Eq. (B.18) similar to the way we did for pure substances gives

$$\frac{\partial A}{\partial \lambda} = \frac{1}{2}\sum_{\alpha}^{C}\sum_{\gamma}^{C}\rho_\alpha\rho_\gamma\int w_{1\alpha 2\gamma}(1\alpha\ 2\gamma)g_{\lambda,1\alpha 2\gamma}(1\alpha\ 2\gamma)\mathrm{d}\widetilde{\mathbf{r}}_{1\alpha}\mathrm{d}\widetilde{\mathbf{r}}_{2\gamma} \tag{B.20}$$

Again, by using $g_{\lambda=0,1\alpha2\gamma}(1\alpha\ 2\gamma) = g^{\mathrm{hs}}_{1\alpha2\gamma}(1\alpha\ 2\gamma)$ and applying the short notation for the orientational averaging, this becomes

$$\begin{aligned}\left(\frac{\partial A}{\partial\lambda}\right)_{\lambda=0} &= \frac{1}{2}\sum_{\alpha}^{C}\sum_{\gamma}^{C}\rho_\alpha\rho_\gamma\int\langle w_{1\alpha2\gamma}(1\alpha\ 2\gamma)\rangle\, g^{\mathrm{hs}}_{1\alpha2\gamma}(1\alpha\ 2\gamma)\mathrm{d}\mathbf{r}_{1\alpha}\mathrm{d}\mathbf{r}_{2\gamma}\\ &= \frac{\rho^2}{2}V\sum_{\alpha}^{C}\sum_{\gamma}^{C}x_\alpha x_\gamma\int\langle w_{1\alpha2\gamma}(1\alpha\ 2\gamma)\rangle\, g^{\mathrm{hs}}_{1\alpha2\gamma}(1\alpha\ 2\gamma)\mathrm{d}\mathbf{r}_{1\alpha2\gamma}\end{aligned} \tag{B.21}$$

with $x_\alpha = N_\alpha/N$ and $x_\gamma = N_\gamma/N$ being the molar fractions of the components. By slightly changing the index (without any loss of information), we get the dimensionless first order contribution as

$$a_1 = \beta\frac{\rho}{2}\sum_{\alpha=1}^{C}\sum_{\gamma=1}^{C}x_\alpha x_\gamma\int\langle w_{\alpha\gamma}(12)\rangle\, g^{\mathrm{hs}}_{\alpha\gamma}(12)\mathrm{d}\mathbf{r}_{12} \tag{B.22}$$

Generally, it can be seen that the Kronecker operator cancels out when introducing the two particle correlation function. We will make use of this observation for the mixture terms of higher orders.

Application of the electrostatic potentials

Having derived the general 1st order perturbation term for any mixture, we can apply the electrostatic potentials used in this work to Eq. (B.22). For brevity, we here use the standard potentials as given by Eq. (2.2) to (2.4) in the main document. Using the damped potentials [...] gives the exactly same results for the orientational averaged potentials and for a_1.

According to the nonprimitive approach, an electrolyte solution is a ternary mixture of cations (index $+$), anions (index $-$) and dipoles (index d), and therefore $\alpha,\gamma \in \{+,-,d\}$. Using equally charged ions with an absolute charge of q, the potentials are

$$w_{++}(12) = w_{--}(12) = \frac{q^2}{r_{12}} \tag{B.23}$$

$$w_{+-}(12) = -w_{++}(12) = -\frac{q^2}{r_{12}} \tag{B.24}$$

and electroneutrality of the mixture requires

$$x_+ = x_- \tag{B.25}$$

For the pair potentials containing dipoles, we get

$$w_{+d}(12) = \frac{q\mu}{r_{12}^2}\left(\hat{\boldsymbol{\mu}}_2 \cdot \hat{\mathbf{r}}_{12}\right) \tag{B.26}$$

$$w_{-d}(12) = -w_{+d}(12) = -\frac{q\mu}{r_{12}^2}\left(\hat{\boldsymbol{\mu}}_2 \cdot \hat{\mathbf{r}}_{12}\right) \tag{B.27}$$

$$w_{dd}(12) = -\frac{\mu^2}{r_{12}^3}\left[3\left(\hat{\boldsymbol{\mu}}_1 \cdot \hat{\mathbf{r}}_{12}\right)\left(\hat{\boldsymbol{\mu}}_2 \cdot \hat{\mathbf{r}}_{12}\right) - \left(\hat{\boldsymbol{\mu}}_1 \cdot \hat{\boldsymbol{\mu}}_2\right)\right] \tag{B.28}$$

and

$$x_d = 1 - x_+ - x_- \tag{B.29}$$

where μ is the dipole moment of the solvent.
The (unweighted) orientational averaged potentials as they are required for Eq. (B.22) are

$$\langle w_{+d}(12)\rangle = \frac{\int w_{+d}(12)\mathrm{d}\boldsymbol{\omega}_2}{\int \mathrm{d}\boldsymbol{\omega}_2} = 0 \tag{B.30}$$

$$\langle w_{-d}(12)\rangle = \frac{\int w_{-d}(12)\mathrm{d}\boldsymbol{\omega}_2}{\int \mathrm{d}\boldsymbol{\omega}_2} = 0 \tag{B.31}$$

$$\langle w_{dd}(12)\rangle = \frac{\int w_{dd}(12)\mathrm{d}\boldsymbol{\omega}_1\mathrm{d}\boldsymbol{\omega}_2}{\int \mathrm{d}\boldsymbol{\omega}_1\mathrm{d}\boldsymbol{\omega}_2} = 0 \tag{B.32}$$

From this, one can already see that the terms containing dipoles in Eq. (B.22) vanish, and the remaining ones are the terms where α and γ are charges. Applying those remaining terms to the equation for a_1 gives one '++'–term, one '−−'–term and two '+−'–terms. Since the concentrations of the ionic components are identical and the potentials given in Eq. (B.23) to Eq.(B.25) have the same magnitude but opposite signs, the sum of the contributions due to the cations and anions also vanishes.
Therefore, for our model electrolyte solution, $a_1 = 0$.

2nd order contribution

Pure substances

The second order contribution can be obtained by differentiating Eq. (B.9) with respect to λ. Doing this gives

$$\begin{aligned}\frac{\partial^2 A}{\partial\lambda^2} &= \frac{\partial}{\partial\lambda}\left[\frac{1}{Z_\lambda}\int W(\widetilde{\mathbf{r}}^N)\exp\left(-\beta U(\widetilde{\mathbf{r}}^N,\lambda)\right)\mathrm{d}\widetilde{\mathbf{r}}^N\right]\\ &= -\frac{1}{Z_\lambda^2}\frac{\partial Z_\lambda}{\partial\lambda}\int W(\widetilde{\mathbf{r}}^N)\exp\left(-\beta U(\widetilde{\mathbf{r}}^N,\lambda)\right)\mathrm{d}\widetilde{\mathbf{r}}^N\\ &\quad -\frac{\beta}{Z_\lambda}\int W(\widetilde{\mathbf{r}}^N)W(\widetilde{\mathbf{r}}^N)\exp\left(-\beta U(\widetilde{\mathbf{r}}^N,\lambda)\right)\mathrm{d}\widetilde{\mathbf{r}}^N\end{aligned} \tag{B.33}$$

From Eq. (B.5) we see that

$$\frac{\partial Z_\lambda}{\partial\lambda} = -\beta Z_\lambda\frac{\partial A}{\partial\lambda} \tag{B.34}$$

Applying Eq. (B.8), (B.9) and (B.34) to Eq. (B.33) gives

$$\frac{\partial^2 A}{\partial\lambda^2} = \beta\left(\frac{\partial A}{\partial\lambda}\right)^2 - \frac{\beta}{Z_\lambda}\int\left(\sum_i^N\sum_{j>i}^N w_{ij}(ij)\sum_k^N\sum_{l>k}^N w_{kl}(kl)\right)\exp\left(-\beta U(\widetilde{\mathbf{r}}^N,\lambda)\right)\mathrm{d}\widetilde{\mathbf{r}}^N \tag{B.35}$$

As we did for the 1st order contribution, we again count the distinguishable interaction contributions arising from the product of the double sum over the pair potentials. The results of that counting are summarized in Tab. B.1. Using those results in Eq. (B.35)

Interaction type	Number of identical contributions
$w_{12}(12)w_{12}(12)$	$N(N-1)/2$
$w_{12}(12)w_{13}(13)$	$N(N-1)(N-2)$
$w_{12}(12)w_{34}(34)$	$N(N-1)(N-2)(N-3)/4$

Tab. B.1: Contributions to 2nd order term for pure substances.

gives

$$\begin{aligned}\frac{\partial^2 A}{\partial\lambda^2} =& \beta\left(\frac{\partial A}{\partial\lambda}\right)^2 - \frac{\beta}{Z_\lambda}\left[\frac{N(N-1)}{2}\int w_{12}^2(12)\exp\left(-\beta U(\widetilde{\mathbf{r}}^N,\lambda)\right)\mathrm{d}\widetilde{\mathbf{r}}^N\right.\\ &+ N(N-1)(N-2)\int w_{12}(12)w_{13}(13)\exp\left(-\beta U(\widetilde{\mathbf{r}}^N,\lambda)\right)\mathrm{d}\widetilde{\mathbf{r}}^N\\ &\left.+ \frac{N(N-1)(N-2)(N-3)}{4}\int w_{12}(12)w_{34}(34)\exp\left(-\beta U(\widetilde{\mathbf{r}}^N,\lambda)\right)\mathrm{d}\widetilde{\mathbf{r}}^N\right]\end{aligned} \tag{B.36}$$

Applying the n–particle distribution functions (for pure substances)

$$g_\lambda^n(\widetilde{\mathbf{r}}^n) = \frac{1}{\rho^n}\frac{N!}{(N-n)!}\frac{1}{Z_\lambda}\int \exp\left(-\beta U(\widetilde{\mathbf{r}}^N,\lambda)\right)\mathrm{d}\widetilde{\mathbf{r}}^{N>n} \tag{B.37}$$

Eq. (B.35) becomes

$$\begin{aligned}\frac{\partial^2 A}{\partial\lambda^2} = \beta\left(\frac{\partial A}{\partial\lambda}\right)^2 - \beta\Bigg[&\frac{1}{2}\rho^2\int w_{12}^2(12)g_\lambda(12)\mathrm{d}\widetilde{\mathbf{r}}_1\mathrm{d}\widetilde{\mathbf{r}}_2\\ &+\rho^3\int w_{12}(12)w_{13}(13)g_\lambda(123)\mathrm{d}\widetilde{\mathbf{r}}_1\mathrm{d}\widetilde{\mathbf{r}}_2\mathrm{d}\widetilde{\mathbf{r}}_3\\ &+\frac{1}{4}\rho^4\int w_{12}(12)w_{34}(34)g_\lambda(1234)\mathrm{d}\widetilde{\mathbf{r}}_1\mathrm{d}\widetilde{\mathbf{r}}_2\mathrm{d}\widetilde{\mathbf{r}}_3\mathrm{d}\widetilde{\mathbf{r}}_4\Bigg]\end{aligned} \tag{B.38}$$

and

$$\begin{aligned}\left(\frac{\partial^2 A}{\partial\lambda^2}\right)_{\lambda=0} = \beta\left(\frac{\partial A}{\partial\lambda}\right)^2_{\lambda=0} - \beta\Bigg[&\frac{1}{2}\rho^2 V\int\left\langle w_{12}^2(12)\right\rangle g^{\mathrm{hs}}(12)\mathrm{d}\mathbf{r}_{12}\\ &+\rho^3 V\int\left\langle w_{12}(12)w_{13}(13)\right\rangle g^{\mathrm{hs}}(123)\mathrm{d}\mathbf{r}_{12}\mathrm{d}\mathbf{r}_{13}\\ &+\frac{1}{4}\rho^4 V\int\left\langle w_{12}(12)w_{34}(34)\right\rangle g^{\mathrm{hs}}(1234)\mathrm{d}\mathbf{r}_{12}\mathrm{d}\mathbf{r}_{13}\mathrm{d}\mathbf{r}_{14}\Bigg]\end{aligned} \tag{B.39}$$

For the dimensionless 2nd order term for pure substances, using Eq. (B.14), we get

$$\begin{aligned}a_2 = \frac{\beta}{2N}\left(\frac{\partial^2 A}{\partial\lambda^2}\right)_{\lambda=0} = &\frac{1}{8}\beta^2\rho^2 N\left(\int\left\langle w_{12}(12)\right\rangle g^{\mathrm{hs}}(12)\mathrm{d}\mathbf{r}_{12}\right)^2\\ &-\frac{1}{4}\beta^2\rho\int\left\langle w_{12}^2(12)\right\rangle g^{\mathrm{hs}}(12)\mathrm{d}\mathbf{r}_{12}\\ &-\frac{1}{2}\beta^2\rho^2\int\left\langle w_{12}(12)w_{13}(13)\right\rangle g^{\mathrm{hs}}(123)\mathrm{d}\mathbf{r}_{12}\mathrm{d}\mathbf{r}_{13}\\ &-\frac{1}{8}\beta^2\rho^3\int\left\langle w_{12}(12)w_{34}(34)\right\rangle g^{\mathrm{hs}}(1234)\mathrm{d}\mathbf{r}_{12}\mathrm{d}\mathbf{r}_{13}\mathrm{d}\mathbf{r}_{14}\end{aligned} \tag{B.40}$$

Mixtures

As can be seen from Eq. (B.40), deriving the 2nd order term for mixtures requires a rather excessive use of indices. However, the structure of the equations observed in Sec. B allows us to directly formulate the 2nd order term for mixtures from Eq. (B.40)

as

$$
\begin{aligned}
a_2 = \frac{1}{8}\beta^2\rho^2 N \left(\sum_{\alpha=1}^{C}\sum_{\gamma=1}^{C} x_\alpha x_\gamma \int \langle w_{\alpha\gamma}(12)\rangle \, g^{\mathrm{hs}}_{\alpha\gamma}(12)\mathrm{d}\mathbf{r}_{12} \right)^2 \\
- \frac{1}{4}\beta^2\rho \sum_{\alpha=1}^{C}\sum_{\gamma=1}^{C} x_\alpha x_\gamma \int \left\langle w^2_{\alpha\gamma}(12)\right\rangle g^{\mathrm{hs}}_{\alpha\gamma}(12)\mathrm{d}\mathbf{r}_{12} \\
- \frac{1}{2}\beta^2\rho^2 \sum_{\alpha=1}^{C}\sum_{\gamma=1}^{C}\sum_{\tau=1}^{C} x_\alpha x_\gamma x_\tau \int \langle w_{\alpha\gamma}(12) w_{\alpha\tau}(13)\rangle \, g^{\mathrm{hs}}_{\alpha\gamma\tau}(123)\mathrm{d}\mathbf{r}_{12}\mathrm{d}\mathbf{r}_{13} \\
- \frac{1}{8}\beta^2\rho^3 \sum_{\alpha=1}^{C}\sum_{\gamma=1}^{C}\sum_{\tau=1}^{C}\sum_{\varphi=1}^{C} x_\alpha x_\gamma x_\tau x_\varphi \int \langle w_{\alpha\gamma}(12) w_{\tau\varphi}(34)\rangle \, g^{\mathrm{hs}}_{\alpha\gamma\tau\varphi}(1234)\mathrm{d}\mathbf{r}_{12}\mathrm{d}\mathbf{r}_{13}\mathrm{d}\mathbf{r}_{14}
\end{aligned}
\tag{B.41}
$$

Application of the electrostatic potentials

Applying the electrostatic potentials as given in Sec. B, the first, third and fourth term in Eq. (B.41) vanish for the same reasons that have been discussed for the a_1 term. The second term remains since the square of the charge-charge potentials given by Eq. (B.23) and (B.24) have the same sign and do not cancel. Also, neither the orientational average of the squared charge-dipole nor of the squared dipole-dipole potential vanishes, as can be seen from Eq. (2.41) and (2.42) of the main document. Thus, the remaining 2^{nd} order term in our work is

$$
a_2 = -\frac{1}{4}\beta^2\rho \sum_{\alpha=1}^{C}\sum_{\gamma=1}^{C} x_\alpha x_\gamma \int \left\langle w^2_{\alpha\gamma}(12)\right\rangle g^{\mathrm{hs}}_{\alpha\gamma}(12)\mathrm{d}\mathbf{r}_{12} \tag{B.42}
$$

3^{rd} order contribution

In this document, we do not derive the higher order terms. As shown for a_1 and a_2, this can be easily done by differentiating Eq. (B.35) once more with respect to λ, and the resulting general equation for a_3 contains correlation integrals of up to 6 particles. After applying the electrostatic potentials, the remaining term for the 3^{rd} order is

$$
a_3 = \frac{1}{6}\rho^2\beta^3 \sum_{\alpha=1}^{C}\sum_{\gamma=1}^{C}\sum_{\tau=1}^{C} x_\alpha x_\gamma x_\tau \int \langle w_{\alpha\gamma}(12) w_{\alpha\tau}(13) w_{\gamma\tau}(23)\rangle \, g^{\mathrm{hs}}_{\alpha\gamma\tau}(123)\mathrm{d}\mathbf{r}_{12}\mathrm{d}\mathbf{r}_{13} \tag{B.43}
$$

C Slow equilibration behavior

Equilibration of some of the systems is very demanding. This is the case especially for state points with high ion mole fraction x_I and/or low ratio q^{*2}/μ^{*2}.
Slow equilibration behavior is manifested by a small, but constant decrease of potential energy $U^* = \beta U/N$ during the entire pre-equilibration phase. The effect is rather easy to overlook, because it is not unambiguously apparent for, say, 100,000 cycles, where each cycle consists of N MC moves. In this section, we discuss the behavior for one exemplary state point and assess its influence on the chemical potential data given in this work.
The drift in U^* can be revealed by subdividing the pre-equilibration simulation into blocks and regarding the block averages over simulation time. In Fig. C.1, U^* is shown for various block averaged values for a system for which we observed slow equilibration behavior. The pre-equilibration simulation was subdivided into 25 blocks, each consisting of 60,000 MC cycles. As can be seen, there is a constant decrease of U^* during the entire simulation. The scale of U^* in Fig. C.1 shows that the drift of energy, however, is lower than 1 % for the here considered system as well as all other systems.

Although the effect of slow equilibration is quite low when regarding U^* only, it is important to assess its impact on chemical potential. Hence, we also subdivided the simulations (multistage sampling) for the same state point as the one that led to Fig. C.1 into 25 blocks (instead of 10 like we did for error estimation) consisting of 8000 MC cycles each. In Fig. C.2, the block averages of $\beta\Delta\mu^c$ are displayed for these 25 block averages. Note, that the simulations were initialized with the possibly not entirely equilibrated system. We observe no obvious drift of chemical potential over simulation time. In addition to this examination, we did not observe any systematical increase or decrease of the 10 block averages we calculated for error estimation in each simulation, neither with the multistage sampling approach nor with the EETM method. We thus do not expect large impact of the slow equilibration on values of the chemical potential we report in this work.

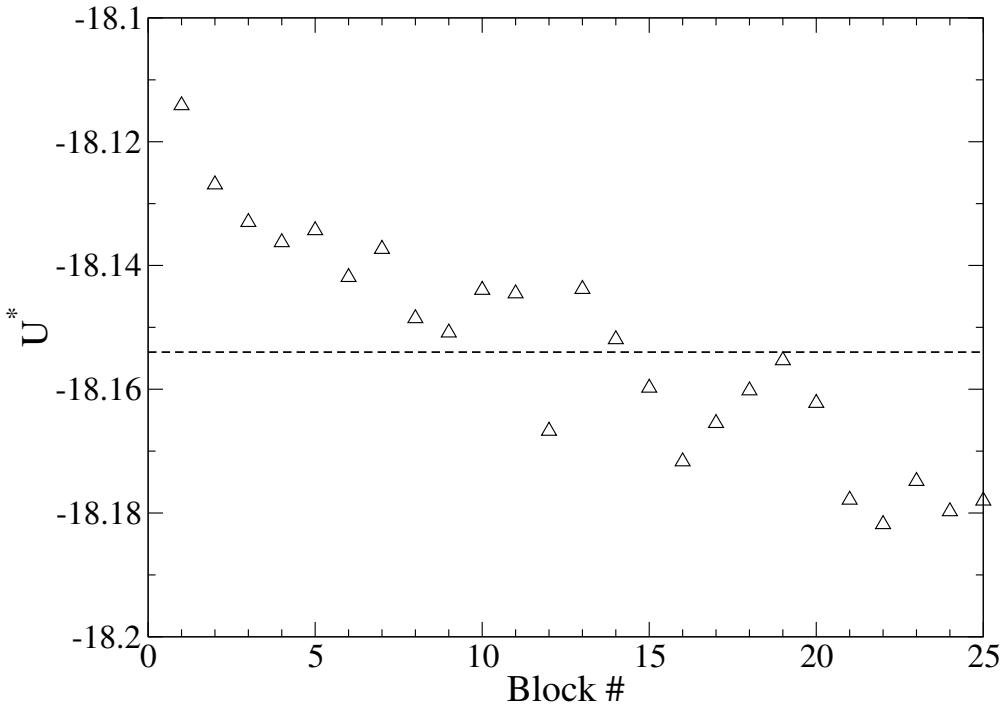

Fig. C.1: Block averages of U^* of the pre-equilibration simulation for the state point with $\rho^* = 0.6786$, $\mu^{*2} = 4.0$, $q^{*2} = 100$, $x_I = 0.160$. The dashed rule represents the total average.

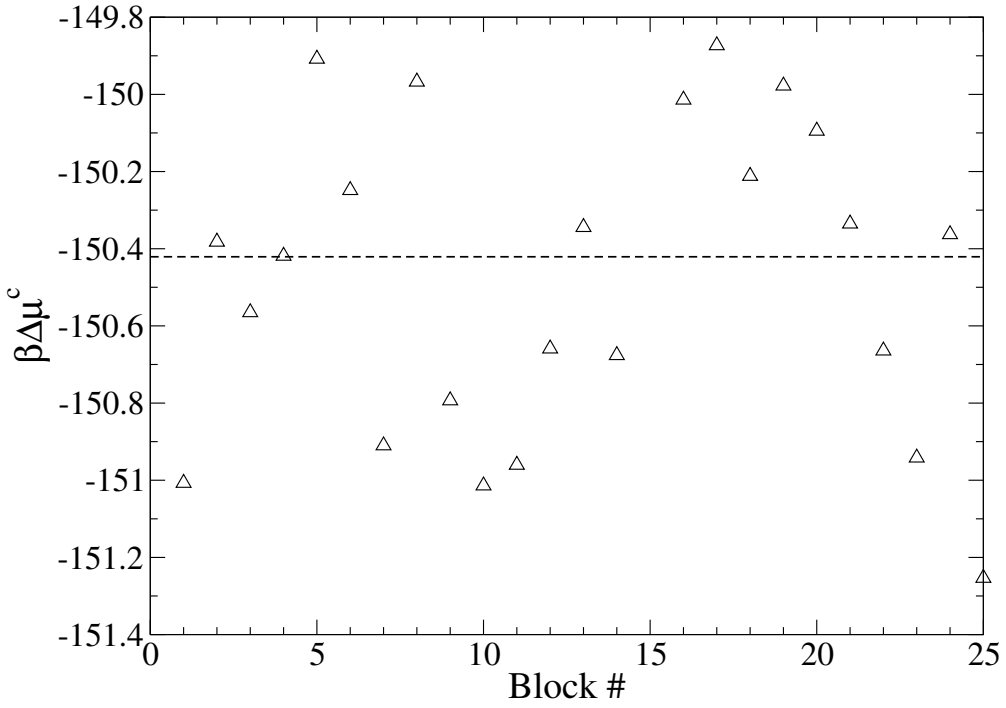

Fig. C.2: Block averages of $\beta\Delta\mu^c$ of the multistage sampling simulation for the state point with $\rho^* = 0.6786$, $\mu^{*2} = 4.0$, $q^{*2} = 100$, $x_I = 0.160$. The dashed rule represents the total average.

D Removing the test particle to test particle interactions in Ewald summation

To test an alternative way of mimicing an infinitely large system with Ewald summation, we omitted the interactions between a test particle and its periodic images when sampling the transition probabilities. Omitting pair interactions is not entirely straightforward in the Ewald summation. In this section, we briefly describe how this can be done in a computationally efficient way. For detailed derivations or discussions of Ewald summation we refer to standard textbooks on molecular simulation techniques, e.g. in Refs. 123 and 122.

The basic Ewald sum equation for calculating the electrostatic part U^{es} of the total potential energy is

$$U^{\text{es}} = U^{\text{real}} + U^{\text{fourier}} - U^{\text{self}} \tag{D.1}$$

with

$$U^{\text{real}} = \sum_{i=1}^{N_c} \sum_{j>i}^{N_c} \frac{q_i q_j \text{erfc}(\alpha\, r_{ij}/L)}{r_{ij}} \tag{D.2}$$

$$U^{\text{fourier}} = \frac{1}{2L^3} \sum_{\mathbf{k}\neq 0} \frac{4\pi}{k^2} \left| \sum_{i=1}^{N_c} q_i \exp(i\, \mathbf{k}\cdot\mathbf{r}_i) \right|^2 \exp\left(-k^2 L^2/(4\alpha^2)\right) \tag{D.3}$$

$$U^{\text{self}} = \frac{\alpha}{\sqrt{\pi} L} \sum_{i=1}^{N_c} q_i^2 \tag{D.4}$$

where N_c is the number of charges, α is the Ewald parameter, $\mathbf{k}$ is the Fourier transformed lattice vector, $\mathbf{r}_i$ is the position of the charge, L is the length of the simulation box and $k^2 = |\mathbf{k}|^2$.

The first term, U^{real}, is a sum of pair potentials in which interactions between the test

particles can easily be omitted. The second term, U^{fourier}, does not explicitly contain pair interactions but only a single sum over all charges and all k-vectors. Thus, it is not possible to simply omit certain pair interactions in this term.
The third term, U^{self}, is a correction term that subtracts the interactions of the charges with themselves. Those self interactions are inherent in U^{fourier}.
In order to enable us to identify certain pair interactions in Eq. (D.3), we use the alternative formulation

$$U^{\text{fourier}} = \frac{1}{2L^3} \sum_{\mathbf{k}\neq 0} \frac{4\pi}{k^2} \sum_{i=1}^{N_c} \sum_{j=1}^{N_c} q_i q_j \exp(i\,\mathbf{k}\cdot(\mathbf{r}_j - \mathbf{r}_i)) \exp\left(-k^2L^2/(4\alpha^2)\right) \tag{D.5}$$

We could now just substitute Eq. (D.3) with Eq. (D.5) in the simulations and omit the test particle interactions (and, at the same time, also omit those interactions in the self interaction term, Eq. (D.4)). However, Eq. (D.5) contains a double sum over all charges for each k-vector, which is of course a disadvantage of this formulation of U^{fourier} compared to Eq. (D.3) (that only contains a single sum). A more efficient way for omitting interactions is to first calculate the total U^{fourier} from Eq. (D.3) and then subtract the contribution arising from test particle-test particle interactions. This contribution can be obtained by Eq. (D.5). In doing so, one implicitly subtracts the self interactions of the test particles. Thus, the test particles have to be omitted in the self interaction term, Eq. (D.4), in order to not subtract them twice.
Applying this procedure, the expression for the total electrostatic potential without the interactions of the test particle to its periodic images is

$$\begin{aligned}
\tilde{U}^{\text{es}} =& \sum_{\substack{i=1\\ i\notin tp}}^{N_c} \sum_{\substack{j>1\\ j\notin tp}}^{N_c} \frac{q_i q_j \text{erfc}(\alpha\, r_{ij}/L)}{r_{ij}} \\
&+ \frac{1}{2L^3} \sum_{\mathbf{k}\neq 0} \frac{4\pi}{k^2} \left| \sum_{i=1}^{N_c} q_i \exp(i\,\mathbf{k}\cdot\mathbf{r}_i) \right|^2 \exp\left(-k^2L^2/(4\alpha^2)\right) \\
&- \frac{1}{2L^3} \sum_{\mathbf{k}\neq 0} \frac{4\pi}{k^2} \sum_{i\in tp}^{N_{tp}} \sum_{j\in tp}^{N_{tp}} q_i q_j \exp(i\,\mathbf{k}\cdot(\mathbf{r}_j - \mathbf{r}_i)) \exp\left(-k^2L^2/(4\alpha^2)\right) \\
&- \frac{\alpha}{\sqrt{\pi}L} \sum_{\substack{i=1\\ i\notin tp}}^{N_c} q_i^2
\end{aligned} \tag{D.6}$$

where '*tp*' denotes all test particles.
From Eq. (D.6), an expression for calculating $\Delta\tilde{U}^{\text{es}}$ in the trial moves ($\kappa_i \to \kappa_j$) can easily be obtained.

E Tabulated simulation results of the study presented in Sec. 3

In this section, the simulation results of our study are tabulated. In Tabs. E.1 and E.2, the results for a^{sr} from α-integration are given. The results for a^{res} are summarized in Tab. E.3.

Tab. E.1: Simulation results for a^{sr} from α-integration (Eq. (3.8)) for $\rho^* = 0.6786$, $\mu^{*\,2} = 4.0$, $q^{*\,2} = 160$

α^*	$x = 0$	$x = 0.032$	$x = 0.064$	$x = 0.12$	$x = 0.176$
0.2	0.000 (0)	0.000 (0)	0.000 (0)	0.000 (0)	0.000 (0)
0.25	0.000 (0)	0.000 (0)	0.000 (0)	0.000 (0)	0.000 (0)
0.3	0.000 (0)	0.000 (0)	0.000 (0)	0.000 (0)	0.000 (0)
0.35	0.000 (0)	0.000 (0)	0.000 (0)	0.000 (0)	0.000 (0)
0.4	−0.003 (0)	−0.003 (0)	−0.003 (0)	−0.003 (0)	−0.003 (0)
0.45	−0.026 (0)	−0.026 (0)	−0.025 (0)	−0.025 (0)	−0.024 (0)
0.5	−0.111 (0)	−0.113 (0)	−0.115 (0)	−0.117 (1)	−0.120 (1)
0.55	−0.307 (0)	−0.319 (1)	−0.331 (1)	−0.352 (1)	−0.372 (1)
0.6	−0.619 (1)	−0.660 (1)	−0.701 (1)	−0.773 (2)	−0.843 (2)
0.65	−1.010 (1)	−1.106 (1)	−1.202 (2)	−1.366 (3)	−1.532 (3)
0.7	−1.428 (1)	−1.603 (2)	−1.780 (3)	−2.084 (5)	−2.390 (5)
0.75	−1.830 (2)	−2.107 (3)	−2.384 (3)	−2.865 (6)	−3.350 (7)
0.8	−2.194 (2)	−2.585 (3)	−2.977 (4)	−3.659 (7)	−4.348 (8)
0.85	−2.511 (2)	−3.024 (4)	−3.537 (4)	−4.432 (9)	−5.333 (10)
0.9	−2.781 (2)	−3.418 (4)	−4.051 (5)	−5.164 (9)	−6.279 (12)
0.95	−3.009 (2)	−3.766 (4)	−4.518 (6)	−5.843 (10)	−7.173 (14)
1.0	−3.200 (3)	−4.074 (4)	−4.942 (6)	−6.468 (11)	−8.004 (15)
1.1	−3.497 (3)	−4.586 (5)	−5.667 (7)	−7.566 (12)	−9.483 (17)
1.2	−3.709 (3)	−4.988 (5)	−6.257 (7)	−8.489 (14)	−10.744 (18)
1.3	−3.864 (3)	−5.310 (5)	−6.745 (8)	−9.270 (14)	−11.818 (20)
1.4	−3.979 (3)	−5.572 (5)	−7.153 (8)	−9.936 (15)	−12.741 (21)
1.5	−4.066 (3)	−5.788 (6)	−7.498 (8)	−10.507 (15)	−13.541 (22)
1.6	−4.133 (3)	−5.969 (6)	−7.793 (9)	−11.004 (16)	−14.240 (23)
1.7	−4.186 (3)	−6.124 (6)	−8.049 (9)	−11.438 (16)	−14.854 (24)
1.8	−4.227 (3)	−6.256 (6)	−8.273 (9)	−11.821 (17)	−15.399 (25)
1.9	−4.261 (3)	−6.372 (6)	−8.471 (9)	−12.162 (17)	−15.885 (25)
2.0	−4.288 (3)	−6.473 (6)	−8.646 (9)	−12.467 (17)	−16.320 (25)
2.1	−4.310 (3)	−6.562 (6)	−8.803 (9)	−12.743 (17)	−16.714 (26)
2.2	−4.329 (3)	−6.642 (6)	−8.944 (9)	−12.991 (17)	−17.070 (26)
2.3	−4.344 (3)	−6.714 (6)	−9.071 (9)	−13.217 (17)	−17.394 (26)
2.4	−4.357 (3)	−6.778 (6)	−9.187 (9)	−13.424 (17)	−17.691 (26)
2.5	−4.368 (3)	−6.836 (6)	−9.293 (9)	−13.613 (18)	−17.964 (26)
2.6	−4.378 (3)	−6.890 (6)	−9.390 (9)	−13.787 (18)	−18.215 (27)
2.7	−4.386 (3)	−6.939 (6)	−9.480 (10)	−13.948 (18)	−18.448 (27)
2.8	−4.394 (3)	−6.985 (6)	−9.563 (10)	−14.098 (18)	−18.664 (27)
2.9	−4.403 (3)	−7.029 (6)	−9.643 (10)	−14.239 (18)	−18.866 (27)
3.0	−4.416 (3)	−7.074 (6)	−9.720 (10)	−14.373 (18)	−19.058 (27)

Tab. E.2: Simulation results for a^{sr} from α-integration (Eq. (3.8)) for $\rho^* = 0.8$, $\mu^{*\,2} = 2.5$, $q^{*\,2} = 100$

α^*	$x = 0$	$x = 0.032$	$x = 0.064$	$x = 0.12$	$x = 0.176$
0.2	0.000 (0)	0.000 (0)	0.000 (0)	0.000 (0)	0.000 (0)
0.25	0.000 (0)	0.000 (0)	0.000 (0)	0.000 (0)	0.000 (0)
0.3	0.000 (0)	0.000 (0)	0.000 (0)	0.000 (0)	0.000 (0)
0.35	0.000 (0)	0.000 (0)	0.000 (0)	0.000 (0)	0.000 (0)
0.4	−0.002 (0)	−0.002 (0)	−0.002 (0)	−0.001 (0)	−0.001 (0)
0.45	−0.015 (0)	−0.014 (0)	−0.014 (0)	−0.014 (0)	−0.014 (0)
0.5	−0.062 (0)	−0.063 (0)	−0.064 (0)	−0.065 (0)	−0.067 (1)
0.55	−0.168 (0)	−0.175 (0)	−0.182 (1)	−0.194 (1)	−0.206 (1)
0.6	−0.338 (1)	−0.361 (1)	−0.385 (1)	−0.426 (2)	−0.467 (2)
0.65	−0.553 (1)	−0.606 (1)	−0.660 (1)	−0.755 (3)	−0.851 (3)
0.7	−0.783 (1)	−0.882 (1)	−0.982 (2)	−1.156 (3)	−1.332 (4)
0.75	−1.008 (2)	−1.164 (2)	−1.321 (2)	−1.596 (4)	−1.877 (5)
0.8	−1.214 (2)	−1.434 (2)	−1.658 (3)	−2.050 (4)	−2.452 (7)
0.85	−1.395 (2)	−1.685 (2)	−1.979 (3)	−2.496 (5)	−3.029 (8)
0.9	−1.550 (2)	−1.912 (2)	−2.279 (3)	−2.924 (6)	−3.589 (8)
0.95	−1.682 (2)	−2.116 (3)	−2.554 (4)	−3.326 (6)	−4.123 (10)
1.0	−1.794 (2)	−2.296 (3)	−2.804 (4)	−3.700 (7)	−4.626 (11)
1.1	−1.967 (2)	−2.599 (3)	−3.237 (4)	−4.367 (8)	−5.532 (12)
1.2	−2.092 (2)	−2.839 (3)	−3.593 (5)	−4.931 (9)	−6.308 (14)
1.3	−2.184 (2)	−3.033 (3)	−3.890 (5)	−5.410 (9)	−6.974 (15)
1.4	−2.252 (2)	−3.191 (3)	−4.139 (5)	−5.821 (10)	−7.548 (15)
1.5	−2.303 (2)	−3.322 (4)	−4.351 (6)	−6.174 (10)	−8.046 (16)
1.6	−2.343 (2)	−3.433 (4)	−4.532 (6)	−6.483 (10)	−8.480 (17)
1.7	−2.375 (2)	−3.527 (4)	−4.690 (6)	−6.753 (11)	−8.863 (17)
1.8	−2.399 (2)	−3.608 (4)	−4.828 (6)	−6.991 (11)	−9.203 (17)
1.9	−2.419 (2)	−3.679 (4)	−4.950 (6)	−7.204 (11)	−9.506 (17)
2.0	−2.435 (2)	−3.741 (4)	−5.058 (6)	−7.394 (11)	−9.778 (18)
2.1	−2.449 (2)	−3.796 (4)	−5.155 (6)	−7.565 (11)	−10.024 (18)
2.2	−2.460 (2)	−3.846 (4)	−5.243 (6)	−7.720 (11)	−10.246 (18)
2.3	−2.469 (2)	−3.890 (4)	−5.322 (7)	−7.861 (11)	−10.449 (18)
2.4	−2.477 (3)	−3.929 (4)	−5.394 (7)	−7.989 (11)	−10.634 (18)
2.5	−2.483 (3)	−3.966 (4)	−5.460 (7)	−8.107 (12)	−10.805 (18)
2.6	−2.489 (3)	−3.999 (4)	−5.521 (7)	−8.216 (12)	−10.962 (18)
2.7	−2.495 (3)	−4.030 (4)	−5.577 (7)	−8.317 (12)	−11.107 (18)
2.8	−2.502 (3)	−4.060 (4)	−5.631 (7)	−8.412 (12)	−11.244 (18)
2.9	−2.510 (3)	−4.091 (4)	−5.683 (7)	−8.503 (12)	−11.372 (18)
3.0	−2.525 (3)	−4.125 (4)	−5.737 (7)	−8.592 (12)	−11.497 (18)

Tab. E.3: Simulation results for a^{res} from λ-integration (Eq. (3.3))

$x = 0$	$x = 0.032$	$x = 0.064$	$x = 0.12$	$x = 0.176$
$\rho^* = 0.6786$; $\mu^{*\,2} = 4.0$; $q^{*\,2} = 160$				
$-4.450\,(5)$	$-8.055\,(6)$	$-11.675\,(10)$	$-18.041\,(14)$	$-24.424\,(19)$
$\rho^* = 0.8$; $\mu^{*\,2} = 2.5$; $q^{*\,2} = 100$				
$-2.532\,(3)$	$-4.728\,(5)$	$-6.934\,(6)$	$-10.828\,(10)$	$-14.766\,(14)$